December 2016

A Multi-Model Approach to Design a Robust Fixed-Order Controller to Improve Power System Stability

Abdlmnam Abdlrahem Abdlrahem
Clemson University, aabdlra@clemson.edu

A MULTI-MODEL APPROACH TO DESIGN A ROBUST FIXED-ORDER CONTROLLER TO IMPROVE POWER SYSTEM STABILITY

A Dissertation
Presented to
the Graduate School of
Clemson University

In Partial Fulfillment
of the Requirements for the Degree
Doctor of Philosophy
Electrical Engineering

---

by
Abdlmnam Abdlrahem
December 2016

Accepted by:
Richard E. Groff, Committee Chair
Taufiquar R. Khan
Randy Collins
Ramtain Hadidi

ABSTRACT

The rapid increase in power system grid has resulted in additional challenges to reliable power transfer between interconnected systems of a large power network. Large-scale penetration of intermittent renewable energy increases uncertainty and variability in power systems operation. For secure operation of power systems under conditions of variability, it is imperative that power system damping controllers are robust. Electromechanical oscillations in the range of 0.2 Hz to 1 Hz are categorized as inter-area modes. These modes arise due primarily to the weak interconnections characterized by long transmission lines between different operating areas of an interconnected power system. One of the main challenges to secure operation of interconnected power systems is the damping of these inter-area modes.

This dissertation introduces two multi-model approaches (loop shaping and H_∞) to designing a fixed-order robust supplementary damping controller to damp inter-area oscillations. The designed fixed-order supplementary damping controller adjusts the voltage reference set point of the Static Var Compensator (SVC). The two main objectives of the controller design are damping low-frequency oscillations and enhancing power system stability. The proposed approaches are based on the shaping of the open-loop transfer function in the Nyquist diagram through minimizing the quadratic error between the actual and the desired open-loop transfer functions in the frequency domain. The H_∞ constraints are linearized with the help of a desired open-loop transfer function. This condition can be achieved by using convex optimization methods. Convexity of the

problem formulation ensures global optimality. One of the advantages of the proposed approach is the consideration of multi-model uncertainty. Also, in contrast to the methods that have been studied in literature, the proposed approach deals with full-order model (i.e., model reduction is not required) with lower controller order. In addition, most of the current robust methods are heavily dependent on selecting some weighting filters: such filters are not required in the loop-shaping approach. The proposed approaches are compared with different existing techniques in order to design a robust controller based on H_∞ and H_2 under pole placement. With large-scale power systems, it is difficult to handle large number of states to obtain the system model. Thus, it becomes necessary to use only input/output data measured from the system, and this data can be utilized to construct the mathematical model of the plant. In this research, the mentioned approaches are offered in order to design a robust controller based only on data by using system identification techniques. The mentioned techniques are applied to the two-area four-machines system and 68 bus system. The effectiveness and robustness of the proposed method in damping inter-area oscillations are validated using case studies.

ACKNOWLEDGMENTS

First of all, I am thankful to God for giving me the strength to complete this dissertation.

I would like to express my sincere gratitude to my academic and research advisor, Dr. Elham Makram, for her supervision and support in making this work possible.

I would also like to express my appreciation to Dr. Ramtain Hadidi and Dr. Alireza Karimi for their support and valuable assistance during my research.

I also thank all the power group members for their help and research ideas, especially Parimal Saraf, Karthikeyan Balasubramaniam and Hani Albalawy.

I would like to say thank you (I know that is not enough) to my beloved one who prays every day and night for me to succeed in life: my Mother; even though you are far away, your prayers are with me every minute. I want also to extend my deep appreciation to my father, and my brothers and sisters for their prayers.

I owe my sincere gratefulness to my wife, who has been the main support during these years. I want to extend my deep thankfulness to my children for their sweet smiles and understanding.

TABLE OF CONTENTS

Page

Page

Page

Page

Page

LIST OF FIGURES

Page

Page

Page

LIST OF TABLES

Page

LIST OF SYMBOLS

x_1	Leakage reactance
R_a	Armature resistance
x_d	D-Axis synchronous reactance
x'_d	D-Axis transient reactance
x''_d	D-Axis sub-transient reactance
T'_{do}	Direct transient filed winding time constant
T''_{do}	Direct sub-transient filed winding time constant
x_q	Q-Axis synchronous reactance
x'_q	Q-Axis transient reactance
x''_q	Q-Axis sub-transient reactance
T'_{qo}	Quadrature transient filed winding time constant
T''_{qo}	Quadrature sub-transient filed winding time constant
H	Inertia Constant
D	Machine Damping

$1/R$	Steady State Gain
T_a, T_b, T_c	Exciter voltage regulator time constants
$E_{fd,max}$, $E_{fd,min}$	Exciter max and min voltage regulator output
K_r	Exciter constant
E_{ref}	Exciter reference voltage
Tr	Exciter Time Constant
ω_{ref}	Governor speed set point
T_{max}	Governor maximum Power Order On Generator Base
T_1	Governor servo time constant
T_2	HP turbine time constant
T_3	Governor transient Gain Time Constant
T_4	HP Section Time Constant
T_5	Reheater Time Constant
T_{n1}	PSS lead Time Constant
T_{d1}	PSS lag Time Constant
T_{n2}	PSS lead Time Constant
T_{d2}	PSS lag Time Constant

Y_{max}	PSS maximum Output Limit
Y_{min}	PSS minimum Output Limit
T_w	PSS washout Time Constant
K_{stab}	PSS gain
δ	Machine rotor Angle
ω	Generator angular speed
e'_q	Transient quadrature axis voltage
e'_d	Transient direct axis voltage
e''_q	Sub-transient quadrature axis voltage
e''_d	Sub-transient direct axis voltage
E_{fd}	Field voltage
T_{AA}	D-Axis Additional Leakage Time Constant
τ_m	Generator Input Mechanical Torque
τ_e	Generator Electromagnetic Torque

CHAPTER ONE

INTRODUCTION

1.1 Motivation

Over the years, maintaining system stability has been a challenge to power engineers. This problem can be categorized as power system modeling and correct assessment of power system stability [1, 2]. A power system is modeled on algebraic and differential equations. For large-scale power systems, these equations are more difficult to solve. To achieve behavior similar to the real system, a detailed model has to be developed. Once a mathematical model that is based on algebraic and differential equations is developed, then the solution through numerical techniques is obtained.

Historically, solutions to the stability problem have been attempted since 1920. At that time, computations of power systems were based on hand calculations. In 1950, analog computers started to be used in power systems to simulate the transient stability problem. In 1956, the first computer program on digital computers was created to make simulating the transient stability problem easier.

Over the years, a high response of the excitation system was achieved to improve transient stability. However, high response of the excitation system caused poor damping in power system oscillations. The problem of poor damping has been coped with by using power system stabilizers.

A power system has never been in steady state condition all the time; disturbances may occur at any time, and the challenge is to keep the system stable during these disturbances.

Power system stability is the ability of a power system at specified operating conditions to keep the system stable after being subjected to a disturbance, i.e. maintaining the system variables, voltage and frequency within their limit [1]. The disturbance could be large or small depending on the severity of the disturbance. Large disturbance includes sizable change in generation, significant change in loads, line outages and the different types of faults. Small disturbance is characterized by minimal changes in generation or load.

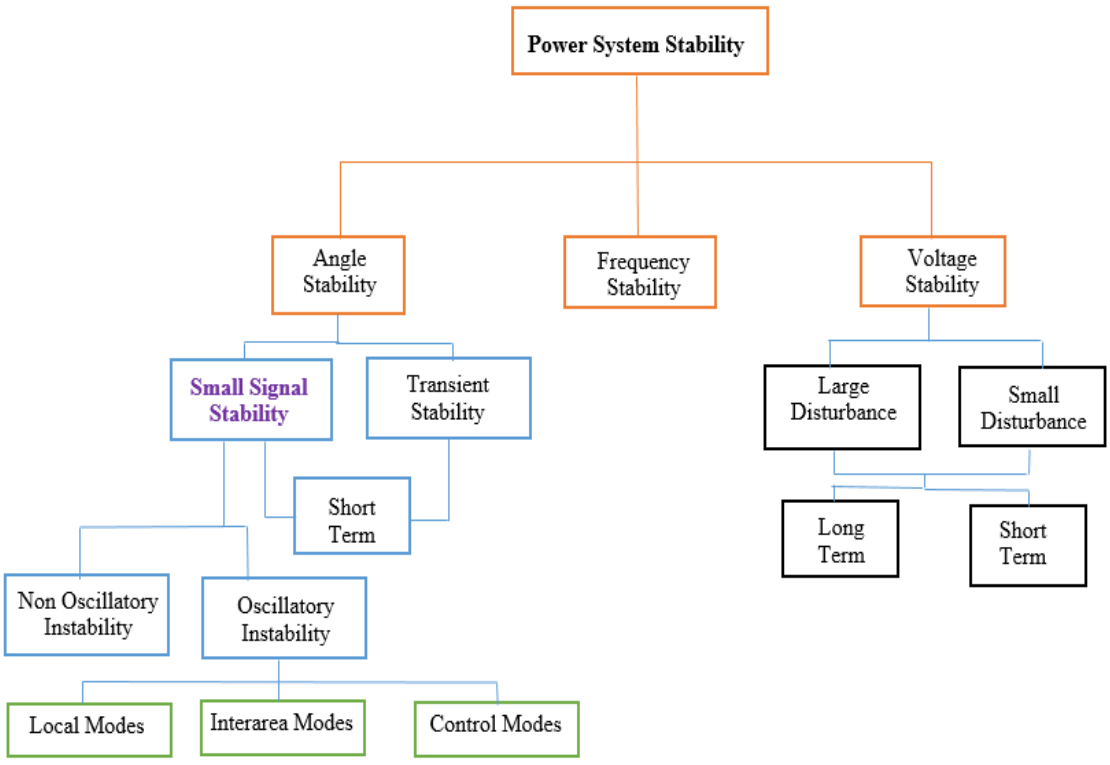

Figure 1.1 Classification of power system stability

Power system stability generally falls into three categories: rotor angle, voltage, and frequency stability. Rotor angle, voltage and frequency stability have been classified as large disturbance or small disturbance, short term or long term. These classifications are shown in Figure 1.1.

The model of any system, no matter how detailed and complex, never represents the real physical system. Normally, in conventional control design, uncertainty is incorporated with the stability margin. The stability margin is a kind of safety factor: if any changes occur (such as uncertainties and disturbances), they will not affect the stability of the system, and the system will continue to behave in a satisfactory manner. However, the uncertainties or perturbations are not quantified, nor has performance been taken into account in terms of disturbance, noise, etc. The robust control method came to the field to address these problems. The aim of the robust control is to achieve robust performance and stability under a limit number of changes, uncertainties and disturbances.

The power system is a nonlinear system, and it can be linearized around an operating point. The nonlinearity and time-varying properties of the power system are modeled by multi-model uncertainty and have been overcome by a robust design approach. In this research, a fixed-order robust controller is designed based on different operating points, which include the normal operating point as well as the worst operating point, to overcome the uncertainties in the power system.

Power system grid has been increased rapidly, an achievement that has added more challenges to reliable power transfer between interconnected systems of a large power

network. Large-scale penetration of intermittent renewable energy increases uncertainty and variability in power systems operation. For secure operation of power systems under conditions of variability, it is imperative that power system damping controllers are robust. Electromechanical oscillations in the range of 0.2 Hz to 1 Hz are categorized as inter-area modes [1-5]. These modes arise due primarily to the weak interconnections characterized by long transmission lines between different operating areas of an interconnected power system. One of the main challenges in secure operation of interconnected power systems is the damping of these inter-area modes. System stability could be affected without adequate damping of these low-frequency oscillations [6]. Events such as the 1996 western interconnection blackout is an example.

Recently, Flexible AC Transmission System (FACTS) devices are being widely used in power systems. The main purpose of these devices is to increase the capability of transferred power between interconnected areas and to enhance the voltage profile as well [3, 5, 7-26]. Static Var Compensator (SVC) is a shunt FACTS device that injects reactive power to maintain the voltage at a point of connection in a certain range to enhance system stability [27]. Controlling SVCs helps to damp inter-area oscillations. A supplementary signal could be added to adjust the voltage reference set point of SVC to achieve the desired damping [3, 19, 20, 24, 28, 29]. The location of SVCs for damping inter-area oscillations is important; they are usually placed at either end of a tie-line. Depending on system configuration, multiple SVCs might be required to improve the overall system damping.

1.2 Literature Review

Damping of inter-area oscillations in power systems using H_2, H_∞, H_∞ loop-shaping, and μ-synthesis methods has been previously studied [3, 10, 11, 24, 30-36]. The results show that these methods of designing the controller have the ability to damp out inter-area oscillations and enhance the stability of the power system. The solution to the H_∞ control design problem is based on the Riccati equation approach. Generally, the controller design based on this solution suffers from pole-zero cancellations between the controller and the plant model. Recently, a linear matrix inequalities (LMIs) method has been used to solve the H_∞ control design problem [35-37]. The main concept of the H_∞ loop-shaping method introduced is to augment the open-loop model by pre- and post-compensators to get the desired shape. Then the controller is designed by solving the H_∞ optimization problem [38].

Most of these designs are based on nominal operating point, i.e. the control objectives from H_2 and H_∞ formulations are guaranteed an operating point [39]. On some occasions, the system might not be operating close to a nominal operating point, and the controller might not work as expected. The order of the controller is considered a key factor, since the controller is implemented in computers and devices that have limited memory and computing power. Implementing a high-order controller both in hardware and software is a challenging task and leads to numerical problems. Even though there are some methods to reduce the order of the controller, they do not guarantee that the reduced controller will achieve the requirements of stability and performance.

New techniques are presented in [10, 11] for designing a robust controller for multi-modal uncertainty using H_2 and H_∞ under pole placement; however, these techniques require reducing the order of the plant model. Also, the designed controller based on these techniques leads to high-order controller, compared with the proposed approach.

Recently, Wide Area Measurements (WAMs) have been used to design the controller [2, 4, 14, 15, 23, 40-42]. Phasor Measurements Units (PMUs) are installed in specific locations to monitor and control modern power systems and improve their stability and security [43-49]. Inter-area oscillations could be damped out using wide area measurements. Good results have been achieved by applying WAMs to the damping controller as shown in [14, 23].

The main challenge of using WAMs to design a robust controller to damp the inter-area oscillations is the issue of the signal transmission delay [43, 46, 48]. The signal provided to the controller from PMUs has some delay in communications channels, and this delay may affect the performance of the controller. In [48], a summary of communication delays is shown among six PMUs installed in different locations at Jiangsu, China. The summary shows that the PMU signal could be delayed in the range (7 to 81 ms). Also, the latency of PMU data of the QUEBEC power system is listed in [50], which shows the total estimated latency (109 ms).

Large interconnected power systems have thousands of generators, and it is not possible to model each generator in detail. For example, to model one single generator, a simple generator can be modeled as a 3rd-order model. The 6th-order model of a synchronous machine gives enough information by having a complete detailed model.

Each generator has a turbine model, governor model, exciter model, and automatic voltage regulator model. Each of these models has a different number of state variables that will correspond to the number of state variables of the machine. So, as a whole, one generator has to be modeled by at least 12 to 13 states, and if the system has a huge number of generators, the number of the state variables will be very high. Thus it becomes quite difficult to handle this number of states to obtain the system model. Most of the control approaches in literature used to damp inter-area oscillations are based on plant models (parametric models). In such situations, input/output data measured from the plant can be used to construct the mathematical model of the plant. This approach is called data driven and can be achieved by using system identification techniques. In this approach, the knowledge of the plant is not required. PMUs can be used to provide input/output data to the control center.

To summarize, the challenges of the existing approaches are:

1- The power system is known as a high-order system. These approaches are based on reducing the order of the plant model (system). The model reduction is the process of reducing the order of a given system to the extent that the response of the reduced system is similar to that of the full-order system. Hence, there is loss of information. The level of loss of information is dependent on the order to which the system is reduced and the method used. On the other hand, the proposed method does not require any model order reduction. In addition, model

order reduction is an $O(n\hat{}3)$ operation. Hence, computing model order reduction for large systems is computationally expensive.

2- The order of the controller based on existing approaches is comparatively high for large systems with the proposed approach, since it is the sum of the orders of the reduced plant model plus the order of the weighting filters as mentioned in [2]. For example, in reference [14] the order of the controller is 10 and it is 7 in reference [10].

3- Most of the existing designs are based on the nominal operating point, i.e. the control objectives from H_2 and H_∞ formulations are guaranteed an operating point. However, a power system is a non-stationary system wherein operating points change for every dispatch at the system operator level. Hence, performance of such controllers degrades depending on the deviation between current operating point and the nominal operating point for which the controller was designed.

4- In literature most of the control approaches that were used to damp inter-area oscillations are based on parametric models.

1.3 Objective and Contributions

The contribution of this research is introducing a new technique to design a fixed-order linearly parameterized controller using the H_∞ approach. The main idea of the proposed approach is based on the shaping of the open-loop transfer function under an infinite

number of convex constraints on the Nyquist diagram. The control objective is to reduce the distance between the designed open-loop transfer function and the desired one by minimizing their quadratic error in the frequency. The desired transfer function needs to be specified in order to carry out the optimization and design of the controller. The proposed technique can handle both stable and unstable plant models. In this work, however, only stable plant models are considered. Frequency Domain Robust Control (FDRC) Toolbox, which is introduced in [51], is used in this research to design the fixed-order robust controller in both approaches. This technique doesn't suffer from other methods' drawbacks.

Thus, the contributions of the dissertation are as outlined below:

- The proposed techniques do not need model order reduction. The controller design techniques presented in this research can be used in full-order systems for designing a robust H_∞ controller, since the order of the controller is fixed, without sacrificing the computational time required (which is taken care of by convexifying the problem). Therefore, the need for using an approximate reduced order model is eliminated. The proposed approaches can also use a reduced order system.
- The resulting controller order is less than that of other existing methods. For example, the IEEE 68 bus test system used in this research has 190 states, and it is considered a large system. To design a robust controller using conventional methods, the system has to be reduced, and the order of the controller is equal to the order of the reduced system. The IEEE 68 bus system (190 states) is

reduced to 7 states. Thus, the order of the controller using, for example H_∞, will be the order of the reduced system 7 plus the order of the weighting filters. On the other hand, only the 4^{th}-order controller is designed based on the proposed approach for the same system, and it demonstrates very good results.

- The designed controller is fixed order, which means that the user can specify the order of the controller; it does not depend on the order of the system.
- Multi-model uncertainty is considered, which means that the robustness is guaranteed in a wide range of changing the operating point. The controller can be designed based on different operating points to overcome the uncertainty of the power system.
- The issue of time delay of feedback signals has been addressed using a multi-model optimization approach.
- Convex formulation guarantees a global optimal solution while minimizing the norm between open-loop transfer function and desired transfer function.
- The designed controller has been integrated into the Power System Toolbox (PST). The results are verified by matching the Eigenvalues of the test systems after adding the controller in both the FDRC Toolbox and the PST.
- In chapter five, a fixed-order robust controller has been designed based only on frequency-domain data (obtained using spectral analysis of measured I/O data); no parametric model is required.

1.4 Organization of the Dissertation

The dissertation is divided into six chapters as follows:

Chapter one: gives an introduction and definition of power system stability and also describes the issue of inter-area oscillations. Research review related to the topic of this dissertation is summarized in this chapter. The challenges of the existing approaches as well as the contributions of this research are also mentioned in this chapter.

Chapter two: describes the dynamic model of the components of power systems, including synchronous machine, excitation system, governor, and power system stabilizer. The dynamic equations of wind turbine are also explained in this chapter. Introduction to small signal stability and linearization of the power system around an equilibrium point are discussed.

Chapter three: the loop-shaping approach based on shaping the open-loop transfer function on the Nyquist diagram through minimizing the distance between the actual and the desired open-loop transfer function is introduced in this chapter. The controller design procedure is explained in detail. The proposed approach is applied to the two-area four-machines system and the IEEE 68 bus system. The effectiveness and robustness of the proposed method in damping inter-area oscillations are validated through case studies.

Chapter four: introduces the H_∞ approach to designing a robust fixed-order controller. The proposed H_∞ approach is based on shaping the closed-loop sensitivity functions in the Nyquist diagram through constraints on their infinity norm. The H_∞ constraints are

linearized with the help of a desired open-loop transfer function. In this chapter, a multi-model optimization method is used to include the effect of time delay. The IEEE 68 bus system is cited to verify the designed controller under different operating conditions.

Chapter five: the method explained in chapter three is extended to design a robust controller based on input/output data using system identification techniques. In this approach, the knowledge of the plant is not required. Phasor measurement units (PMUs) can be used to provide input/output data to the control center.

Chapter six: summarizes results, conclusions, and future work.

CHAPTER TWO

POWER SYSTEM MODELING

In this chapter, the dynamic model of power system components is explained. The power system contains different dynamic components that are used to maintain system stability. These components need to be modeled in order to find the nonlinear dynamic model of the power system. The dynamic model of these devices can be modeled by several algebraic and differential equations as explained in the following sections [1, 2].

2.1 Synchronous Machine Model

Synchronous generators are the main source of electric energy in power systems. The stability of a power system is defined as the ability of interconnected synchronous generators in different areas to maintain synchronism after the system becomes subjected to a disturbance. Basically, system stability depends on different factors that determine the severity of the disturbance: the initial operating condition, and the nature and size of the disturbance. Consequently, it becomes important to understand the modeling and dynamic behavior of the synchronous generators. The synchronous generator equations describe the dynamic behavior of synchronous machines. There are different types of models for synchronous machines, and the order of the model depends upon the purpose of study [1].

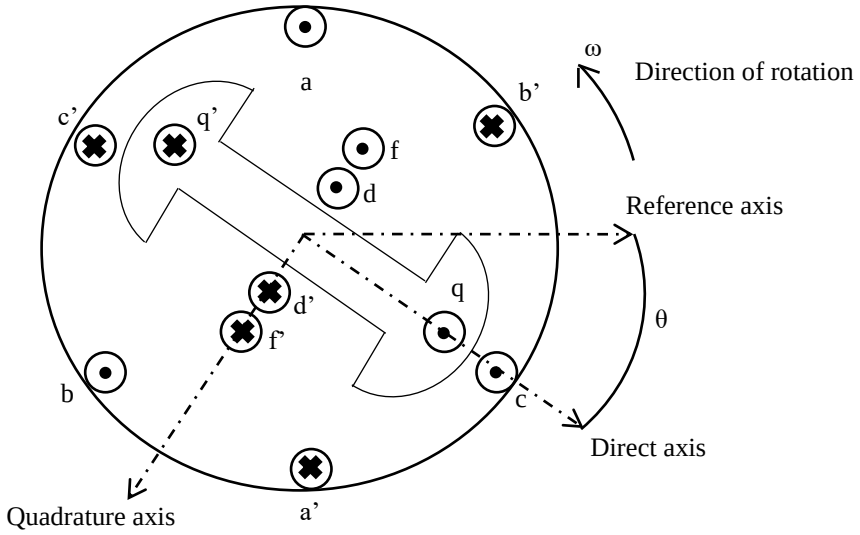

Figure 2.1 Synchronous machine schematic

The 6th-order model of a synchronous machine provides enough information by having a complete detailed model. In this dissertation, a 6th-order model of a synchronous machine, as described herein, has been used.

The dynamic equations of the 6th-order synchronous machine model that is used in this thesis are given below in (2.1) – (2.6).

$$\dot{\delta} = \Omega_b(\omega - \omega_s) \tag{2.1}$$

$$\dot{\omega} = \frac{1}{2H}\left(T_m - T_e - D(\omega - \omega_s)\right) \tag{2.2}$$

$$\dot{e}'_q = \frac{1}{T'_{d0}}\left(-e'_q - (x_d - x'_d - \gamma_d)i_d + \left(1 - \frac{T_{AA}}{T'_{d0}}\right)E_{fd}\right) \quad (2.3)$$

$$\dot{e}'_d = \frac{1}{T'_{q0}}\left(-e'_d - \left(x_q - x'_q - \gamma_q\right)i_q\right) \quad (2.4)$$

$$\dot{e}''_q = \frac{1}{T''_{d0}}(-e''_q + e'_q - (x'_d - x''_d + \gamma_d)i_d + \frac{T_{AA}}{T'_{d0}}\mathrm{E_{fd}}) \quad (2.5)$$

$$\dot{e}''_d = \frac{1}{T''_{d0}}(-e''_d + e'_d + (x'_q - x''_q + \gamma_q)i_q) \quad (2.6)$$

where γ_d and γ_q are given as follows:

$$\gamma_d = \frac{T''_{d0}}{T'_{d0}}\frac{x''_d}{x'_d}(x_d - x'_d), \qquad \gamma_q = \frac{T''_{q0}}{T'_{q0}}\frac{x''_q}{x'_q}(x_q - x'_q) \quad (2.7)$$

The solution of power flow reveals the initial values of active and reactive power as well as the voltage and the angle (P_g, Q_g, V, θ) of the system. The power system variables are related to the machine equations by the equations given in (2.7) – (2.9)

$$I = \frac{P_g + i * Q_g}{V} \quad (2.8)$$

$$\delta = \angle\left(V + \left(r_a + i * x_q\right)I\right) \quad (2.9)$$

$$v_d = V\sin(\delta - \theta)$$

$$v_q = V\cos(\delta - \theta) \quad (2.10)$$

2.2 Excitation System

The main purpose of an excitation system is to provide a direct current to the field winding of a synchronous machine. An excitation system provides two essential functions: control and protection, to satisfy the power system performance. The control function includes controlling voltage and reactive power flow to enhance power system stability. The protective functions of the excitation system are responsible for monitoring the limits of the synchronous machine and the other equipment to avoid exceeding their limit. Generally there are three different types of excitation system: DC, AC, and static excitation systems [52]. A basic block diagram of the standard excitation system is shown in Fig.2.2.

The excitation system can b represented by the following dynamic equations (2.11) to (2.13):

$$\dot{E}_r = \frac{1}{T_r}(K_r E - E_r) \tag{2.11}$$

$$\dot{E}_a = \frac{1}{T_b}\left(\left(1 - \frac{T_c}{T_b}\right)(E_{ref} - E_r) - E_a\right) \tag{2.12}$$

where E_a is an internal state of the lead-lag compensator.

$$\dot{E}_{fd} = \frac{1}{T_a}(K_a E_a - E_{fd}) \tag{2.13}$$

The value of E_{fd} is used in the machine equations

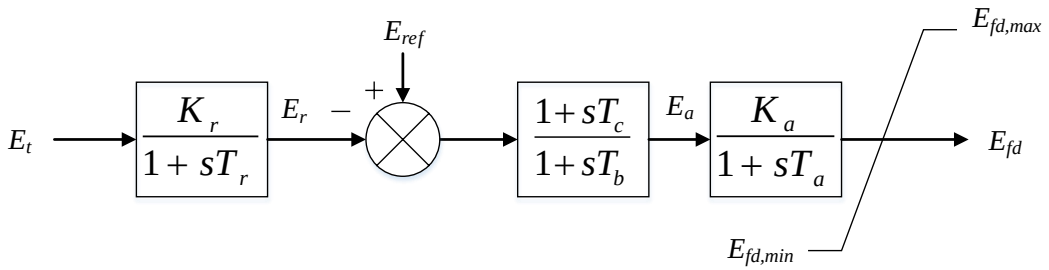

Figure 2.2 Simplified block diagram of standard excitation system

2.3 Governor

The main function of the governor is to control the output power of a synchronous machine as the power system changes. The speed of the synchronous machine accelerates or de-accelerates depending on the change in loads. The governor increases the speed of the synchronous machine by increasing the input of real power until the frequency settles at the synchronous speed. The governor control action is relatively slow compared with other controllers, so the time constants associated with the governor are small. The block diagram of the governor dynamic model is shown in Fig 2.3 [2].

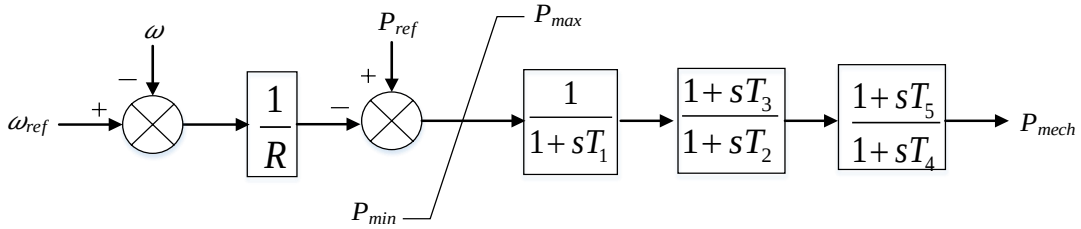

Figure 2.3 Block diagram of governor system

The dynamic equations that represent the governor model have been listed in (2.14) – (2.16).

$$\dot{x}_{g1} = \frac{1}{T_1}\left(P_{in} - x_{g1}\right) \tag{2.14}$$

$$\dot{x}_{g2} = \frac{1}{T_2}\left(\left(1 - \frac{T_3}{T_2}\right)x_{g1} - x_{g2}\right) \tag{2.15}$$

$$\dot{x}_{g3} = \frac{1}{T_4}\left(\left(1 - \frac{T_5}{T_4}\right)\left(x_{g2} + \frac{T_3}{T_2}x_{g1}\right) - x_{g3}\right) \tag{2.16}$$

2.4 Power System Stabilizer (PSS)

The power system stabilizer is normally installed in the system to damp out the local power system oscillations. PSS is very useful for improving the dynamic stability of the power system. It helps the damping of these oscillations by adding a supplementary damping signal to the reference of the excitation circuit. PSS has three main blocks: gain, phase compensation, and washout circuit or reset block. Fig 2.4 shows the simple block diagram of PSS.

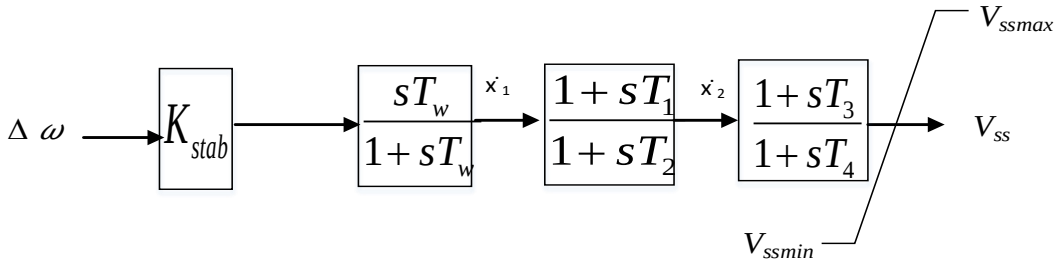

Figure 2.4 A common structure of PSS

The dynamic equations related to the PSS are given in (2.17) – (2.19).

$$\dot{x}_1 = \frac{1}{T_w}(-K_{stab}\Delta\omega + x_1) \tag{2.17}$$

$$\dot{x}_2 = \frac{1}{T_2}\left(\left(1 - \frac{T_3}{T_2}\right)(K_{stab}\Delta\omega + x_1) - x_2\right) \tag{2.18}$$

$$\dot{V}_{ss} = \frac{1}{T_4}\left(\left(1 - \frac{T_5}{T_4}\right)\left(x_2 + \left(\frac{T_3}{T_2}(K_{stab}\Delta\omega + x_1)\right)\right) - V_{ss}\right) \tag{2.19}$$

2.5 Wind Energy Conversion Systems

Due to an ever increasing penetration of renewable energy sources in the power grid, it has become essential to study the impact of these sources on the dynamics and stability of the system. A Wind Energy Conversion System (WECS) essentially comprises a wind turbine, a generator and power electronic controls. An important assumption for modeling WECS in fundamental frequency simulations is that the power electronic converters are represented as current sources. This is a routine methodology used for modeling of power electronic components in power system dynamic studies. One more important assumption in this work is that multiple wind generators are aggregated into a single machine for the purpose of dynamic analysis [53].

2.5.1 Wind turbine

The wind turbine extracts the kinetic energy from the wind and converts it into mechanical energy that in turn rotates the rotor of the wind generator and generates electricity. The mechanical power output of the turbine shaft is given as:

$$P_m = \frac{n_{gen}}{2} \rho_{air} A_{blade} C_p(\beta, \lambda) v^3{}_w \tag{2.20}$$

Tip-speed ratio, $\lambda = \frac{R_{blade}\omega_m}{v_w}$

where n_{gen} is the number of wind generators, ρ_{air} is the density of air, A_{blade} is the area of the blades swept by the rotor [m^2], v_w is the wind speed [m/s], β is called the pitch angle, ω_m is the angular speed of the blades, and R_{blade} is the radius of the rotor blades. Pitch angle control is necessary to protect the blades from damage when the wind speeds are very high. It curtails the amount of power extracted from wind by pitching the blades of the turbine. $C_p(\beta, \lambda)$ is called the 'coefficient of performance,' and it is a function of the tip-speed ratio and the pitch angle. The $C_p(\beta,\lambda)$ curve is approximated as given in (2.21) using (2.22) [54].

$$C_p = 0.22\left(\frac{116}{\lambda_i} - 0.4\beta - 5\right) e^{-\frac{12.5}{\lambda_i}} \tag{2.21}$$

$$\frac{1}{\lambda_i} = \frac{1}{\lambda + 0.08\beta} - \frac{0.035}{\beta^3 + 1} \tag{2.22}$$

The dynamic equation representing pitch angle control is given in (2.23).

$$\dot{\beta} = \frac{\left(K_p \varphi\left(\omega_m - \omega_{ref}\right) - \beta\right)}{T_p} \tag{2.23}$$

where φ is a function that allows changing the pitch angle only when the difference $\left(\omega_m - \omega_{ref}\right)$ is above a certain threshold. Since pitch angle control only operates in super-synchronous speeds (speed greater than synchronous speed), an anti-windup limiter sets β to zero for sub-synchronous speeds.

The electromechanical equation associated with the shaft of the turbine is given in (2.24).

$$\dot{\omega}_m = \frac{T_m - T_e}{2H_m} \tag{2.24}$$

where ω_m is the rotor speed, T_m is the mechanical torque, T_e is the electrical torque and H_m is the inertia of the rotor.

2.5.2 Doubly-fed induction generator

The most commonly used type of generator for wind power generation is a Doubly-Fed Induction Generator (DFIG). A grid connected to a DFIG involves a wound rotor induction machine and has terminals on both stator and rotor. However, with an induction machine, the rotor frequency is dependent on the operating slip of the machine. So, an AC/DC/AC converter is used to connect the rotor terminals to the grid. The AC/DC/AC converter enables variable speed operation and also enables the control of output real and reactive power. The machine stator and rotor voltages in terms of machine currents and rotor speed ω_m are given in (2.25) – (2.28) [55]. A schematic diagram of DFIG is shown

in Fig. 2.5. The bidirectional arrows signify that the power can flow in either direction depending on the mode of operation (sub-synchronous or super-synchronous).

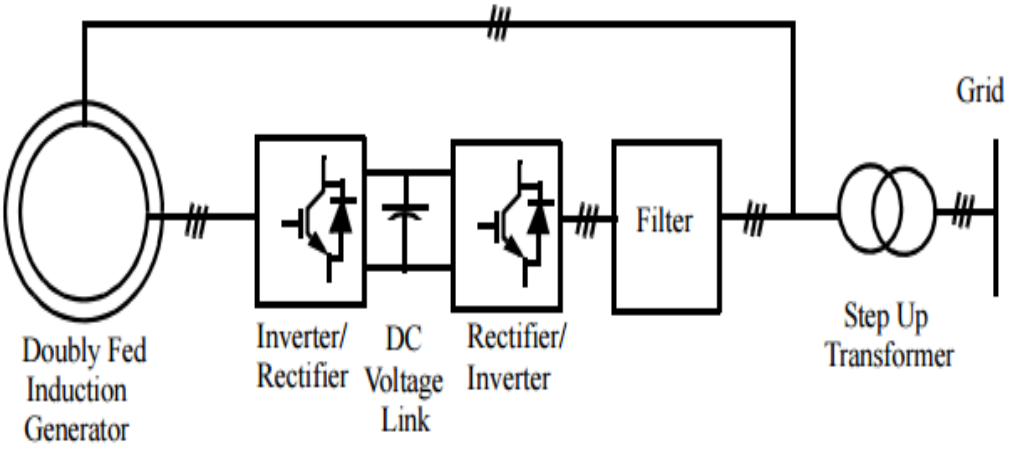

Figure 2.5 Schematic of a DFIG

$$v_{ds} = -r_s i_{ds} - \frac{d\lambda_{ds}}{dt} + \lambda_{qs} \tag{2.25}$$

$$v_{qs} = -r_s i_{qs} - \frac{d\lambda_{qs}}{dt} + \lambda_{qs} \tag{2.26}$$

$$v_{dr} = -r_r i_{dr} - \frac{d\lambda_{dr}}{dt} + (1 - \omega_m)\lambda_{qr} \tag{2.27}$$

$$v_{qr} = -r_r i_{qr} - \frac{d\lambda_{qr}}{dt} + (1 - \omega_m)\lambda_{dr} \tag{2.28}$$

where $i_{ds}, i_{qs}, i_{dr}, i_{qr}$ are the direct and quadrature axis stator and rotor currents, $v_{ds}, v_{qs}, v_{dr}, v_{qr}$ are the direct and quadrature axis stator and rotor voltages, $\lambda_{qs}, \lambda_{qr}, \lambda_{ds}, \lambda_{sr}$ are the stator and rotor direct and quadrature axis fluxes, r_s and r_r are

stator and rotor resistances. It has to be noted that the equations (2.25) – (2.28) are shown per unit.

The DFIG is represented as a constant power load for the purpose of dynamic simulation. This choice influences the update of bus voltages (algebraic variables) during dynamic simulations. For representing DFIG in dynamic studies, the transients associated with stator and rotor flux have been neglected. It is normal to neglect stator flux transients (even in synchronous machines) in fundamental frequency simulations since they are very fast to die out. The rotor flux transients are neglected because the current control loops of the voltage source converters counteract them. Therefore, the differential terms in equations (2.25) – (2.28) are set to zero. The electrical torque output of the machine in terms of stator and rotor currents is given in (2.29) [56].

$$\tau_e = x_m\left(i_{qr}i_{ds} - i_{dr}i_{qs}\right) \tag{2.29}$$

where x_m is the magnetizing reactance.

As mentioned previously, the dynamics associated with the voltage source converters (VSC) are quite fast, and thus the converter can be modeled as an ideal current source. The rotor direct and quadrature currents i_{dr} and i_{qr} form the state variables. The current i_{dr} is used to control the bus voltage (in other words reactive power injection), whereas i_{qr} is used for controlling the rotor speed. The dynamic equations associated with the VSC are given in (2.30) and (2.31).

$$i_{qr} = \frac{\left(\left(-\frac{x_s + x_m}{x_m v_{bus}}\right)\frac{P_m(\omega_m)}{\omega_m} i_{qr}\right)}{T_\epsilon} \tag{2.30}$$

$$i_{dr} = K_v\left(v_{bus} - v_{ref}\right) - \frac{v_{bus}}{x_m} - i_{dr} \tag{3.31}$$

where x_s is the stator reactance, v_{bus} is the voltage of the bus where the DFIG is connected, K_v is the voltage control gain, $P_m(\omega_m)$ is the power extracted from the wind as a function of the rotor speed, and T_ϵ is the power control time constant. Since, i_{qr} and i_{dr} cannot exceed certain physical limits, anti-windup limiters are used.

2.6 Small Signal Stability

Small signal stability is defined as the ability of the power system to maintain synchronism under small perturbations [1]. Small perturbations may occur in any part of the power system due to the daily changes in loads and generations. The first step in studying the small signal stability of any power system is to linearize it around an operating point since small disturbance is considered a small change in the system. Thus, a linear model can be made around this operating condition. The effect of small signal stability can be studied by applying small disturbances on the resulting model. Furthermore, there are different types of control theories that have been used to design a controller based on a linear model.

2.6.1 Linearized state space model of a power system

A large-scale power system consists of a large number of machines and each machine has its own controller. The components of a power system are represented by Differential

and Algebraic Equations (DAE), and some of the differential equations are nonlinear. Consequently, the first step in performing small signal analysis is to linearize the dynamic model of the interconnected power system. The set of differential and algebraic equations that represent the power system can be listed as given in (2.32a-c) [1, 2].

$$\dot{x} = f(x, x_a, u) \tag{2.32a}$$

$$0 = g(x, x_a, u) \tag{2.32b}$$

$$y = h(x, x_a, u) \tag{2.32c}$$

where x and x_a are the vectors of state and algebraic variables respectively, u and y represent the variables of input and output vectors, equation (2.32a) represents the power system dynamics. The power flow equation is described in (2.32b). Equation (2.32c) describes output in terms of state and input variables.

In small signal stability, the dynamic behavior of a power system is linearized around an equilibrium point where $\dot{x} = 0$. Then, the system can be analyzed around this point. The state space matrices (A, B, C and D) can be obtained based on the linearized model of the power system around the equilibrium point. The equilibrium point of a power system is obtained from the power flow results.

Two approaches exist that can determine state space matrices:

1) Using analytic Jacobian.
2) Using numerical differentiation for approximating the Jacobian.

In this work, the power system toolbox (PST) software package based on MATLAB is used. PST employs the second approach to obtain the state space matrices. The differential and algebraic equations are solved in PST successively. The modified Euler's method, which is also known as the predictor and corrector method, is used to calculate and update the state and algebraic variables. This approach has two steps: the first one applies a small change to the variables (x and u) and the changes are ($\Delta x \; and \; \Delta u$). In the second step, the change in the nonlinear function f in equation (2.32a) are ($\frac{\partial f}{\partial x}$) and ($\frac{\partial f}{\partial u}$), which produces the matrices *A* and *B.* A similar approach is used to calculate matrix *C*. In the transfer function that represents the power system components, the order of the numerator is less than or equal to the order of the denominator, so the *D* matrix is composed of zeros. Thus, the power system can be represented by the state space form as given in (2.33).

$$\dot{x} = Ax + Bu$$

$$y = Cx \tag{2.33}$$

For small disturbance resulting in small change in (($\Delta x \; and \; \Delta u$), the system equations can be written in a linearized form as given in (2.34).

$$\Delta\dot{x} = A\Delta x + B\Delta u$$

$$\Delta y = C\Delta x \tag{2.34}$$

where

$A = \left[\frac{\partial f}{\partial x}\right]$, $B = \left[\frac{\partial f}{\partial u}\right]$ and C= $\left[\frac{\partial g}{\partial x}\right]$

Note that *A* is the state matrix, *B* is the input matrix and *C* is the output matrix.

The matrix *A* provides important information about the system behavior. It can be shown that the closed loop poles of the system represented by these matrices are the roots of the characteristic equation:

$$det(A - \lambda I) = 0 \tag{2.35}$$

These roots are called Eigenvalues $\lambda(\lambda = \lambda_1, \lambda_2, \ldots\ldots, \lambda_n)$ of the state matrix *A*. Eigenvalues are very important in analyzing power system dynamics; they indicate how much the system is close to or far from the stability limit. Eigenvalues can be obtained by solving equation (2.35). By looking at the Eigenvalues $\lambda_i = \alpha_i \pm j\omega_i$, in which numbers can be real or complex, a full picture of small signal stability can be gained.

Properties of Eigenvalues

1- The system is said to be stable if all the real parts of the Eigenvalues have a negative sign (α_i).

2- The system is said to be unstable if all the real parts of the Eigenvalues have a positive sign.

3- The system becomes marginally stable if all the real parts of the Eigenvalues have a negative sign except one that has only an imaginary part ($\pm j\omega$), and the system in this case will be in oscillatory mode.

There are two important parameters for analyzing the small signal stability of the oscillatory mode: its damping (ξ_i) and frequency (f_i), which can be given as:

$$\xi_i = \frac{-\alpha_i}{\sqrt{\alpha_i^2 + \omega_i^2}} \tag{2.36}$$

$$f_i = \frac{\omega_i}{2\pi}$$

Two Eigenvectors—"Right Eigenvector (REV) and Left Eigenvector (LEV)" —are associated with each Eigenvalue, as described in equation (2.37).

$$A\Phi_i = \lambda_i \Phi_i$$

$$\Psi_i A = \lambda_i \Psi_i \tag{2.37}$$

where Φ_i and Ψ_i are the vectors of the right and left Eigenvectors respectively as shown below:

$$\Phi_i = [\Phi_1\ \Phi_2 \dots \dots . \Phi_n]$$

$$\Psi_i = [\Psi_1\ \Psi_2 \dots \dots . \Psi_n]^T$$

Φ and Ψ are orthogonal matrices.

The parameters of REV define the existence of the mode in different state variables, while LEV indicates the excitation of the mode when it is perturbed. Based on these two vectors, the participation factor is defined. The matrix of the participation factor P is shown in (2.38).

$$P = [P_1, P_2, \dots\dots, P_n] \tag{2.38}$$

The participation of an i^{th} mode in K^{th} states can be given in (2.39)

$$P_{ki} = \Phi_{ki}\Psi_{ki} \tag{2.39}$$

2.6.2 Power system oscillations

The power system is considered a complex system, and it has different modes of oscillations. These modes can be classified as:

- Local modes of oscillation: these occur when a synchronous machine located in a power system plant oscillates with respect to the rest of the system, and the frequency range of these oscillations lies between (1.0 to 2.0).
- Inter-area modes of oscillation: this phenomenon involves a group of generators in one area swinging against another group of generators in the neighboring area connected by a weak tie line. The frequency of these oscillations ranges between (0.2 to 1.0).
- The control modes of oscillation: these oscillations are mainly associated with generators and poorly tuned voltage regulators, turbine governors, SVC controls and HVDC converters.

2.6.3 Inter-area oscillations

The work of this dissertation focuses on damping inter-area oscillations. Damping of inter-area oscillations is one of the main challenges in maximizing the tie-line power transfer in power systems. These oscillations are the outcome of weakly interconnected power systems. The inter-area oscillations become worse as the power system becomes stressed. Recently, Flexible AC Transmission System (FACTS) devices have been used in power systems to control the bus voltages and tie-line power. They can also damp power system oscillations and improve system stability by providing a supplementary control signal to the reference value of these devices. Large-scale integration of renewable resources in a modern power system has added extra uncertainty to the power system. As a result of this variability, it becomes necessary for the damping controllers to be robust.

2.7 Static VAR Compensator (SVC)

The Static VAR Compensator (SVC) is a shunt FACTS device; it is mainly used to maintain the bus voltage by varying its injected reactive power. Fig. 2.6 shows a basic circuit of SVC, which consists of a fixed series capacitor bank, *C*, connected in parallel with a thyristor-controlled reactor, *L*. By sensing the bus voltage and providing a firing pulse signal to the thyristor, the reactance *L* can be controlled. Consequently, the whole admittance of SVC will vary and provide reactive power support accordingly.

The injected reactive power (*Q*) of SVC connected to the bus *j* in the power system as shown in Fig 2.6 can be written as:

$$Q_j = V_j^2 B_{svc} \tag{2.40}$$

where $B_{svc} = B_C - B_L$ and B_C is the susceptance of the fixed capacitor and B_L is the susceptance of the thyristor controlled reactor.

The block diagram of the dynamic model of an SVC is given in Fig 2.7.

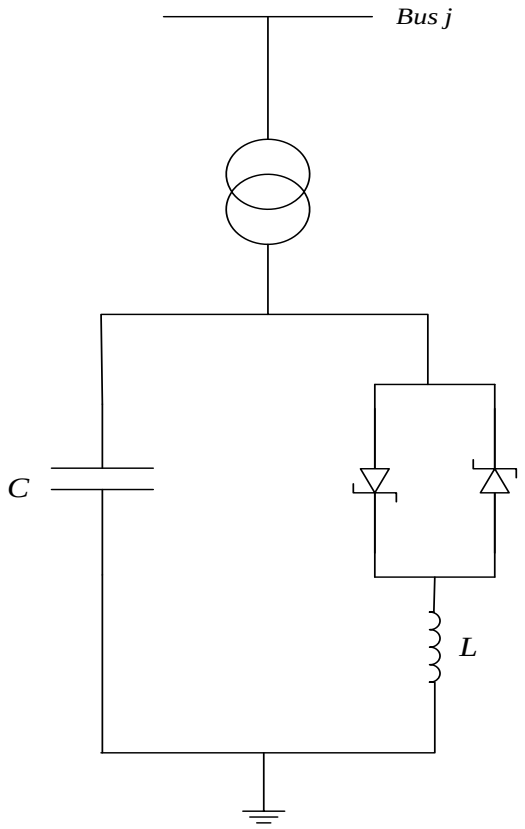

Figure 2.6 The SVC circuit

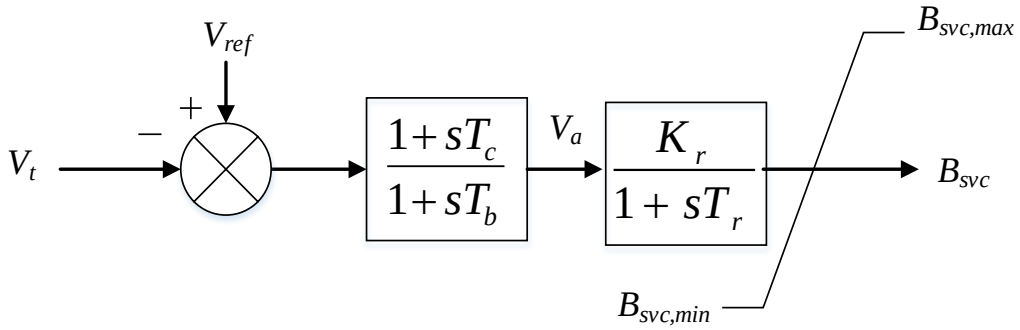

Figure 2.7 Block diagram of the dynamic model of an SVC

The differential equation associated with the SVC can be given as:

$$\dot{B}_{svc} = \frac{1}{T_r}(K_r V_a - B_{svc}) \tag{2.41}$$

$$\dot{V}_a = \frac{1}{T_b}\left(\left(1 - \frac{T_c}{T_b}\right)(V_{ref} - V_t) - V_a\right) \tag{2.42}$$

CHAPTER THREE

H_∞ ROBUST CONTROLLER DESIGN

This chapter introduces a multi-model approach to designing a robust supplementary damping controller. The designed fixed-order supplementary damping controller adjusts the voltage reference set point of SVC. There are two main objectives of the controller design, which are: damping low-frequency oscillations and enhancing power system stability. The proposed H_∞ approach is based on shaping the closed-loop sensitivity functions in the Nyquist diagram through constraints on their infinity norm. The H_∞ constraints are linearized with the help of a desired open-loop transfer function. The controller is designed using convex optimization techniques in which the difference between the open-loop transfer function and the desired transfer function is minimized. Convexity of the problem formulation ensures global optimum. One of the advantages of the proposed approach is the consideration of multi-model uncertainty. Also, in contrast to the methods that have been studied in literature, the proposed approach deals with a full-order model (i.e., model reduction is not required) with lower controller order. The proposed approach is compared with recent existing techniques to design a robust controller that is based on H_2 under pole placement. Both techniques are applied to the 68 bus system to evaluate and validate the robust controller performance under different load scenarios and different wind generations.

3.1 Class of models and controllers

The primary purpose of this chapter is to introduce and design a linearly parameterized robust controller. To demonstrate the capability of the proposed method and controller, it is used to damp out inter-area oscillations. Consider a linearly parameterized controller of the form given in (3.1) [51, 57-60]:

$$K(s) = \rho^T \varphi(s) \tag{3.1}$$

where $\rho = [\rho_1\ \rho_2\ \ldots.\ \rho_n]$

$$\varphi(s) = [\varphi_0(s)\ \varphi_1(s)\ \ldots\ldots\ \varphi_{n-1}(s)]^T$$

where *n* is the number of controller parameters, ρ_i is the controller parameters and $\varphi_i(s)$ is a basis function. For example, the controller parameters of the Proportional Integral Derivative (PID) controller are $[\rho_1\ \rho_2\ \rho_3] = [K_p\ K_i\ K_d]$ and $[\varphi_1(s)\ \varphi_2(s)\ \varphi_3(s)]^T = \left[1\ \frac{1}{s}\ \frac{s}{1+Ts}\right]^T$. The Laguerre function is a commonly used basis function and is given in (3.2) [58].

$$\varphi_0(s) = 1, \varphi_i(s) = \frac{\sqrt{2\zeta}(s-\zeta)^{i-1}}{(s+\zeta)^i}\ \ i \geq 1, \qquad \zeta > 0 \tag{3.2}$$

where $\zeta > 0$ is the Laguerre parameter. It can be shown that for any finite order transfer function *F(s)*, arbitrary Laguerre parameter $\zeta > 0$ and an arbitrary constant $\varepsilon > 0$, there exists a finite *n* such that

$$\|F(s) - \rho^T \varphi(s)\|_p < \varepsilon \quad for\ 0 < p < infinity \tag{3.3}$$

The controller parameterization presented in (3.1) obtains a good approximation of any finite order stable transfer function with a desired level of accuracy by varying the parameter *n*. The result of the optimization problem given in (3.3) is dependent on the difference between the poles of *F(s)* and ζ. A better approximation of any finite order stable transfer function can be obtained for a given controller order if the choice of ζ is proper. More details for optimal selection of the basis function can be found in [58, 60].

The reason behind using the linearly parameterized controller is that all points on the Nyquist diagram of the open-loop transfer function $L(j\omega, \rho)$ can be written as a linear function of the controller parameters ρ as given in (3.4). This property helps in obtaining a convex parameterization of the loop-shaping fixed-order controller.

$$L(j\omega, \rho) = K(j\omega, \rho)G(j\omega) = \rho^T \varphi(j\omega)G(j\omega)$$

$$= \rho^T \mathcal{R}(\omega) + j\rho^T \mathcal{I}(\omega) \tag{3.4}$$

where $\mathcal{R}(\omega)$ and $\mathcal{I}(\omega)$ are respectively the real and imaginary parts of $\varphi(j\omega)G(j\omega)$.

In case of a single model, *G* is a scalar function, whereas for a multi-model controller design $\mathcal{G} = \{G_i(j\omega), i = 1, \ldots, m\}$ is defined as $G_i(j\omega)$ representing the i-th model in the

multi-model uncertainty set. In this case, $L_i(j\omega)$ is the open-loop transfer function for the i-th model.

3.2 H_∞ Robust Constraints

3.2.1 Uncertainty and Robustness Representation

3.2.1.1 Multiplicative uncertainty

Multiplicative uncertainty is represented in (3.5). Suppose that $G_0(j\omega)$ is the normal plant frequency response, and the actual plant that describes the normal plant with uncertainty is $G(j\omega)$, as shown in Fig. 3.1 and (3.5) [61, 62].

$$G(s) = G_0(s)\big(1 + W_2(s)\Delta(s)\big) \tag{3.5}$$

where $\Delta(s)$ is an unknown stable transfer function with $\|\Delta\|_\infty < 1$.

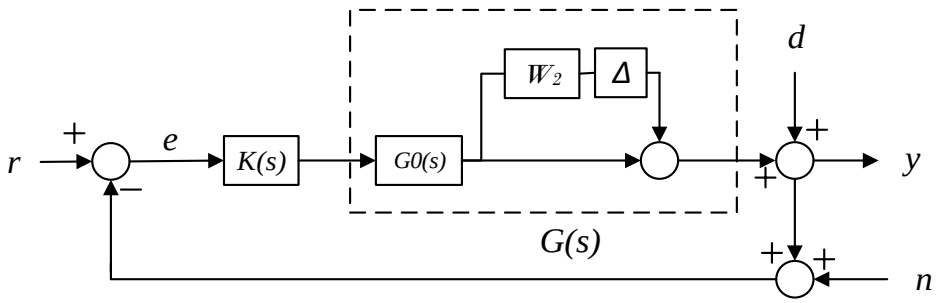

Figure 3.1 Block diagram representing an uncertain feedback system

3.2.2 Robust Stability and Performance

The closed-loop system in Fig. 3.1 can be represented by equation (3.6) as:

$$y = \frac{K(s)G(s)}{1 + K(s)G(s)}(r - n) + \frac{1}{1 + K(s)G(s)}d \tag{3.6}$$

The open-loop transfer function is $L(j\omega) = K(j\omega)G(j\omega)$, the complementary sensitivity function is $T(j\omega) = L(j\omega)/[1 + L(j\omega)]$ and the sensitivity function is $S(j\omega) = 1/[1 + L(j\omega)]$ be defined. It can be seen from (3.6) that $T(j\omega)$ defines the relationship between the reference and the output signals and $S(j\omega)$ defines the relationship between the reference and the error. These transfer functions define the main characteristic of the closed-loop architecture.

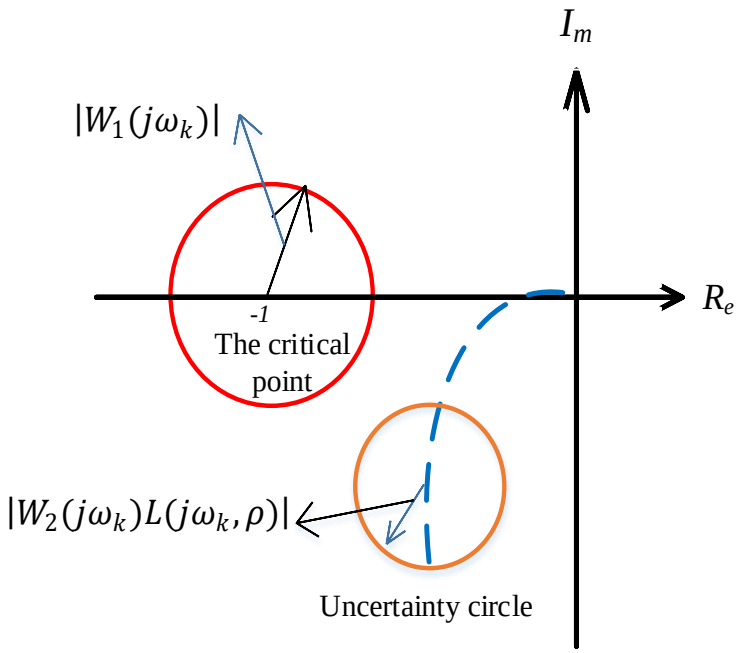

Figure 3.2 Nyquist plot

The Nyquist diagram has been used to derive the criteria of robust performance as well as robust stability. The point $(-1 + j0)$ on the Nyquist plot as shown in Fig. 3.2 is known

as the critical point used to study the closed-loop system stability. The circle centered at the critical point $(-1 + j0)$ with radius $W_1(j\omega)$ is known as the performance disc. The uncertainty disc is represented by the circle with radius $W_2(j\omega)L(j\omega, \rho)$.

Graphically, robust stability is achieved if, and only if, the uncertainty disc centered at the original open-loop transfer function with radius $W_2(j\omega)L(j\omega, \rho)$ does not intersect with the other circle centered at the critical point $(-1 + j0)$ with radius $W_1(j\omega)$ on the Nyquist plot. The absolute value of $|1 + L(j\omega, \rho)|$ defines the distance between the center of the critical point and the center of the uncertainty disc. For robust stability, the radius $W_2(j\omega)L(j\omega, \rho)$ of the uncertainty circle has to be less than the distance $|1 + L(j\omega, \rho)|$ at all frequencies. In other words, $|W_2(j\omega)L(j\omega)| < |1 + L(j\omega, \rho)|$ for all ω. Dividing both sides of this equation by $|1 + L(j\omega, \rho)|$ and knowing the fact $T(j\omega) = L(j\omega)/[1 + L(j\omega)]$ results in:

$$|W_2(j\omega)T(j\omega)| < 1 \qquad \forall\omega \tag{3.7}$$

The normal performance condition of a stable system can be given in the following standard form:

$$|W_1(j\omega)S(j\omega)| < 1 \qquad \forall\omega \tag{3.8}$$

To define the condition of the robust performance of the system given in Fig 3.2, substitute (3.5) with (3.8), as given in (3.9)

$$|W_1 S| = \left|\frac{W_1}{1+(1+\Delta)L}\right| = \left|\frac{W_1 S}{1+\Delta T}\right| < \left|\frac{W_1 S}{1-W_2 T}\right| \tag{3.9}$$

Since $|W_1 S| < 1$, then $\left|\frac{W_1 S}{1-W_2 T}\right| < 1$ from equation (3.9), and this constraint is required for the robust performance. By rearranging this constraint, the result is the standard form of the robust performance, which is given in (3.10).

$$|W_1(j\omega)S(j\omega)| + |W_2(j\omega)T(j\omega)| < 1 \; \forall\omega \tag{3.10}$$

3.3 The proposed approach

The constraints in (3.10) satisfy the robust stability as well as robust performance. The main idea here is to represent these constraints in the Nyquist plot. Then robustness can be achieved by a set of convex constraints on the frequency domain. Now the controller can be designed based on convex optimization, and the solution is to reduce the norm of the distance between the actual $L_i(j\omega_k, \rho)$ and desired $L_d(j\omega_k)$ open-loop transfer function as shown in Fig. 3.1.

Multiplying (3.10) by $|1 + L(j\omega, \rho)|$, one finds:

$$|W_1(j\omega)| + |W_2(j\omega)L(j\omega, \rho)| < |1 + L(j\omega, \rho)| \quad \forall\omega \tag{3.11}$$

The constraints in (3.11) are non-convex, and $L_d(j\omega_k)$ is used to linearize these constraints. Making the problem convex ensures that global optimality can be achieved. Now, line d as shown in Fig. 3.3 is introduced, which is tangent to the performance disc centered at $(-1 + j0)$ and orthogonal to the line that links the center of the performance

disc to $L_d(j\omega_k)$. A sufficient condition for constraints in (3.11) is that the circle centered at the actual open-loop transfer function $L_i(j\omega_k, \rho)$ has to be on the right side of line d for all frequencies as shown in Fig 3.3.

Note that line d is a straight line in the complex plane and can be represented by an infinite number of points. Each point in the complex plane has a real part x and imaginary part y. The equation of the straight line d is a function of $L_d(j\omega_k)$ and W_1 and it can be written at each point as:

$$Line\ d:\ \ y = tan(\alpha)\left[x - \frac{|W_1|}{\sin(\alpha)} + 1\right] \tag{3.12}$$

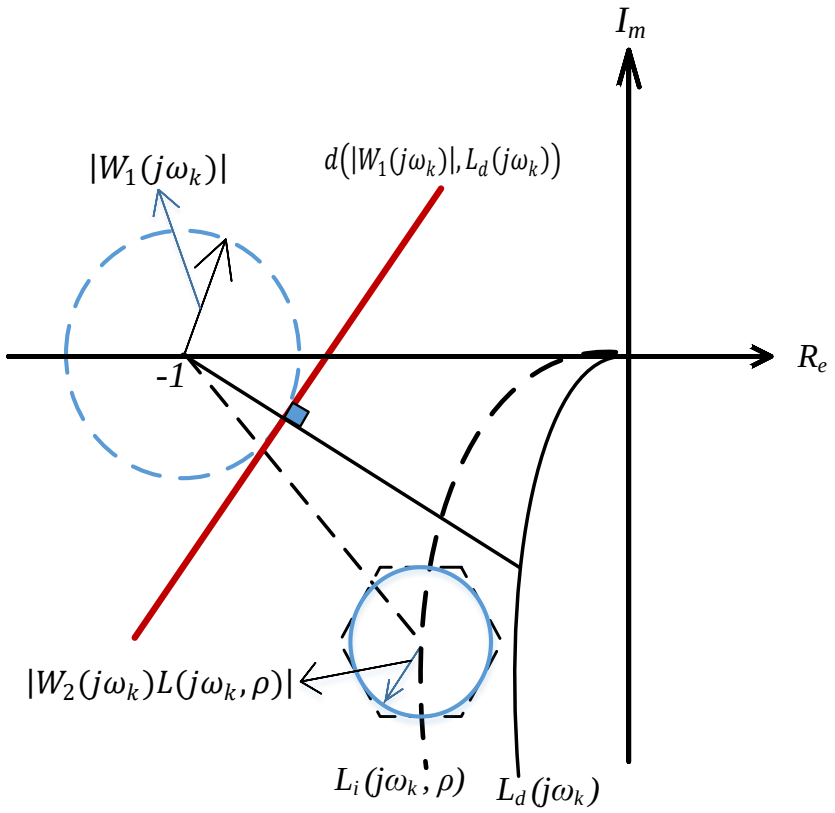

Figure 3.3 Linear constraints on Nyquist plot

where $\sin(\alpha)$ and $\cos(\alpha)$ are:

$$\sin(\alpha) = \frac{R_e\{1 + L_d(j\omega_k)\}}{|1 + L_d(j\omega_k)|}, \quad \cos(\alpha) = -\frac{I_m\{1 + L_d(j\omega_k)\}}{|1 + L_d(j\omega_k)|}$$

By substituting $\sin(\alpha)$ and $\cos(\alpha)$ into the equation (3.12), the result is:

$$|W_1(j\omega_k)[1 + L_d(j\omega_k)]| - I_m\{L_d(j\omega_k)\}y - [1 + R_e\{L_d(j\omega_k)\}][1 + x] = 0 \qquad (3.13)$$

Now, the linear constraints of line *d* that exclude the performance disc are given in (3.14) as:

$$|W_1(j\omega_k)[1 + L_d(j\omega_k)]| - I_m\{L_d(j\omega_k)\}I_m\{L(j\omega_k, \rho)\} - [1 + R_e\{L_d(j\omega_k)\}][1 + R_e\{L(j\omega_k, \rho)\}] < 0 \ \forall\omega \qquad (3.14)$$

The linear constraints in (3.10) can be simplified using the following facts:

$$R_e\{L_d(j\omega_k)\} = 1/2[L_d(j\omega_k) + L_d^*(j\omega_k)]$$

and $$I_m\{L_d(j\omega_k)\} = 1/2[L_d(j\omega_k) - L_d^*(j\omega_k)]$$

The constraints in (3.14) become:

$$|W_1(j\omega_k)[1 + L_d(j\omega_k)]| - R_e\{[1 + L_d^*(j\omega_k)][1 + L(j\omega_k, \rho)]\} < 0 \ \ \forall\omega \qquad (3.15)$$

where $L_d^*(j\omega_k)$ is the complex conjugate of $L_d(j\omega_k)$.

To satisfy the condition in (3.15) for a set of uncertainty models, the circle centered at $L_i(j\omega_k, \rho)$ should be approximated by a polygon with $v > 2$ vertices. To satisfy the

robust uncertainty in (3.10), all the vertices of the polygon located at the uncertainty disc have to be on the right side of line d. This condition can be represented by the linear constraints as shown in equation (3.16) [57]:

$$|W_1(j\omega_k)[1 + L_d(j\omega_k)]| - R_e\{[1 + L_d^*(j\omega_k)][1 + L_i(j\omega_k, \rho)]\} < 0 \ \ \forall\omega \qquad (3.16)$$

where $L_i(j\omega_k, \rho) = K(j\omega_k, \rho)G_i(j\omega)$, and

$$G_i(j\omega) = G(j\omega)\left[1 + \frac{|W_2(j\omega_k)|}{\cos(\pi/v)} e^{-2j\pi i/v}\right] \qquad (3.17)$$

It is observed that the number of linear constraints is multiplied by *v*.

Another way to satisfy the robust condition in (3.11) is to increase the radius of the circle $|W_2(j\omega)L(j\omega, \rho)|$, an increase that leads to the following convex constraints:

$$|W_1(j\omega_k)[1 + L_d(j\omega_k)]| + |W_2(j\omega)L(j\omega, \rho)|[1 + L_d(j\omega_k)] - R_e\{[1 + L_d^*(j\omega_k)][1 + L_i(j\omega_k, \rho)]\} < 0 \ \ \forall\omega \qquad (3.18)$$

Considering all of these examinations, the quadratic optimization problem can be expressed as given in (3.19).

$$\min_{\rho} \sum_{i=1}^{m} \sum_{k=1}^{N_i} |L_i(j\omega_k, \rho) - L_d(j\omega_k)|^2 \qquad (3.19)$$

Subject to:

$$|W_1(j\omega_k)[1 + L_d(j\omega_k)]| + |W_2(j\omega)L(j\omega, \rho)|[1 + L_d(j\omega_k)] - R_e\{[1 + L_d^*(j\omega_k)][1 + L_i(j\omega_k, \rho)]\} < 0 \ \ \forall\omega$$

$for\ k = 1, \ldots\ldots, N_i\ (No.of\ frequencies), \qquad i = 1 \ldots, m.$

where $L_i(j\omega_k, \rho) = \rho^T\ \varphi(j\omega_k) G_i(j\omega_k)$

For multi-model uncertainty cases, the constraints in (3.18) can be repeated for all the plant models $G_i(j\omega)$ for $i = 1\ldots,m$. The constraints in (3.18) still can be used if the uncertainty weighting filters W_1, W_2 and the desired open-loop tansfer function L_{di} are different for each plant model, since these constraints are convex with respect to $G_i(j\omega)$ for multi-model uncertainty.

3.4 IEEE 68 Bus Test System and SVC Model

3.4.1 Test System

The IEEE 16 machines, 68 bus system is used in this study. This test system is particularly suited for small signal stability studies. For instance, reference [2] uses the same test system for damping inter-area modes. There are five distinct areas in the test system with a total load of 18.23 GW. Areas NETS and NYPS are interconnected through two parallel tie-lines. Fig. 3.4 shows the single line diagram of the test system. Parameters of the generators, exciters, governors, and transmission lines of the test system can be found in [2].

Power System Toolbox (PST) is used to simulate the test system, including the SVC and doubly-fed induction generator (DFIG) [63]. The controller was implemented in MATLAB based on the proposed approach and has been integrated in PST.

In order to include renewable generation, a 500MW wind farm is placed in area 2 at bus 39 as presented in Fig. 3.4. The wind farm is installed to add more variability to the system due to the continuous change of the output power of the wind farm. A 3rd-order model of a DFIG is used [64]. The dynamic model of the DFIG contains a set of differential algebraic equations that has been integrated in PST. A single model of DFIG is used to represent the wind farm.

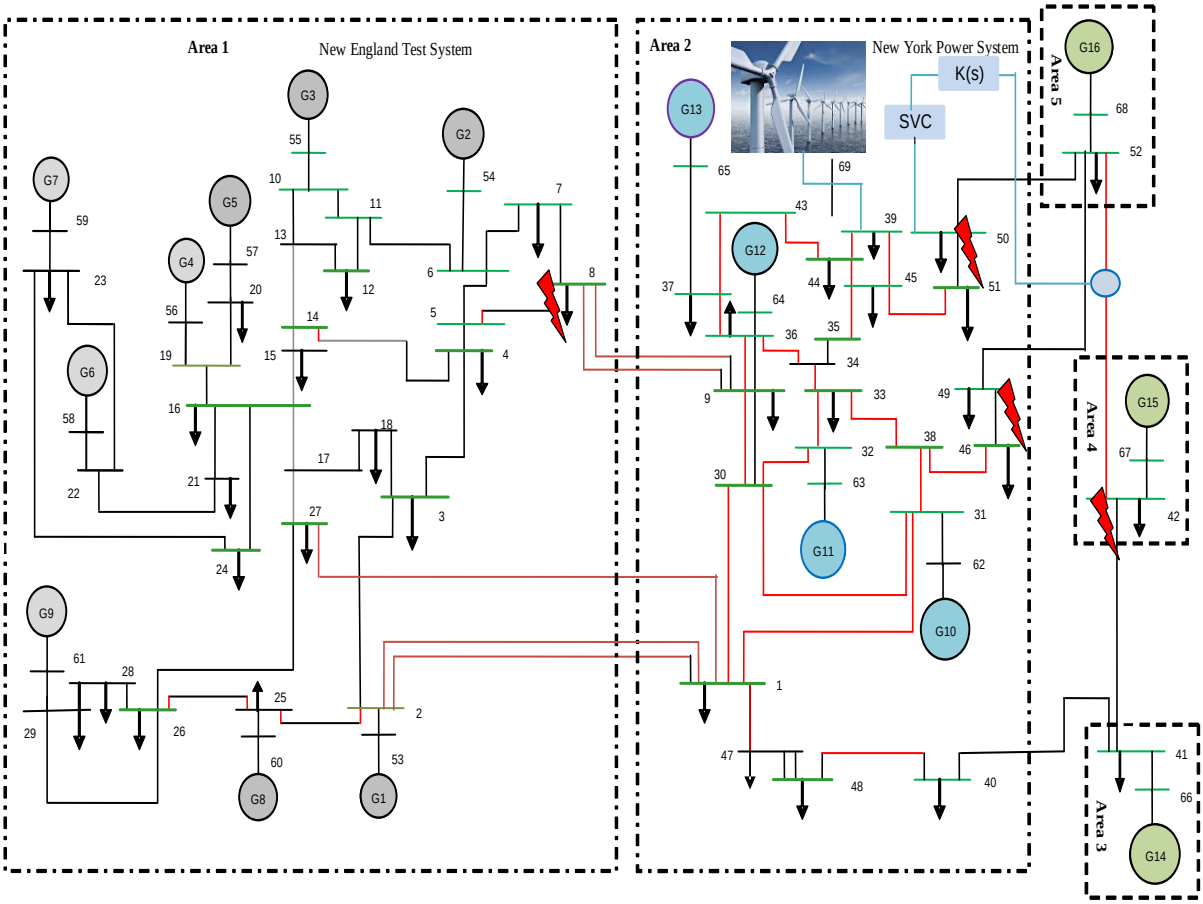

Figure 3.4 Single line diagram of the 68 bus test system

3.4.2 Static Var Compensator

The block diagram of SVC is shown in Fig. 3.5 (a). The test system has an SVC installed at bus 50. The parameters of SVC are given in Table 3.1. The objective of designing the controller is to damp tie-line oscillations by providing additional signal to the set point of the SVC. The control structure of the proposed approach is represented as shown in Fig. 3.5 (b).

Table 3.1 SVC Parameters

B_{svcmax}	B_{svcmin}	K_r	T_r	T_c	T_b
$1pu$	$1pu$	10	$0.05sec$	$0.6sec$	$0.2sec$

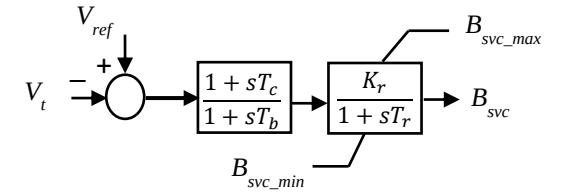

(a)

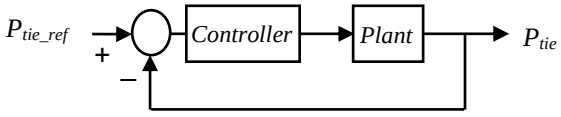

(b)

Figure 3.5 Block diagram of (a) SVC and (b) control representation

3.5 Controller Design Procedure

In this section, the step by step procedure and rationale used in designing the controller are described in detail.

3.5.1 Selecting Inter-Area Modes

For the given test system, under nominal operating condition, two Eigenvalue pairs have damping of less than 5%. In fact, one of the Eigenvalue pairs has damping very close to zero; hence, the system is close to the instability point.

Table 3.2 Eigenvalues, Damping Ratios and Frequencies of the Inter-Area Modes of the Test System

Eigenvalue $\sigma \pm j\omega$	**Damping ratio** $-\frac{\sigma}{\sqrt{\sigma^2+\omega^2}}$	**Frequency (*Hz*)** $\frac{\omega}{2\pi}$
$-0.04052 \pm 3.410j$	0.01188	0.5427
$-0.1539 \pm 4.948j$	0.03108	0.7875

Based on the Eigenvalues for nominal operating point, the inter-area modes that need to be damped for the case study are listed in Table 3.2. Fig.3.6 shows the damping ratios for frequencies of interest corresponding to the nominal operating condition.

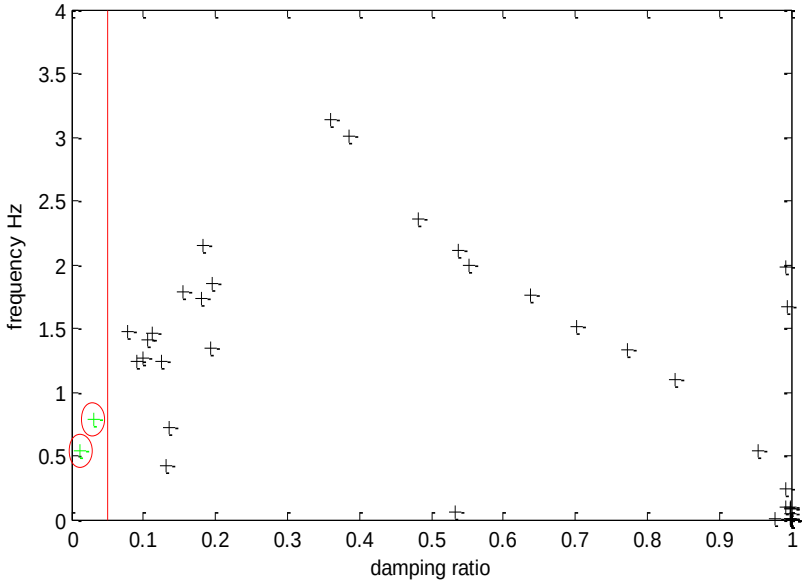

Figure 3.6 Damping ratios and frequencies of Eigenvalues for OP1, normal operating point

3.5.2 Selecting Input/Output Signal

Appropriate selection of the input signal for the designed controller is highly essential to guarantee that the inter-area Eigenvalues are controllable and observable. To this end, controllability metric is used to choose the most effective input signal to damp the inter-area modes. Controllability metric is defined as the amount of displacement that a pole would undergo due to small change in the feedback gain; this condition is given in (3.20) [65]. Using controllability metric as shown in Fig. 3.7, the active power flow of the line 42 to 52 is found as the most controllable measurement to damp the inter-area modes. Therefore, the input signal that feeds the controller is provided from the tie-line (42 to 52), which connects the areas 4 and 5. The controller output is used as an additional control signal to the SVC.

$$\Delta\lambda_i = u_i B \Delta K C v_i \rightarrow \frac{\|\Delta\lambda_i\|}{\|\Delta K\|} \leq \|u_i B\| * \|C v_i\| \tag{3.20}$$

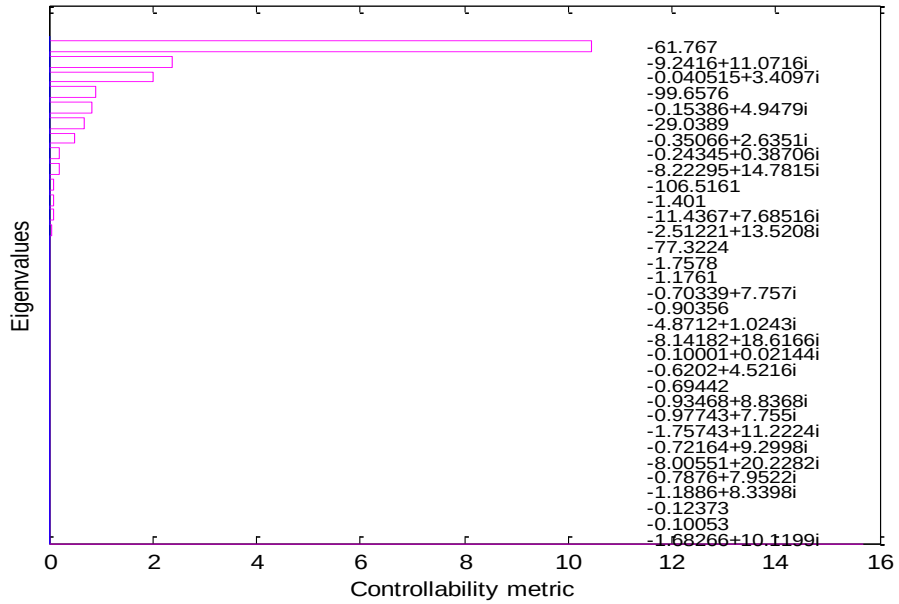

Figure 3.7 Controllability indices of controllable Eigenvalues based on selecting the line 42 to 52

3.5.3 Choice of Operating Points

A power system is a non-stationary system in which a set of new dispatches are computed every five to fifteen minutes. As a result, the total number of possible operating points are innumerable; hence, six different operating points that represent several stress levels of the system are used for controller design and validation. Stress levels of the system in this context are quantified using Eigen-spectrum. Eigenvalues convey two very important attributes: oscillation frequencies and their corresponding damping ratio. Damping ratio illustrates how much energy is dissipated during each cycle for a given frequency.

Thus, six different operating points are created whereby the damping ratio of the Eigenvalues that correspond to inter-area modes of the system are progressively made worse.

Table 3.3. Different Operating Points for 68 Bus System

OP #	**Gen 15**	**Gen 16**	**Wind generation**
1	5	40	5*(Normal model)*
2	*7*	*38*	*5*
3	5	43	2
4*	5	44	1
5*	5	42	3
6*	7	40	3

*It is not used in the control design but is used to validate the controller.

The system has been extensively studied, and these operating points listed in Table 3.3 are considered for this study as they greatly affect the inter-area modes. The generators G_{15} and G_{16} are adjusted to obtain different operating points. In addition, wind generation is also varied between different operating points. All the values in Table 3.3 are in per-unit system.

3.5.4 Desired Open-Loop Transfer Function (L_d)

Selecting L_d is based on design specifications. L_d normally has a high amplitude in low frequencies for reliable tracking, and that means the system follows the reference signal. At high frequencies, L_d should have small amplitude to provide robustness and

noise rejection characteristics. $L_d(s)$ could be chosen as ω_c/s where ω_c is the desired closed-loop bandwidth [51, 57]. Typically, the bandwidth is the range of frequencies for which the gain is significant. Generally high bandwidth is needed to obtain faster response. In the case study, the aim is to damp the inter-area modes in the range of frequencies (0.2-1.0 Hz), so a bandwidth of more than $2\pi f = 2\pi * 1.0 = 6.28\ rad/sec$ is needed. The desired bandwidth ω_c should be more than $6.28\ rad/sec$. For the case study, the resonance mode around ω_1 and ω_2 as shown in Fig. 3.8 is a strong one, and these modes should be cancelled by the controller. So ω_c is selected to be $\omega_c = 9$, which means ($L_{d0} = 9/s$).

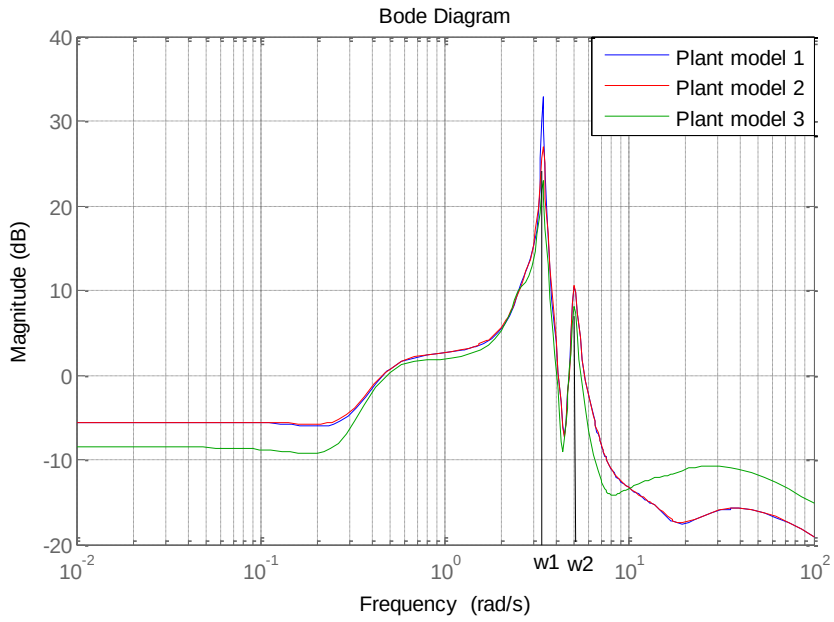

Figure 3.8 Frequency response of the three selected plant models

3.5.5 Weighting Filters (W_1 and W_2)

Selection of W_1 and W_2 are essential for the controller design. In this research, W_1 is designed as a first-order low-pass filter to gain a valid disturbance rejection. W_2 is designed as a high-pass filter to guarantee robustness and minimize the controller effort in high frequencies [2].

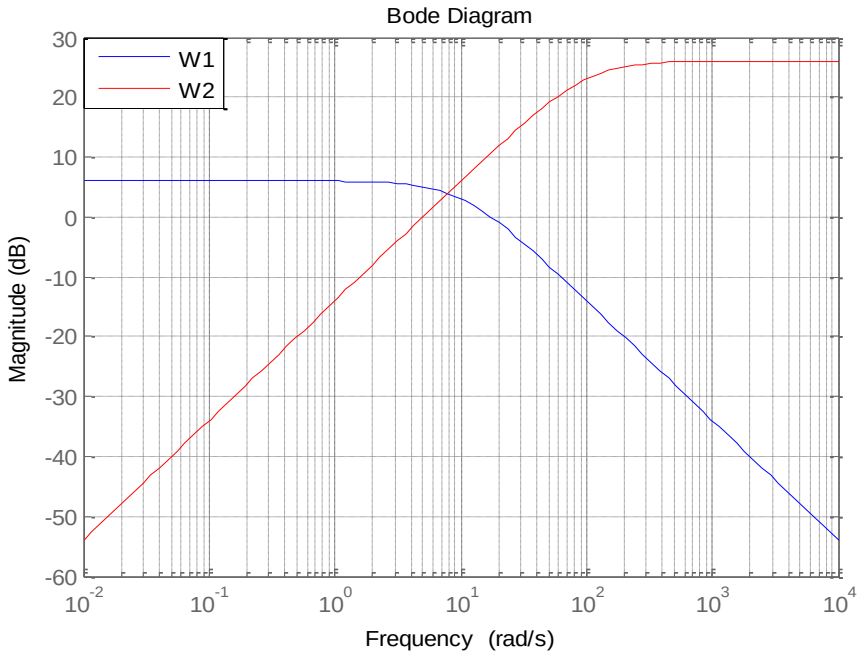

Figure 3.9 Frequency response of the weighting filters

Frequency response of W_1 and W_2 is shown in Fig. 3.9.

$$W_1(s) = \frac{20}{s+10} \qquad W_2(s) = \frac{20s}{s+100} \tag{3.21}$$

3.5.6 Solving the Optimization Problem

The convex quadratic programing problem described by (3.19) is solved to obtain $K_0(s)$. Since the problem is convex, global optimality is guaranteed. Using the relation $L_{di} = K_0 G_i \ , i = 1,2,3,$ the desired open-loop transfer function is computed for operating points OP_1 to OP_3. The three computed L_d with the three models are used to design the final controller $K(s)$ by solving the optimization problem in (3.19). The final controller $K(s)$ is given in (3.22).

$$K(s) = \frac{-43.095(s + 17.13)(s + 0.07859)(s^2 + 0.7662s + 6.429)}{(s + 9)^4} \qquad (3.22)$$

3.6 H_2 Controller under Pole Placement

For comparison, a damping controller is designed using pole placement and H_2 optimization following two steps based on matrices described in [11]. First, a state-feedback controller is developed that uses the system states to generate a control signal. This condition is achieved by solving a set of Linear Matrix Inequalities (LMIs) that places the system poles into a cone area in the complex plane, while minimizing the amplitude of control signal represented by its H_2 norm. Thereafter, a state estimator is developed that constructs system states from the output. A similar set of LMIs is employed for this purpose. The controller can be obtained by a transfer function equivalence of the state-feedback controller and the state estimator combined. This approach considers multi-model so the controller is designed based on different load conditions. However, this approach still suffers from the drawbacks (1 and 2) listed in section 1. For the case study, the damping ratio is set to be 10% as the boundary of the

pole placement region. Also, the weighting filters are selected to be the same as those used in the proposed approach. The same operating points listed in Table 3.3 are used to design the controller using this approach. The plant/system model needs to be reduced based on this approach in such a way that the response of the reduced system is similar to that of the original system in the frequency range of interest. The test system consists of 190 states, including the DFIG and the SVC. For the frequency range of interest, the plant model can be reduced to at least 7th order. In addition, the total order of the controller based on [2] is equal to the order of the reduced system plus the order of weighting filters. In this case, this sum equates to a controller order of 7+2, i.e. 9 states. Fig. 3.10 shows the original and the reduced plant model; it can be seen that they are identical in the frequency range of interest. However, no model order reduction is required for the proposed method. Yet, using the proposed approach, a 4th-order controller is designed that replicates the frequencies of interest. This approach is applied to design a robust controller to compare it with the proposed method. Interested readers are referred to [11] for more details.

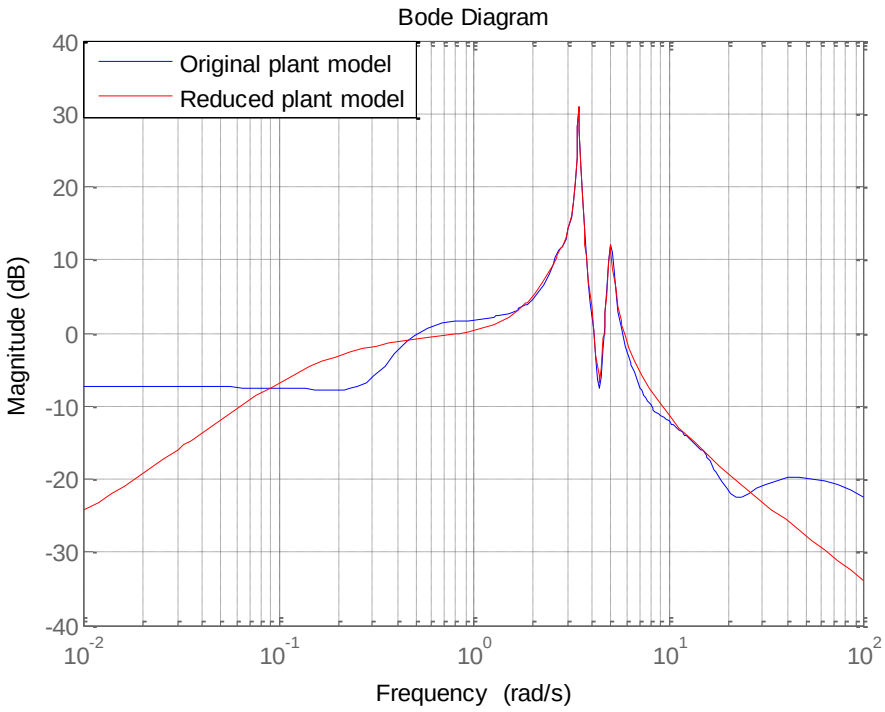

Figure 3.10 Frequency response of the original and the reduced system, OP1

3.7 Results and Discussion

In this section, two parts of validation of the proposed approach are presented. Comparisons of the proposed method, both numerical and time-domain based, with the base case with only SVC are presented. In the first part of validation, Eigenvalue spectrums obtained using the different methods are compared. Specifically, comparisons for damping ratios are drawn for different modes of interest.

In the second part, time-domain performance results are presented. Comparing controllers that have user defined parameters is not straight forward. Clearly, one can use a given control methodology and design a poorly performing controller through an

unwise choice of parameters. One way to avoid this situation is to use a standard set of values for user defined parameters and utilize the same parameters in both approaches. The same parameters approach is used for H_2 under pole placement controller, such as the damping ratio of the boundary of the pole placement region. Also, the same operating points and the weights that the controllers' design is based on are used in both approaches. Furthermore, the focus of the validation process is not to have a quantitative comparison, but rather to show that the proposed controller gives results comparable to those of existing methods with the advantages listed in chapter 1.

3.7.1 Eigenvalue Analysis

Eigenvalue comparisons of the proposed controller with the base case, i.e. with only the SVC for six different operating points, is given in Table 3.4. Substantial improvements in damping ratio are seen with the proposed controller. For instance, consider mode 1 of operating point 4: without the controller the damping ratio is negative and illustrative of an unstable system.

Table 3.4 Damping and Frequencies of the Inter-area Modes under Different Load Conditions of the 68 Bus System

Operating point No.	**SVC**				**SVC with H $_\infty$ controller**			
	Mode 1		***Mode 2***		***Mode 1***		***Mode 2***	
	ξ	***f(H)***	***ξ***	***f(Hz)***	***ξ***		***ξ***	***f(Hz)***
1	0.01188	0.5427	0.03108	0.7875	*0.1935*	0.5085	*0.1337*	0.7200
2	0.01659	0.5448	0.03286	0.7903	*0.1980*	0.5103	*0.1337*	0.7199
3	0.00267	0.5266	0.03026	0.7850	*0.1880*	0.4883	*0.1335*	0.7159
4	**-0.0008**	0.5194	0.03005	0.7838	0.1814	0.4818	0.1326	0.7141
5	0.00596	0.5327	0.03050	0.7860	*0.1921*	0.4951	*0.1339*	0.7175
6	0.01120	0.5353	0.03222	0.7890	*0.1978*	0.4965	*0.1341*	0.7173

With the addition of the proposed controller, the damping ratio is improved to ***(0.1814) from (-0.0008)***. A similar trend of improved damping ratio is seen across all six operating points. The modes of the test system under different load conditions are shown in Fig. 3.11.

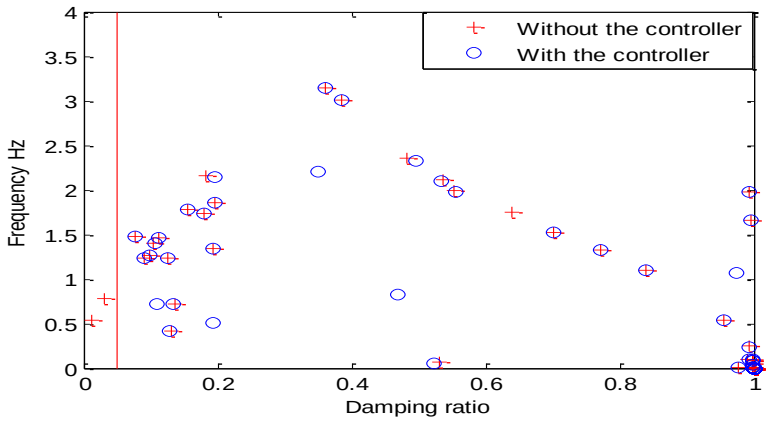

(a) Modes of the test system, OP1

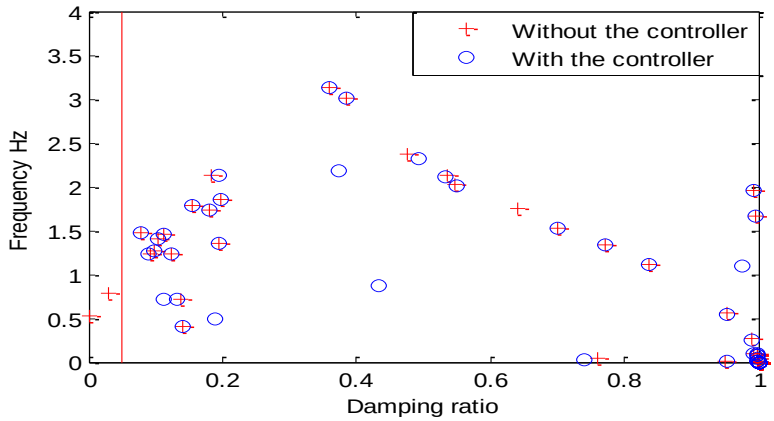

(b) Modes of the test system, OP3

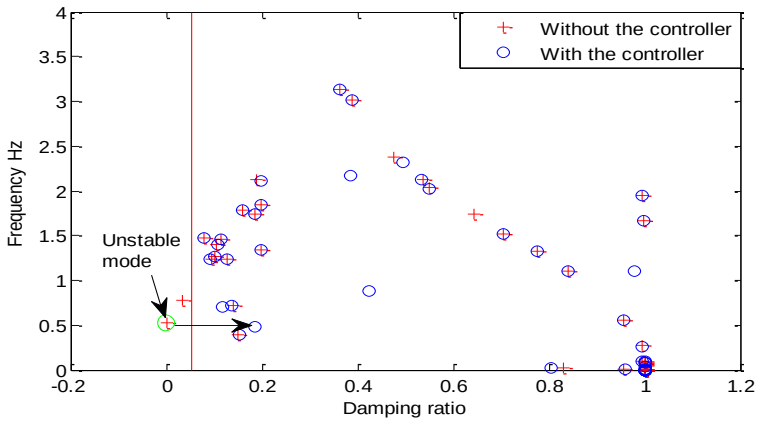

(c) Modes of the test system, OP4

Figure 3.11 Modes of the test system under three different operating points.

3.7.2 Time Domain Analysis

3.7.2.1 Robustness under Variability in Load Conditions and Wind Generation

To investigate the robustness of the proposed controller, three phase fault is placed at different areas with different operating points. Application of a fault in power systems results in a difference between mechanical and electrical power that produces electromechanical oscillations. The tests used for validating controller performance are designed in such a way that different disturbances occur under different operating points and at different parts of the system.

In this scenario, a 50ms three phase fault is applied at bus 8 in area 1, and it is applied under operating points 1, 3 and 4. The resulting tie-line power flow through line 42-52 for the three operating points 1, 3 and 4 is shown in Fig. 3.12 (a)-(c). Rotor angle separation between generators G_{16} and G_1 for this scenario under different operating conditions is shown in Fig. 3.12 (d)-(f).

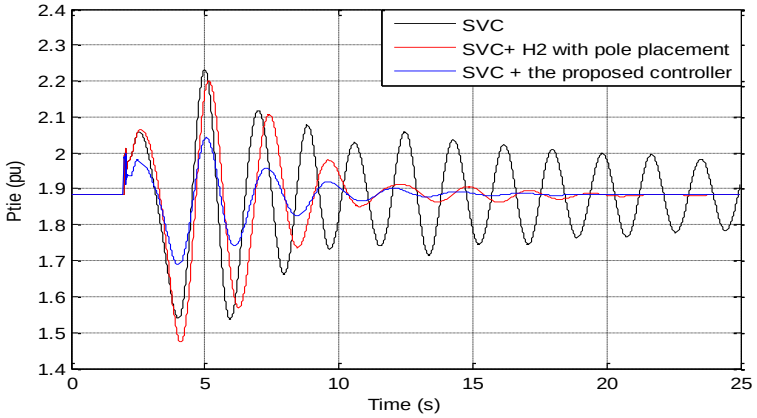

(a) Tie-line power, OP 1

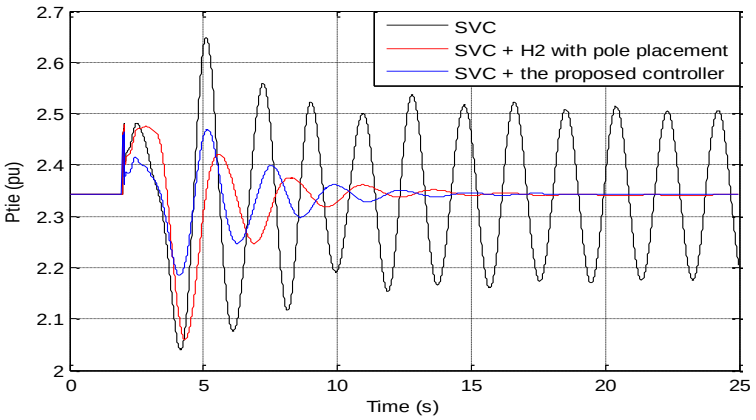

(b) Tie-line power, OP 3

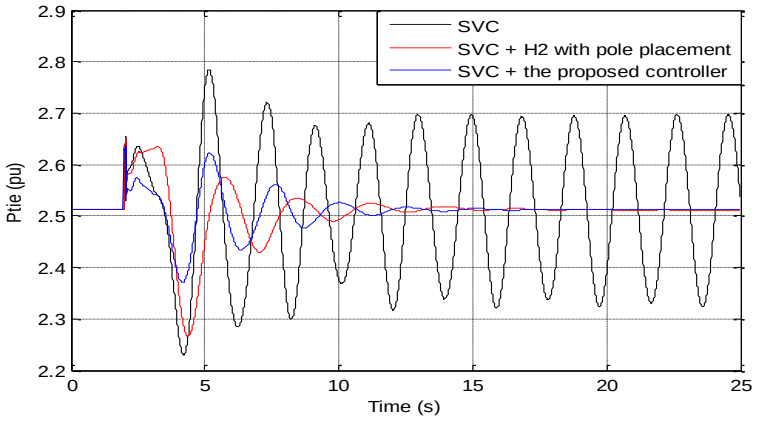

(c) Tie-line power, OP 4

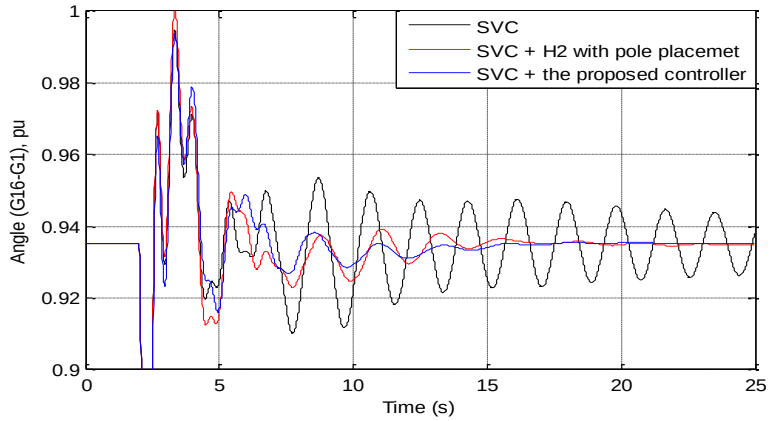

(d) Angle difference, G16 and G1, OP1

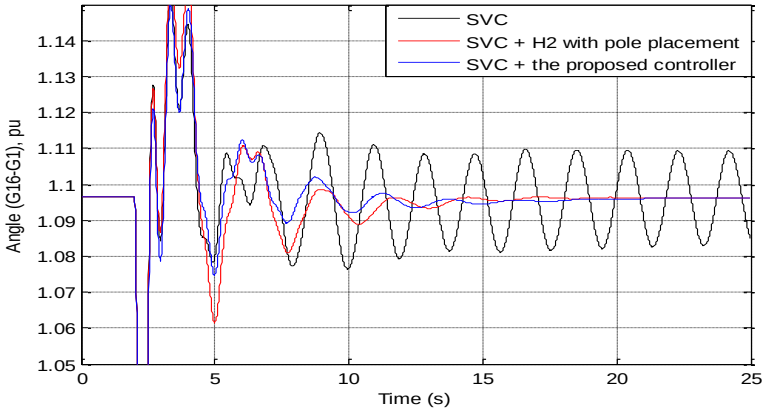

(e) Angle difference, G16 and G1, OP3

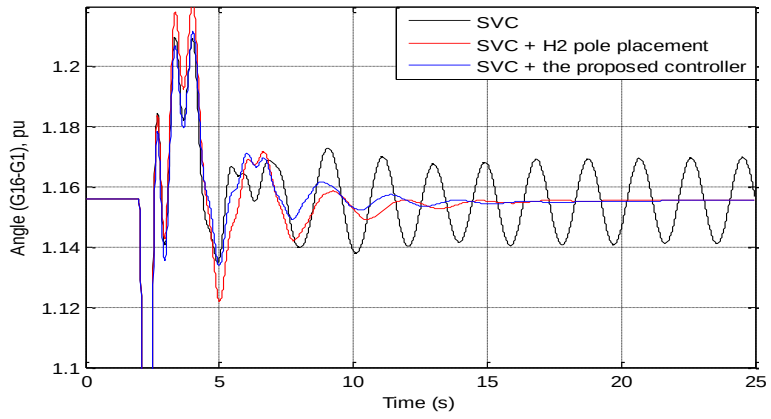

(f) Angle difference, G16 and G1, OP4

Figure 3.12 Dynamic response of the system under three phase fault at bus 8 (Area 1)

Comparisons between the system with and without the proposed controller show that the maximum overshoot and damping are considerably improved with the addition of the proposed controller under all three operating points tested in this scenario. Of particular note are the comparisons for operating point 4. Without the proposed controller, the system becomes marginally unstable as shown in Fig. 3.12 (c) and (f). However, the addition of the proposed controller not only makes the system stable but also damps out oscillations quickly. Both the H_2 under pole placement and the proposed controller have similar performance; however, in some cases the proposed controller has slightly better damping.

In another scenario, a 50ms fault is applied at bus 49 in area 2. This results in a significant drop in tie-line flow through line 42-52 during the fault, as can be seen in Fig. 3.13 (a)-(c). This scenario captures the performance of the proposed controller as the fault is applied relatively close to the SVC. Angular separation between areas 2 and 5, i.e. between generators G_{16} and G_{10}, is shown in Fig. 3.13 (d)-(f).

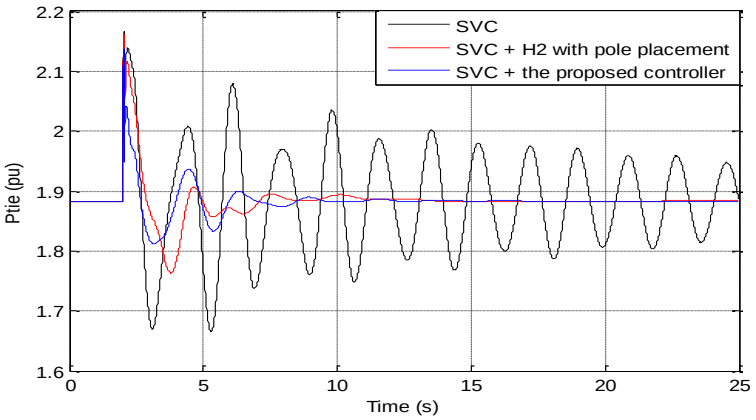

(a) Tie-line power, OP 1

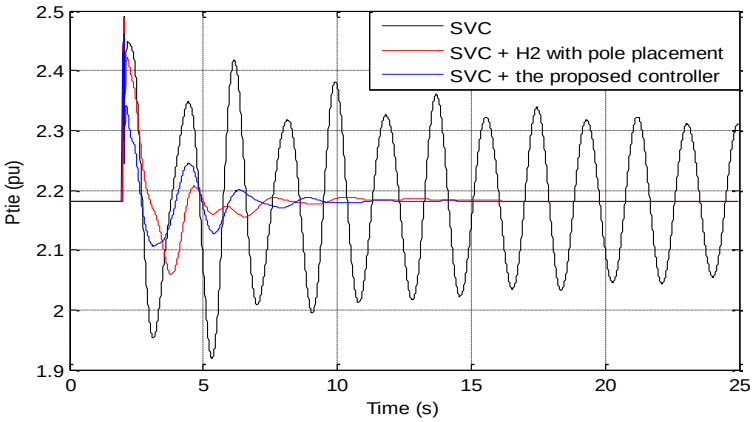

(b) Tie-line power, OP 5

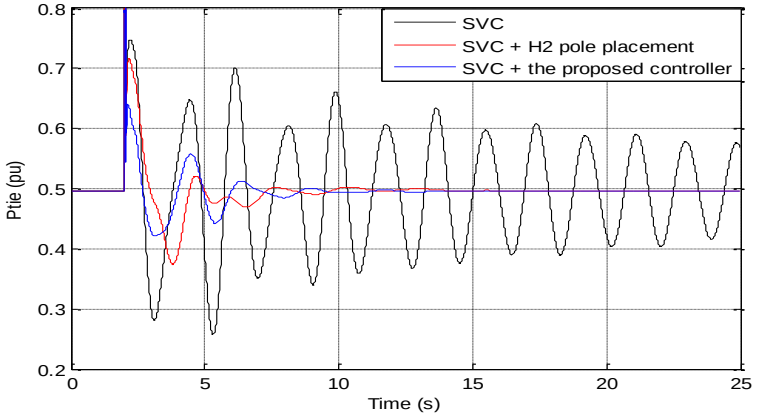

(c) Tie-line power, OP 6

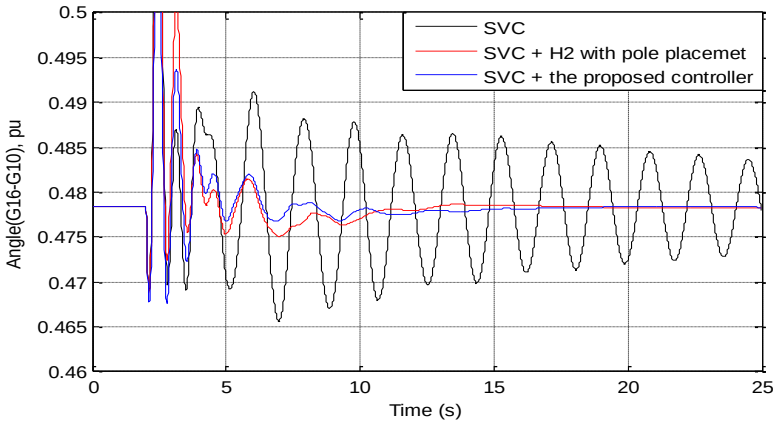

(d) Angle difference, G16 and G10, OP1

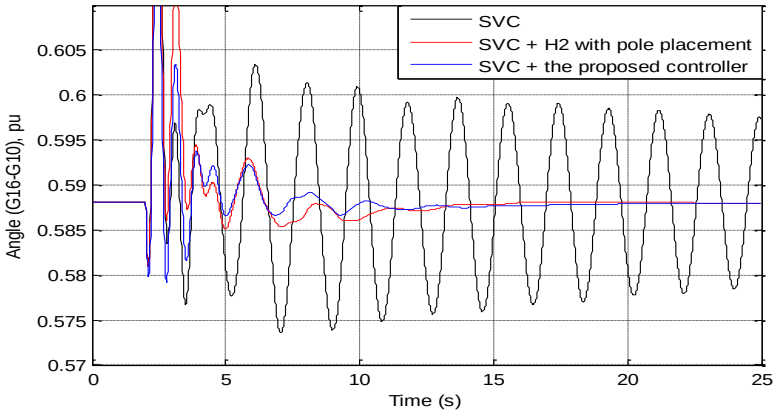

(e) Angle difference, G16 and G10, OP5

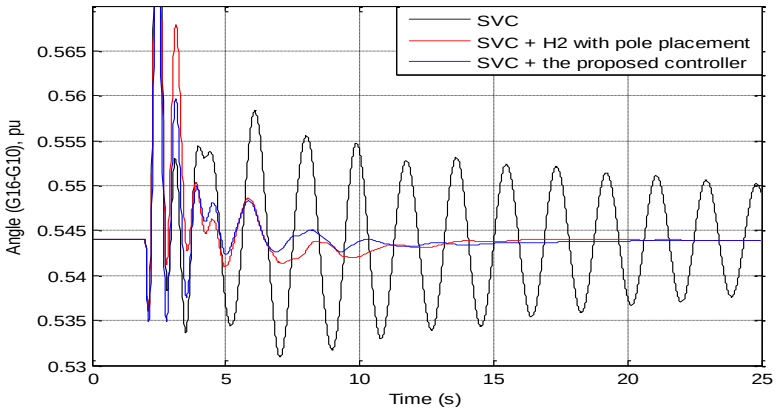

(f) Angle difference, G16 and G10, OP6

Figure 3.13 Dynamic response of the system under three phase fault at bus 49 (Area 2)

The susceptance of the SVC of operating point 1 during different fault locations (bus 8, bus 42 and bus 50) is shown in Fig. 3.14.

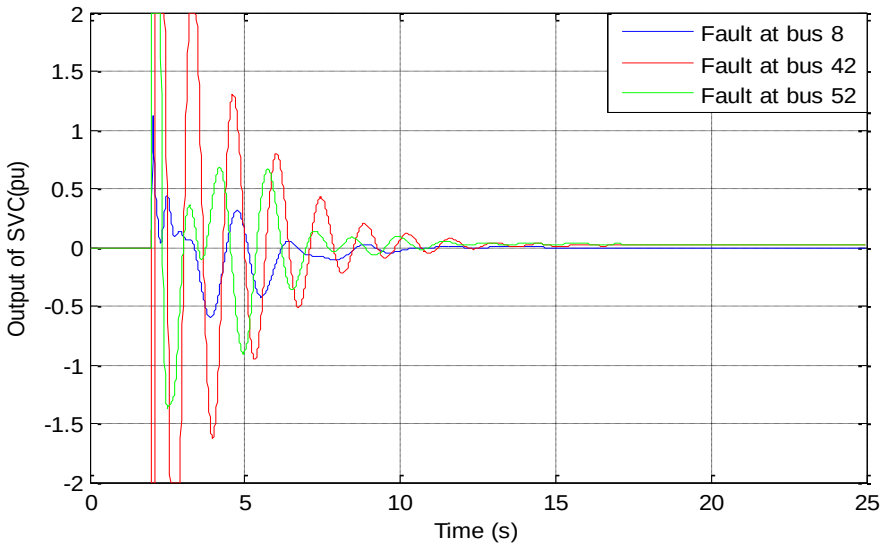

Figure 3.14 Output of the SVC at different fault locations, OP 1

3.8 Time Delay

The major problem in using remote signals is the time delay, and the range of the time delay varies depending on different factors such as the distance of the remote signal [66]. The remote signals can be delayed up to 100ms [48, 50]. Therefore, it is very important to account for an uncertain time delay to ensure the robustness under various time delays. In this chapter, a multi-model optimization method is used to include the effect of time delay. In the previous section, no time delay is considered since the main concern was to show that the method works for different scenarios and it is comparable with the existing approach. The time delay in this section has been approximated by the second order Pade approximation. To design a robust controller based on a multi-model optimization approach for the uncertainty in time delay, the time delay incorporates the worst case (OP3) and the operating points (1 and 2) are also chosen to design the controller. So the new controller is designed based on three operating points using the same procedure in section 3.4. Fig 3.15 shows the block diagram for incorporating the time delay with the feedback signal.

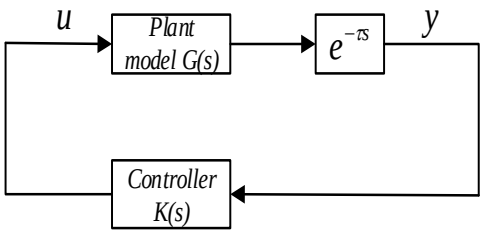

Figure 3.15 Block diagram of output signal time delay

Fig.3.16 shows the dynamic response of the test system with the designed controller for different values of time delay. It can be seen that the controller is able to damp the power system oscillations under a variety of operating points and time delay values. A comparison between the designed controller in section 4 (without incorporating the time delay) and the new controller designed based on incorporating the time delay is shown in Fig. 3.17. As can be seen, both controllers behave similarly when the feedback signal is delayed by 200ms. However, the first controller is not able to damp the inter-area oscillations in case of delay of the feedback signal by 300ms as shown in Fig. 3.17 (b) and (d). On the other hand, the second controller can maintain system stability and is able to damp these oscillations as can be seen in Fig. 3.17 (b) and (d).

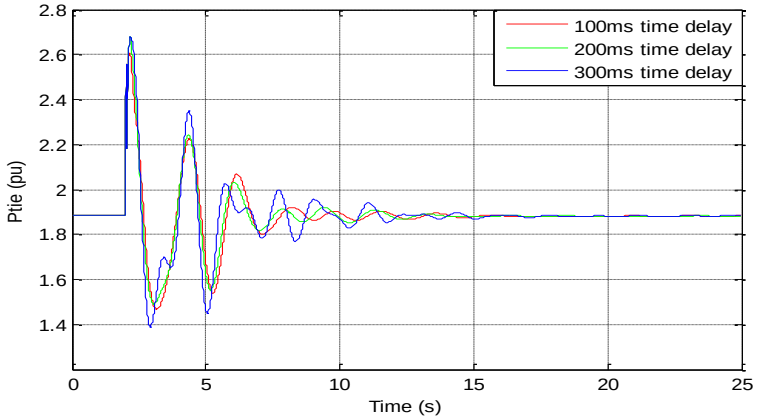

(a) Tie-line power, Fault at 50, OP 1

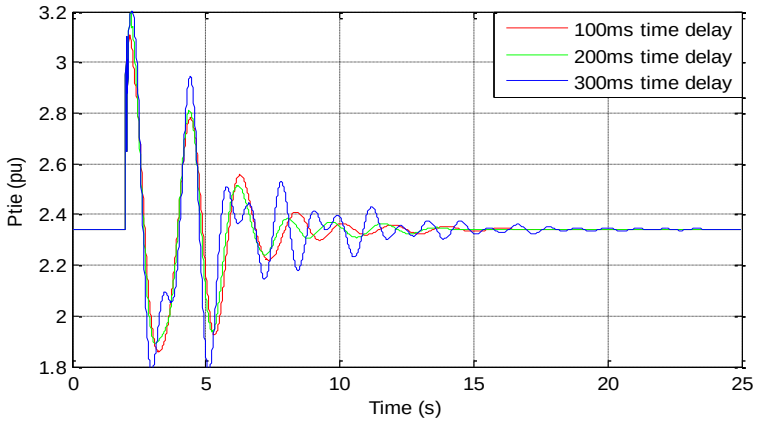

(b) Tie-line power, Fault at 50, OP 3

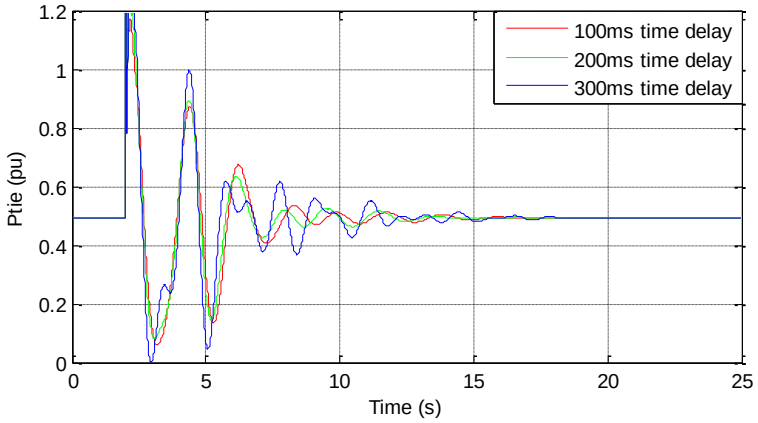

(c) Tie-line power, Fault at 50, OP 6

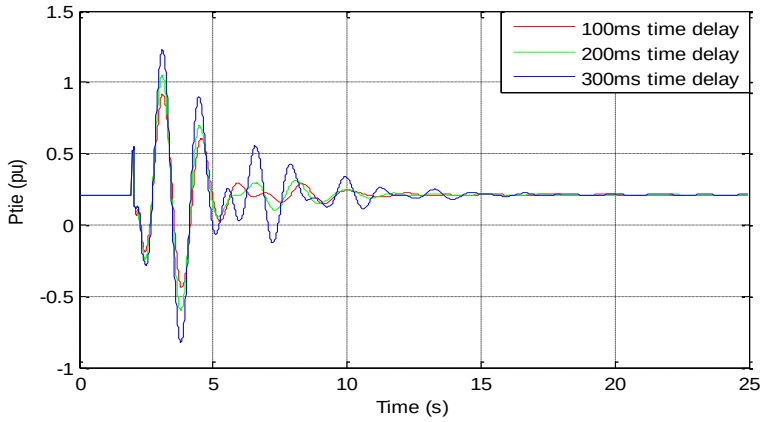

(d) Tie-line power, Fault at 41, OP 2

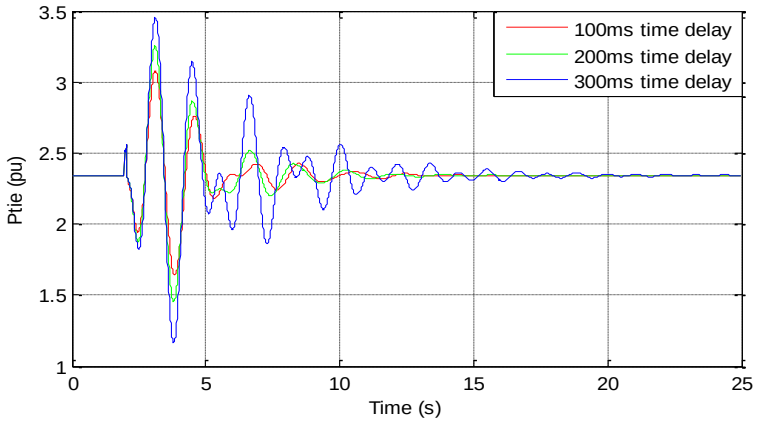

(e) Tie-line power, Fault at 41, OP 3

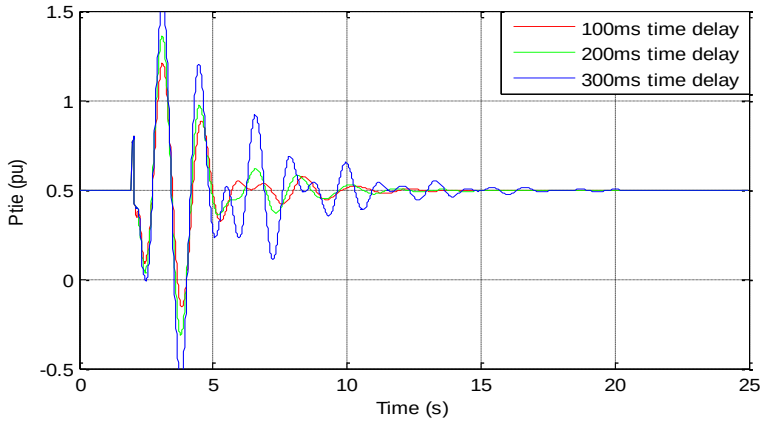

(f) Tie-line power, Fault at 41, OP 4

Figure 3.16 Dynamic response of the test system with different time delay

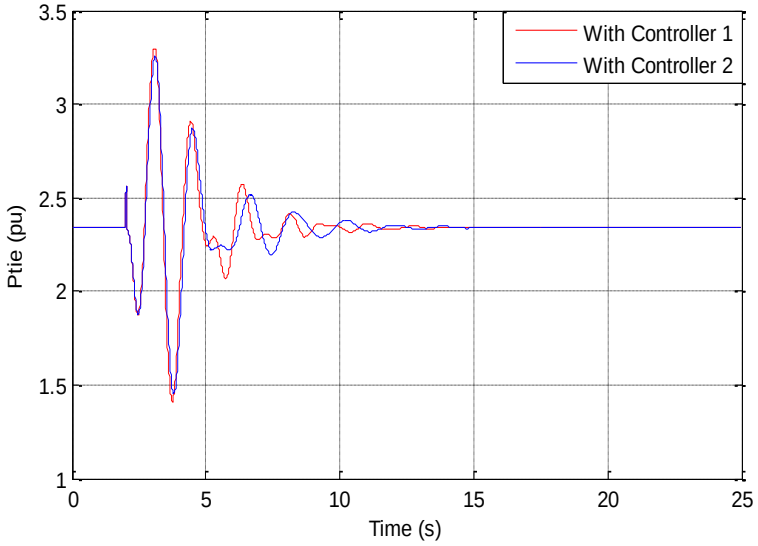

(a) Tie-line power, Fault at 41, OP 3,200ms

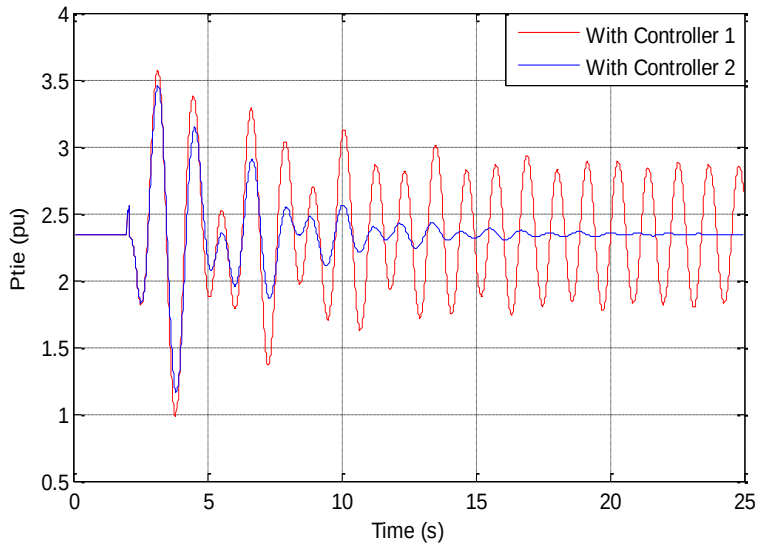

(b) Tie-line power, Fault at 41, OP 3,300ms

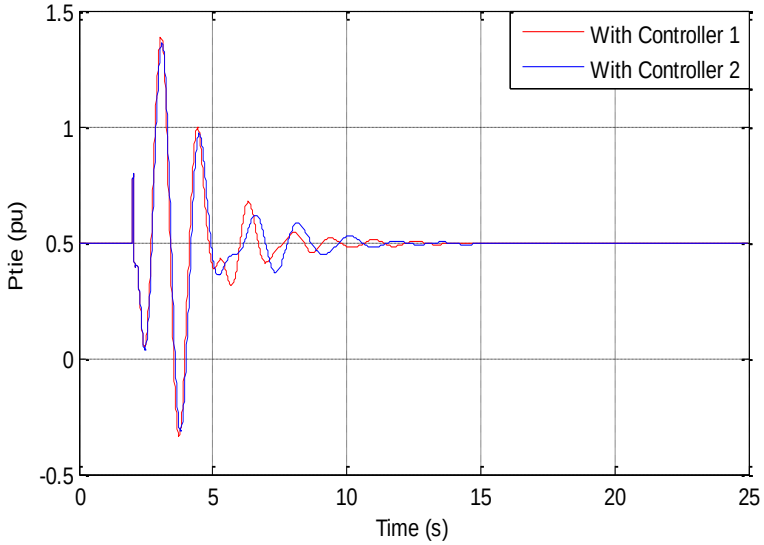

(c) Tie-line power, Fault at 41, OP 6,200ms

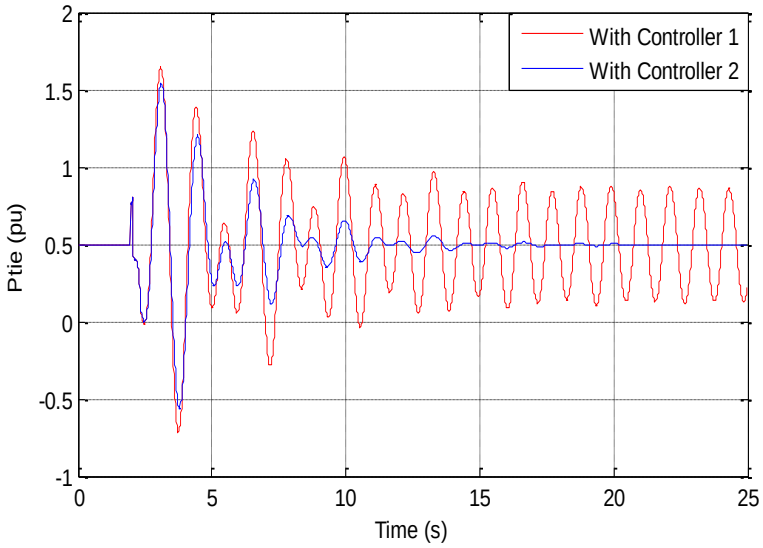

(d) Tie-line power, Fault at 41, OP 3,300ms

Figure 3.17 Dynamic response of the test system with the two controllers under different time delay

3.9 Conclusion

A multi-model approach is used in this chapter to design a robust supplementary damping controller. The designed fixed-order supplementary damping controller provides a supplementary signal to the voltage reference set point of SVC. The main objectives achieved in this chapter are damping low-frequency oscillations and enhancing power system stability. The controller design is based on shaping the closed-loop sensitivity functions in the Nyquist diagram through constraints on their infinity norm. The IEEE 68 bus system with a wind farm is used to demonstrate the controller performance. Test scenarios are designed to emulate real life scenarios seen at system operator level, specifically, uncertainties in operating conditions and changes to system topology are considered. Several test scenarios are run in which disturbances are applied to different areas of the test system under different operating conditions. In all test cases, the proposed controller significantly improved the system's dynamic response and compared favorably with an existing control technique H_2 under pole placement. Improved controller performance with a lower order controller and without the need for model order reduction are the primary advantages of the proposed method—a claim validated using both numerical and time-domain analysis. The issue of delaying the feedback signal has been addressed using multi-model optimization, and the result shows that the designed controller is able to damp out the inter-area oscillations under different values of time delay.

CHAPTER FOUR

LOOP-SHAPING CONTROLLER

This chapter presents the design of a robust fixed-order loop-shaping controller to damp out the inter-area oscillations and to enhance the stability of the power system. The proposed loop-shaping method in this chapter is based on the shaping of the open-loop transfer function in the Nyquist diagram through minimizing the quadratic error between the actual and the desired open-loop transfer functions in the frequency domain. The proposed method is robust with respect to multi-model uncertainty. Despite other robust controller design methods, the proposed approach deals with the entire system, i.e. there is no need to reduce the system, yet it still leads to a lower order controller. In addition, most of the robust methods are heavily dependent on selecting some weighting filters, which is not required in the proposed approach. This method is applied to the two-area four-machines system and the IEEE 68 bus system. The effectiveness and robustness of the proposed method in damping inter-area oscillations are validated using these case studies.

4.1 Class of models and controllers

A model of a system can be represented as parametric or nonparametric; however, in this chapter a parametric model is considered. The class of a controller can be low-order such as the proportional-integral-derivative (PID) controller or high-order. The Laguerre

function is a commonly used basis function for a high-order controller and is given in (3.2) (see chapter three for more details).

4.2 Robust Loop-Shaping Constraints

The main idea of this method is based on minimizing the difference between the desired open-loop transfer function $L_d(j\omega_k)$ and the open-loop transfer function $L_i(j\omega_k, \rho)$ shown in Fig. 4.1. As it is well known, $(-1 + j0)$ is the critical point on the Nyquist plot for analyzing the stability of the closed-loop system [51]. Therefore, the shortest distance between the Nyquist curve and the critical point is a good indicator of the robustness of the system. This distance has been termed the modulus margin. In the present work, modulus margin has been used as the robustness indicator in the controller design. In Fig. 4.1, if the desired modulus margin is *M*, then the robustness is met if the Nyquist plot of $L_i(j\omega_k)$ does not intersect a circle with its radius *M* centered at $(-1 + j0)$. This constraint can be achieved if the Nyquist plot is on the right side of a line $d\big(M, L_d(j\omega_k)\big)$ tangent to the circle and perpendicular to another line d_1. The line d_1 is a line that connects the critical point to $L_d(j\omega_k)$. All the points on line $d\big(M, L_d(j\omega_k)\big)$ can be defined as a function $f(x + iy, d)$, whereby (x, y) are coordinates of the points on the line. The region under this line can be defined as $f(x + iy, d) < 0$. So, the optimization problem involves achieving L_i to be as close as possible to L_d under the constraint that L_i should be on the right side of the line $d\big(M, L_d(j\omega_k)\big)$ as shown in Fig. 4.1. The equation of $d\big(M, L_d(j\omega_k)\big)$ at each frequency ω_k depends only on M and $L_d(j\omega_k)$ and for the situation of Fig. 4.1 can be written as:

$$d\big(M, L_d(j\omega_k)\big): \qquad y = tan(\alpha)\left[x - \frac{M}{\sin(\alpha)} + 1\right] \tag{4.1}$$

Where $\sin(\alpha)$ and $\cos(\alpha)$ are functions of $L_d(j\omega_k)$, $x\ and\ y$ are the real and imaginary parts on a point complex plane.

$$\sin(\alpha) = \frac{R_e\{1 + L_d(j\omega_k)\}}{|1 + L_d(j\omega_k)|}\ , \qquad \cos(\alpha) = -\frac{I_m\{1 + L_d(j\omega_k)\}}{|1 + L_d(j\omega_k)|}$$

Thus, equation (4.1) will be written as:

$d\big(M, L_d(j\omega_k)\big)$:

$$M|1 + L_d(j\omega_k)| - I_m\{L_d(j\omega_k)\}y - R_e\{1 + L_d(j\omega_k)\}[1 + x] = 0 \tag{4.2}$$

The side of the line $d\big(M, L_d(j\omega_k)\big)$ that excludes the critical point can be given by the following linear constraint:

$$M|1 + L_d(j\omega_k)| - I_m\{L_d(j\omega_k)\}\mathcal{I}(\omega)\rho - R_e\{1 + L_d(j\omega_k)\}[1 + \mathcal{R}(\omega)\rho] < 0 \tag{4.3}$$

These linear constraints can be further simplified to:

$$M|1 + L_d(j\omega_k)| - R_e\{[1 + L_d(-j\omega_k)][1 + L_i(j\omega_k, \rho)]\} \tag{4.4}$$

Using the following facts:

$$R_e\{1 + L_d(-j\omega_k)\} = R_e\{1 + L_d(j\omega_k)\}\,, \tag{4.5}$$

and

$$R_e\{[1 + L_d(-j\omega_k)]jI_m\{L(j\omega_k, \rho)\}\} = I_m\{L_d(j\omega_k)\}\mathcal{I}(\omega)\rho\} \tag{4.6}$$

Using all the above analysis, the quadratic optimization problem can be formulated as given in (4.7). The goal is to minimize the distance (the error) between the open-loop transfer function of a given system and the desired one under the constraints in (4.4).

$$\min_{\rho} \sum_{i=1}^{m} \sum_{k=1}^{N_i} |L_i(j\omega_k, \rho) - L_d(j\omega_k)|^2 \tag{4.7}$$

Subject to:

$$M|1 + L_d(j\omega_k)| - R_e\{[1 + L_d(-j\omega_k)][1 + L_i(j\omega_k, \rho)]\} \quad < 0$$

$for\ k = 1, \dots\dots, N_i\ (No.of\ frequencies), \qquad i = 1 \dots, m.$

where $\quad L_i(j\omega_k, \rho) = \rho^T\ \varphi(j\omega_k) G_i(j\omega_k)$

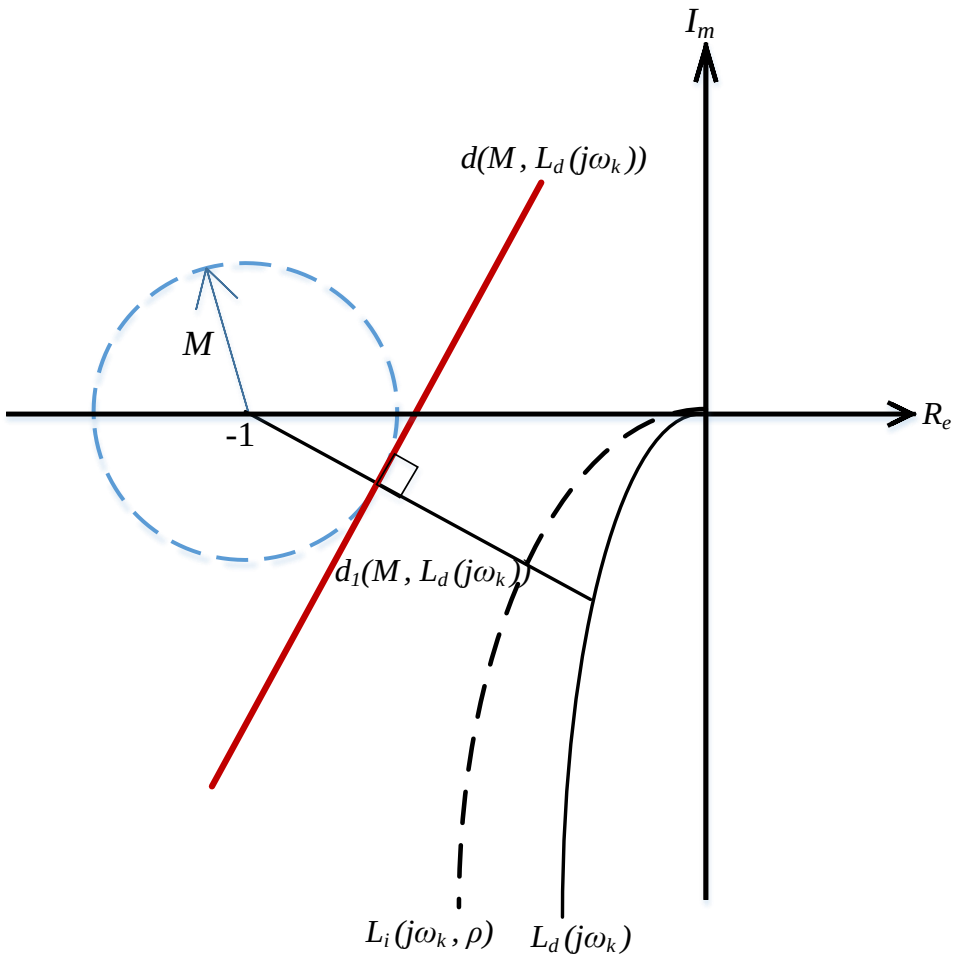

Figure 4.1 Loop shaping in Nyquist plot

4.3 Test Systems

Two test systems have been selected to validate the proposed approach introduced in section 4.1.

4.3.1 Two-Area Four-Machines Test System

The test power system consists of two areas connected through two parallel tie lines; each area consists of two synchronous generators as shown in Fig. 4.2. The four generators are equipped with automatic voltage regulators, power system stabilizers, and turbine governors [2]. The SVC is installed at bus 8. Table 4.1 shows the Eigenvalue pair, the frequency and the damping ratio, which represent the inter-area mode at the normal operating point $P_{tie} = 400MW$ for the two-area system. Controllability metric has been used to select the most effective input signal to damp the inter-area mode. The measured signal ***y*** is the tie-line power through the line 7-8, which is used as an input to the controller *K(s*) as shown in Fig. 4.2. The output signal of the controller ***u*** is used to provide supplementary signal to the reference of the SVC.

Table 4.1 Eigenvalue, Damping Ratio and the Mode Frequency for Two-Area System

Eigenvalue $\boldsymbol{\sigma \pm j\omega}$	**Damping ratio** $-\frac{\sigma}{\sqrt{\sigma^2+\omega^2}}$	**Frequency (*Hz*)** $\frac{\omega}{2\pi}$
$-0.1114 \pm 4.044j$	0.02753	0.6435

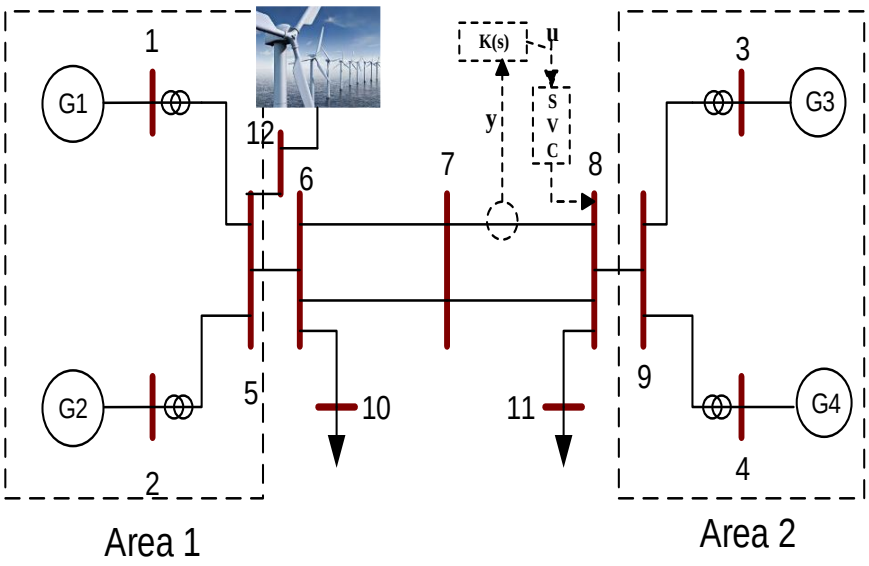

Figure 4.2 Single line diagram of two-area four-machines test system

4.3.2 16 Machines, 68 Bus System

The IEEE 68 bus system has already been described in chapter three; however, it has been modified slightly in this chapter. Table 4.2 shows the Eigenvalue pairs, the frequencies and the damping ratios that represent the inter-area mode at the normal operating point of the system.

Table 4.2 Eigenvalue, Damping Ratio and the Mode Frequency for 68 Bus System

Eigenvalue $\sigma \pm j\omega$	**Damping ratio** $-\frac{\sigma}{\sqrt{\sigma^2+\omega^2}}$	**Frequency (*Hz*)** $\frac{\omega}{2\pi}$
$-0.03597 \pm 3.370j$	0.0107	0.5364
$-0.1712 \pm 5.002j$	0.0342	0.7961

4.4 The Controller Design Procedure

The steps in designing the proposed controller using the loop-shaping approach are similar to the steps that have been explained in chapter three. However, selection of weighting filters (step #5) is not required in this approach, making the approach more advantageous. Also, different operating points are chosen as listed in Tables 4.3 and 4.4 for the two test systems respectively. The desired open-loop transfer function L_{d0} has been chosen as ($L_{d0} = {\omega_c}/{S} = 12/\mathrm{s}$).

Table 4.3 Different operating points for two-area test system

Operating point No.	***Load of Area1***	***Load of Area2***	***Approximate Tie-line power***
1	9.76	17.67	4
2	10.76	16.75	3
3	11.76	15.77	2
4*	14.65	12.82	-1

The final controller $K(s)$ for all the plants of the second case study (IEEE 68 bus system) is given in (4.8).

$$K(s) = \frac{-94.437(s^2 + 0.375S + 10.4)(s^2 + 5.013s + 27.37)}{(s+7)^4} \tag{4.8}$$

To confirm robustness and effectiveness, the controller in (4.8) should be investigated under the selected operating points (the controller designed based on 1, 2 and 5) and also other operating points that are not included in the original design (3* and 4*) as listed in Table 4.4.

Table 4.4 Different operating points for 68 bus system

Operating point	G_{12}	G_{13}	G_{14}	G_{15}	G_{16}
1	13.5	38.15	17.85	10	40
2(line8-9 disconnected)	13.5	38.15	17.85	10	40
3*	15.5	38.15	21.85	6	38
4*	13.5	38.15	17.85	5	45
5	15.5	38.15	20.85	5	40

*Not used in the control design, but used to validate the controller.

4.5 Frequency Response Analysis of the IEEE 68 Bus System

The closed-loop transfer function $T_i = \frac{L_{di}}{1+L_{di}}$ defines the relationship between the reference and the output signals; it is called the complementary sensitivity function. In general the frequency shape of the complementary sensitivity function should resemble a low pass filter. Ideally in low frequency, it is designed to have a flat gain of $0\ dB$. Flat $0\ dB$ gain in low frequency means that the output signal very closely follows or tracks the desired reference. The sharp drop in T in high frequency means that the system will have a good high-frequency noise rejection characteristic. The complementary sensitivity

function T for the second case study is shown in Fig. 4.3 (b). The close-loop transfer function from the reference to the error is $S_i = \frac{1}{1+L_{di}}$, and it is called the sensitivity function.

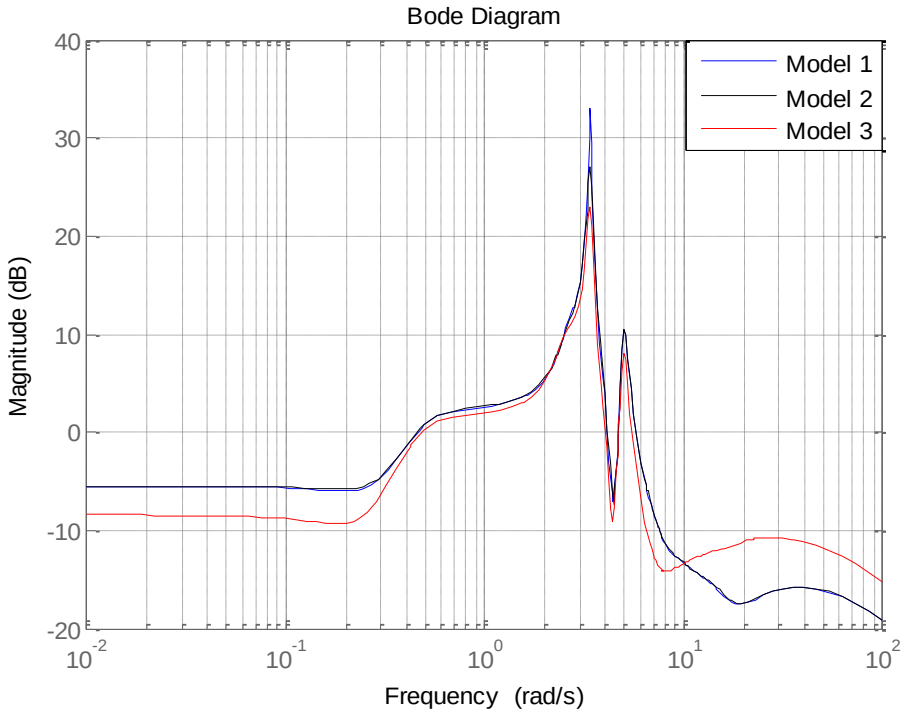

(a) The three models

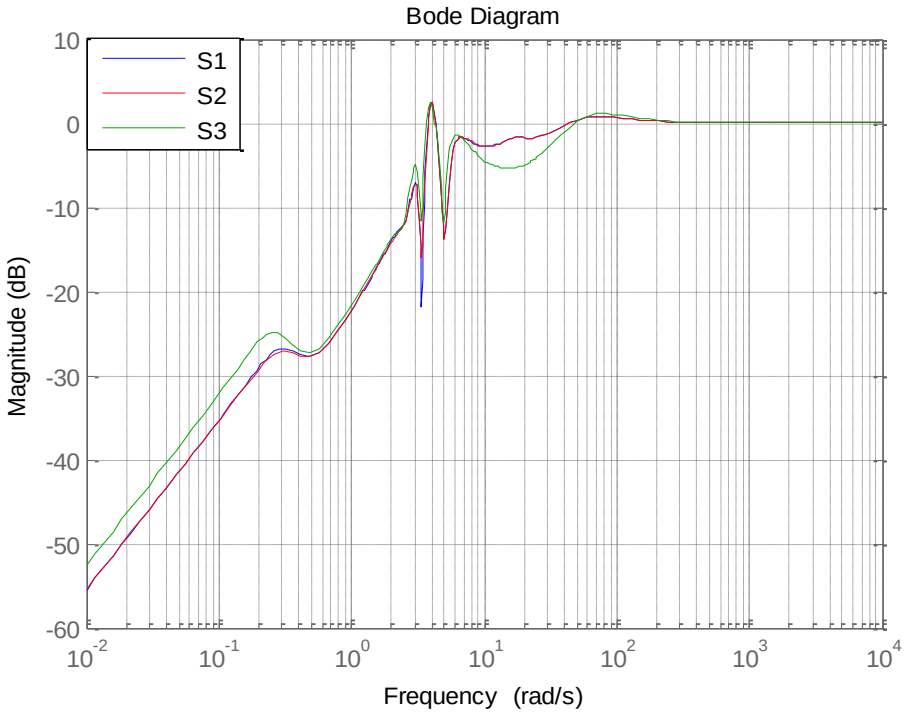

(b) Complementary sensitivity functions

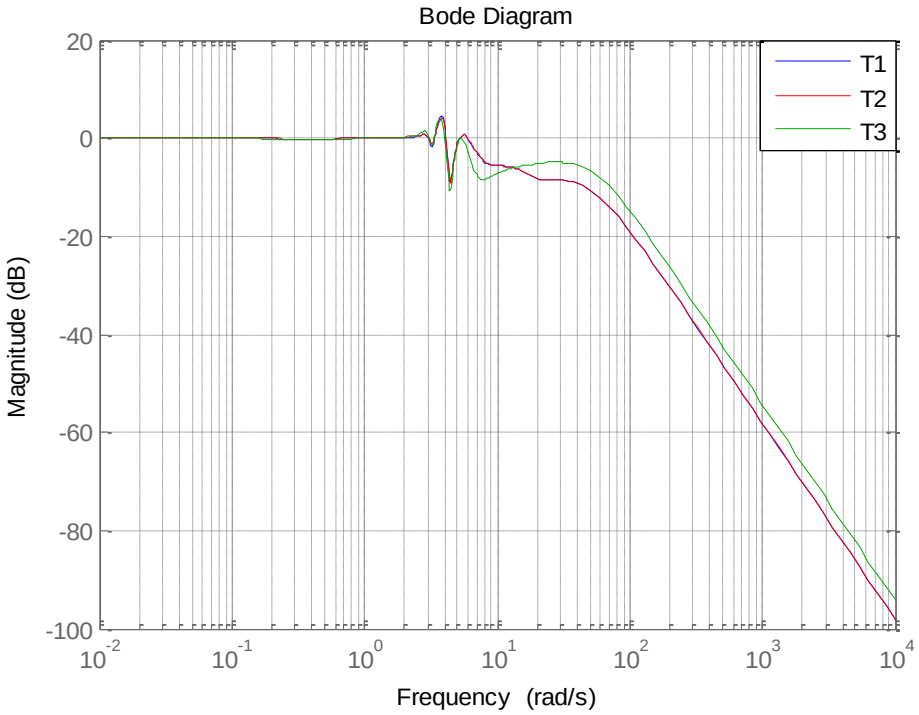

(c) Sensitivity functions

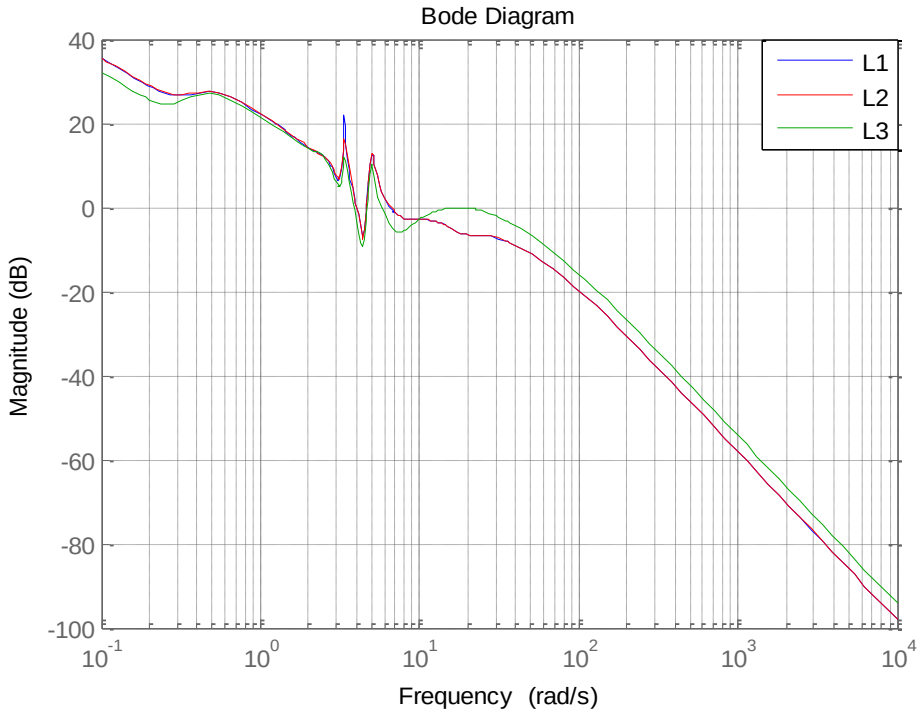

(d) Open loop transfer functions

Figure 4.3 Frequency response of the three (a) models, (b) complementary sensitivity functions (c) sensitivity functions and (d) open loop TFs for the 68 bus system case study

The corresponding frequency shape of S, shown in Fig. 4.3 (c), resembles a high pass filter. Good attenuation at low frequency range means that any disturbances in that frequency range will not significantly affect the output signal. In other words, the system will have good disturbance rejection characteristic. To achieve a solid tracking performance characteristic in T and sufficient disturbance rejection in S, the desired open-loop transfer function has to attain a high enough gain at low frequency; in other words, L_{d0} needs to be above the $0\,dB$. To assure an adequate noise rejection

characteristic, the desired open-loop transfer function should have a sharp drop in high frequency as shown in Fig. 4.3 (d).

4.6 Simulation Results for the Two Case Studies

The test systems with the SVC and DFIG have been simulated in Power System Toolbox (PST). The controller design was implemented in MATLAB, and it is integrated in PST.

4.6.1 Time Domain Results for the Two-Area Test System

The two-area system is studied under different operating points (load conditions shown in Table 4.3), different wind penetrations and fault conditions with and without the SVC supplementary controller $K(s)$. By following the controller design steps mentioned in section 4.4, the operating points 1, 2, and 3 are used to design the controller and the operating point 4^* is used to validate the controller. The two-area system is selected as a sample of small test system. All the values in Tables 4.3 and 4.4 are in per unit system based on 100MVA.

As previously mentioned, one of the advantages of the proposed approach is that the system reduction is not required. The number of states of the two-area test system is 75, including the SVC and DFIG, and a 3rd-order controller is designed to damp out the inter-area oscillations and enhance the system stability, as will be shown in the results. For the methods that require system reduction for the same case study, the order of the

controller will be the sum of the reduced system order plus the order of the weights. In addition, for these methods, selecting the proper weights is still another challenge.

The proposed controller, however, is verified under uncertainty in the system caused by the operating point change, changes in system topology and different levels of wind penetrations.

4.6.1.1 The controller response to different operation conditions

To test the robustness of the test system, a three-phase to ground fault is applied at bus 6, and it is cleared (self-cleared) after 50ms at different operating points as shown in Table 4.3. The tie-line power as well as the speed of generator 1 are presented to demonstrate the effect of the disturbances on the test system. Fig. 4.4 (a) and (b) show the tie-line power under the fault mentioned above with and without the proposed controller for SVC at the operating points 1 and 4* (see Table 4.4) respectively. It can be seen that the tie-line oscillations without the proposed controller have longer settling time; however, in the system with the proposed supplementary controller, the oscillations damped out faster. The speed of generator 1 is shown in Fig. 4.4 (c) under the mentioned fault, showing that the speed of G1 with only SVC oscillates for more than 20 seconds. On the other hand, the oscillations of the speed of G1 with the proposed supplementary controller are smoother and settle down faster.

4.6.1.2 The controller response to changes in system topology

To test the robustness of the proposed controller, the topology of the test system is changed by tripping the line 6-7 due to a three phase fault at bus 7 for 50ms under the operating points 1 and 4*. The steady state value of the tie-line power flow changes due to tripping. It can be seen from the results shown in Fig 4.4 (d) and (e) that with the proposed controller, the oscillations of tie-line power are damped quickly, whereas much more time is needed to damp them out without the supplementary controller.

4.6.2 Two-Area System with different wind penetrations

In this section, the output of the wind turbine is varied and two different values (200 MW and 100MW) are assumed to validate the controller. Fig. 4.4 (f) shows the tie-line power of the operating point 1 with three phase fault occurs at bus 6 when the output of the wind turbine was 200MW. Then the level of wind penetration is decreased to 100MW, and in this scenario the system becomes oscillatory without the controller as shown in Fig.4.4 (g). The change in the system topology is made by tripping line 6-7 with 100MW wind as shown in Fig. 4.4 (h) at the operating point 2. In all these cases the controller is able to damp out the oscillations within 15 seconds.

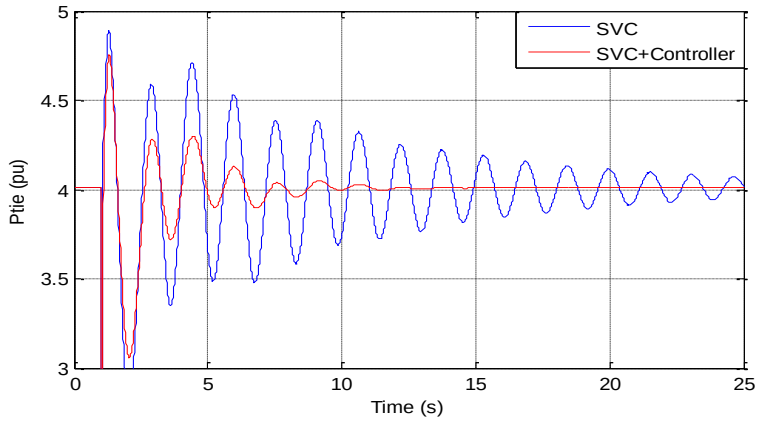

(a). 400MW tie-line, fault at bus 6

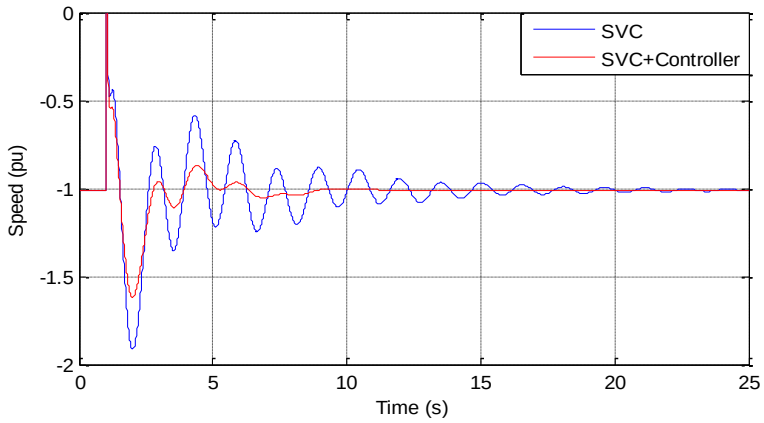

(b) 100MW tie-line, fault at bus 6

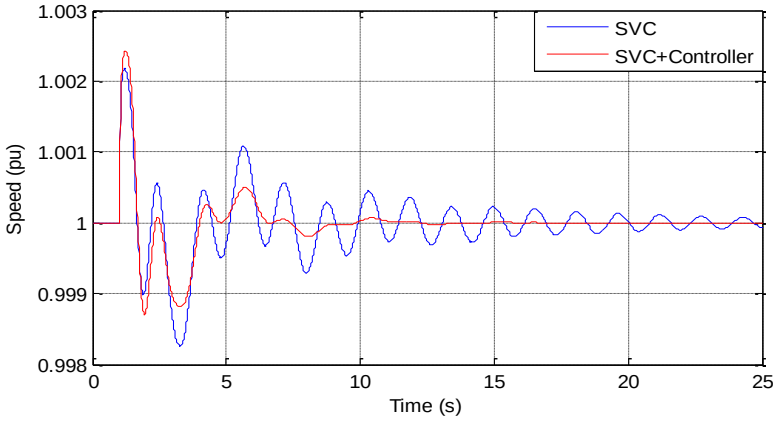

(c) Speed G1, 400MW tie-line fault at bus 6

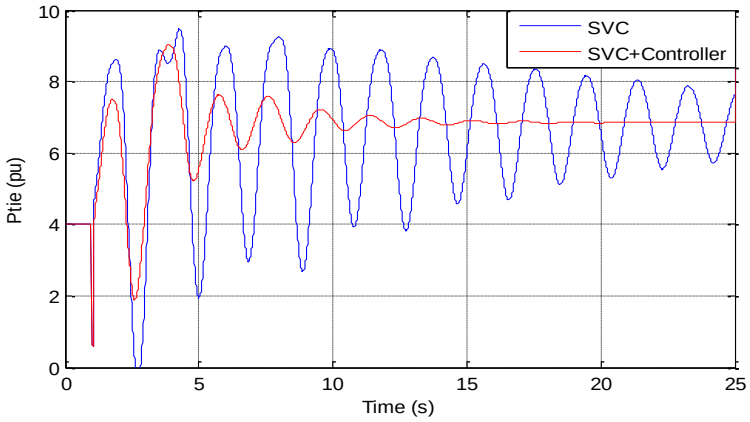

(d) 400MW tie-line, trip the line 6-7

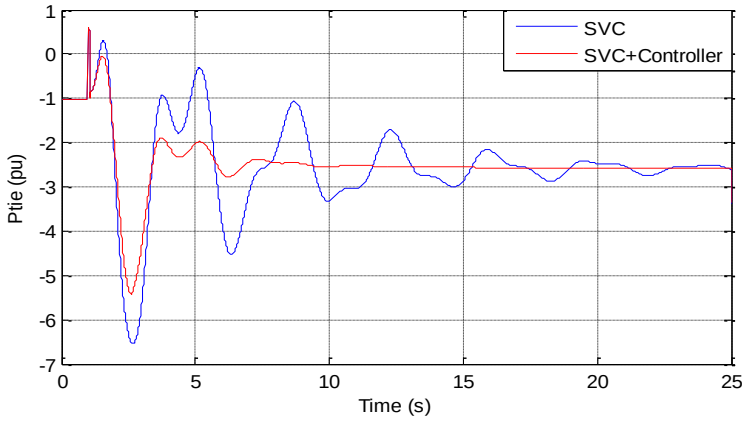

(e) -100MW tie-line, trip the line 6-7

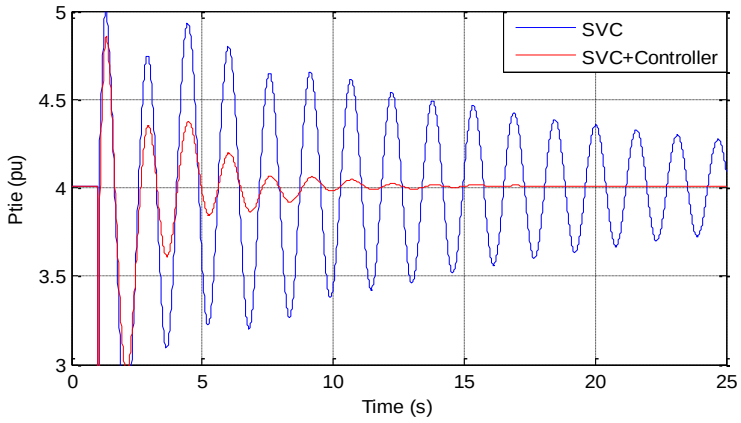

(f) 400MW, 200MW wind, fault at bus 6

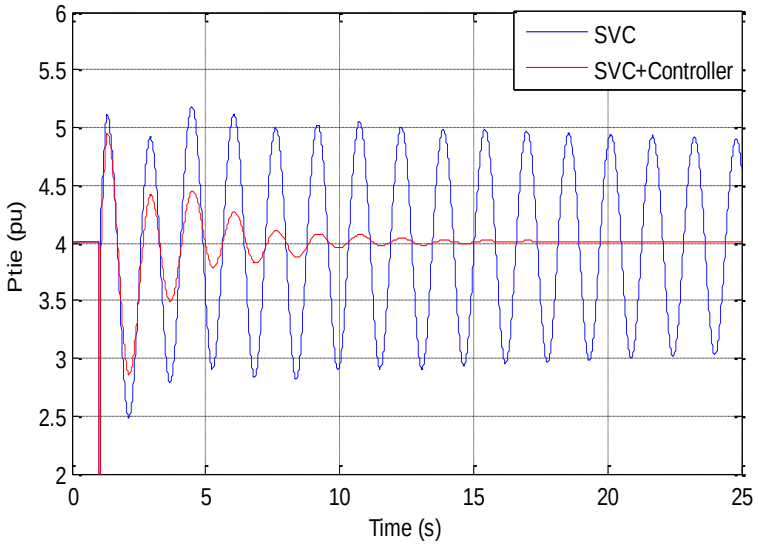

(g) 400MW, 100MW wind, fault at bus 6

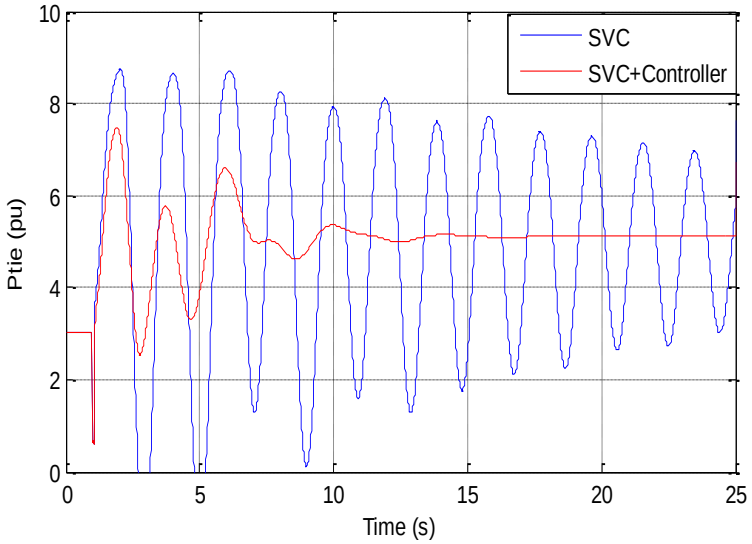

(h) 400MW, 100MW wind, trip the line 6-7

Figure 4.4 Tie-line power and speed of G1 at different load conditions and changes in system topology

4.6.3 Eigenvalue Analysis

The Eigenvalue study has been undertaken to examine the performance of the supplementary controller in terms of improving the damping ratio ξ of the inter-area modes. The results are concluded in Table 4.5. It can be seen that the damping ratios at different load conditions are improved significantly. Table 4.6 summarizes the damping ratios of the inter-area modes under different levels of wind penetrations ($P_{tie} = 400MW$). The results show that the action of the supplementary controller is robust against varying the level of wind penetrations.

Table 4.5 Damping and frequencies of the inter-area modes under different load conditions

Tie-line power (pu)	*SVC*		*SVC with controller*	
	ξ	*f(Hz)*	ξ	*f(Hz)*
4	0.02753	0.6434	0.2840	0.7421
3	0.03318	0.6505	0.3582	0.7163
2	0.03846	0.6550	0.4234	0.6692
1	0.0432	0.6567	0.4666	0.6210

Table 4.6 Damping and frequencies under different wind penetrations

Level of wind penetrations(pu)	*SVC*		*SVC with controller*	
	ξ	*f(Hz)*	ξ	*f(Hz)*
2	0.01392	0.6425	0.2780	0.7472
1	0.00252	0.6408	0.2744	0.7486
0.5	-0.00088	0.6388	0.2746	0.7492

4.7 Time Domain Result for the 68 Bus System

This system is selected as a sample of a large test system. The system contains 190 states including the SVC and DFIG. Since the order of the system is large, an H_∞ controller is also designed and implemented to provide a performance comparison with the proposed controller.

4.7.1 H_∞ Controller

In this study, the proposed method has been compared with H_∞ technique since it is a widely used technique in damping power-system oscillations. This technique shows a solid performance in damping these oscillations as well as maintaining the stability of the power system. The focus of the validation process is not to have a quantitative comparison, but rather to show that the proposed controller gives comparable results to those of existing methods with the advantages listed in section 1.2. In the H_∞ approach,

the order of the system needs to be reduced, so it was reduced to 7. It should be mentioned that the frequency response of both the reduced and the original system has to be the same in the frequency range of interest. For example, the order of the second test system (68 bus system) is 190 and it is reduced to 12. The frequency response of the original and reduced system is shown in Fig. 4.5, and it can be seen that the original and the reduced system match exactly at the entire range of low and high frequencies. This reduced system can be used in the proposed approach and leads to a low-order controller. However, if the same reduced system is used to design a robust controller using for example H_∞, then the order of the controller definitely will be high since it is based on the order of the reduced system, which is 12 in this case. To reduce the order of the controller, the system needs to be reduced even further, and it cannot be reduced to less than 7 as shown in Fig. 4.5. It can be seen that when the order of system is reduced to 6, the reduced order system no longer represents the actual system. For the 7th model, it is clear that the original and reduced system match only in frequency range of interest (0.2 to 1.0) Hz. The same concept can be applied to large-scale power systems (such as a system with 10000 states or more) as well, and the proposed approach will lead to lower order controller.

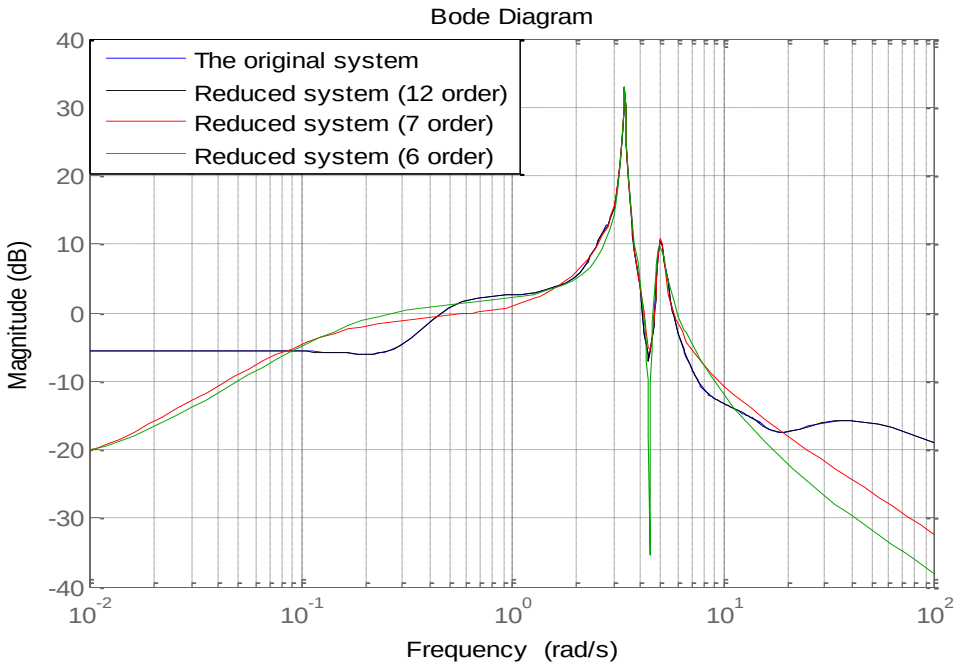

Figure 4.5 Frequency response of original system, 12-, 7- and 6-order reduced system

Also, in this approach weighting filters–$W_1(s)$ and $W_2(s)$ have to be properly selected. For output disturbance rejection, $W_1(s)$ should be selected as a low-pass filter. $W_2(s)$ should be selected as a high-pass filter to ensure robustness in the high frequency range and to reduce the control effort. The weighting filters are tuned to add more weight to the first mode that is close to instability. The robust toolbox in MATLAB is used to design the H_∞ controller for the test system. The order of the designed controller based on the H_∞ approach is 9, which is equal to the order of the reduced system plus the weighting filter order (7+2) [2].

4.7.2 The proposed controller

The system has been extensively studied, and the operating points listed in Table 4.4 are considered for this study as they greatly affect the inter-area modes. The wind is varied, and no effect is found on the inter-area modes. By following the controller design steps in section 4.5, three different operating points—1, 2 and 5—are selected to design the controller. Operating points 3*, 4* and 5 are used for validation. The order of the controller is considered to be 4 for this case study.

4.7.2.1 Controller response to different operation conditions

The robustness is verified by applying three phase fault at buses 41 and 52 at different load conditions. Figures 4.6 (a), (b) and (c) show the tie-line power in the line 52-42 under the fault at bus 41 at the operating points 3*, 4* and 5 as shown in Table 4.4. Figures 4.6 (g), (h) and (i) show the same tie-line power of the same operating points under the fault at bus 52.

The angular separation between machines G16 and G10 under the fault at bus 41 at different operating points is shown in Figures 4.6 (d), (e) and (f). Figures 4.6 (j), (k) and (l) show the same angle under the fault at bus 52. The simulation results illustrate that the proposed approach is able to damp out the oscillations faster than the normal H_∞ approach in most of the scenarios.

4.7.2.2 Controller response to changes in system topology

To test the robustness to changes in the topology, the line 46-49 is assumed to be out of service for maintenance, and three phase fault is placed at bus 38 for 50ms at different operating scenarios. Figures 4.6 (m) and (n) show the tie-line power at operating points 3* and 5 under the above fault and the angular separation between machines G16 and G10 under the same fault are shown in Figures 4.6 (o) and (p). It can be seen that the H_∞ controller cannot perform effectively after changing the topology of the system; however, the proposed approach is able to damp out the oscillations quickly.

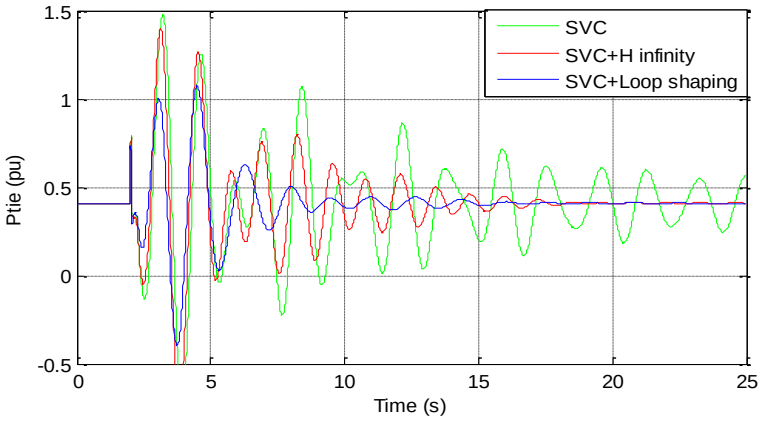

(a) 0.5MW tie-line, OP 3, fault at bus 41

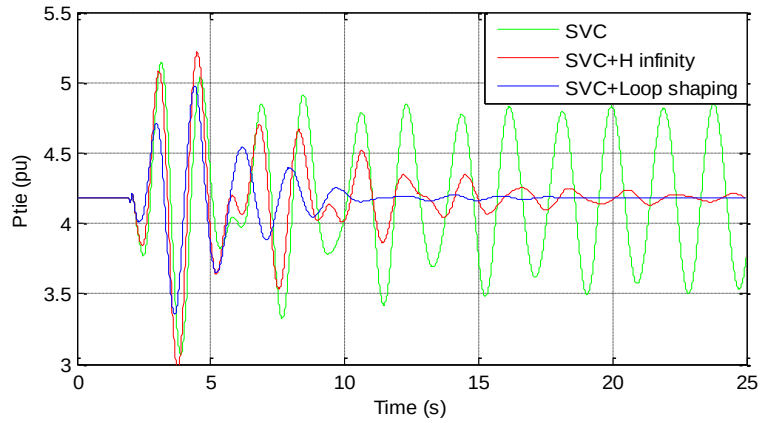

(b) 4.2MW tie-line, OP 4, fault at bus 41

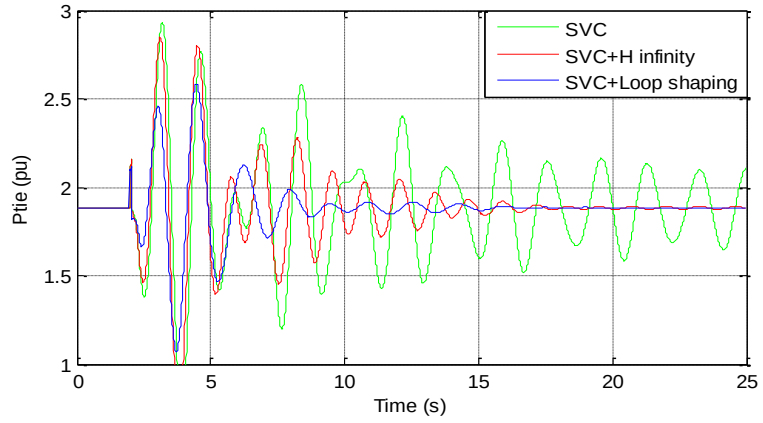

(c) 1.9MW tie-line, OP 5, fault at bus 41

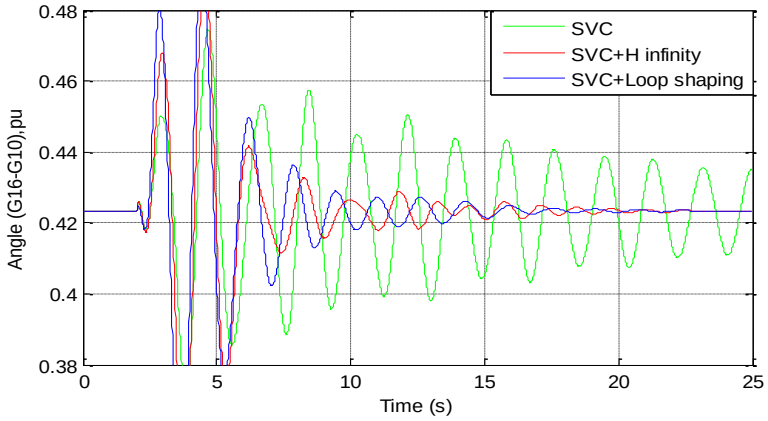

(d) Angle difference, OP 3, fault at bus 41

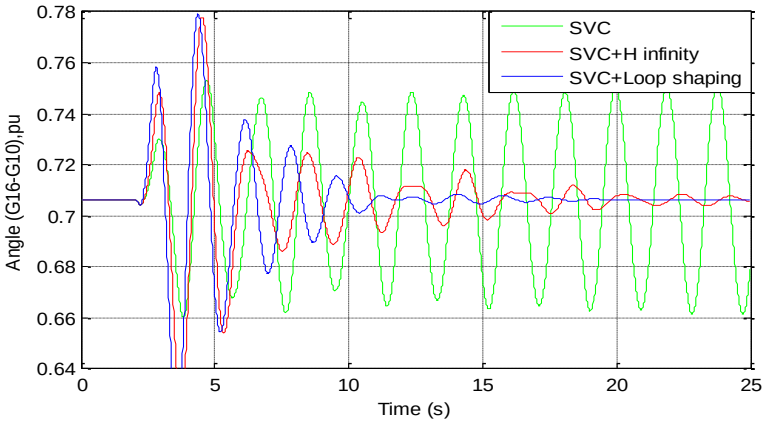

(e) Angle difference, OP 4, fault at bus 41

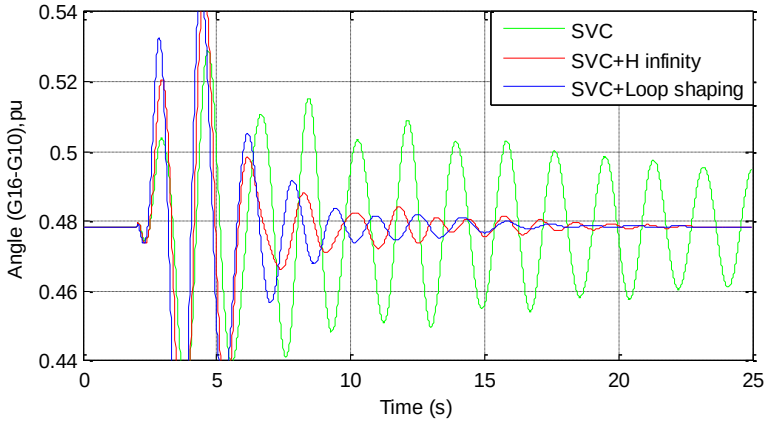

(f) Angle difference, OP 5, fault at bus 41

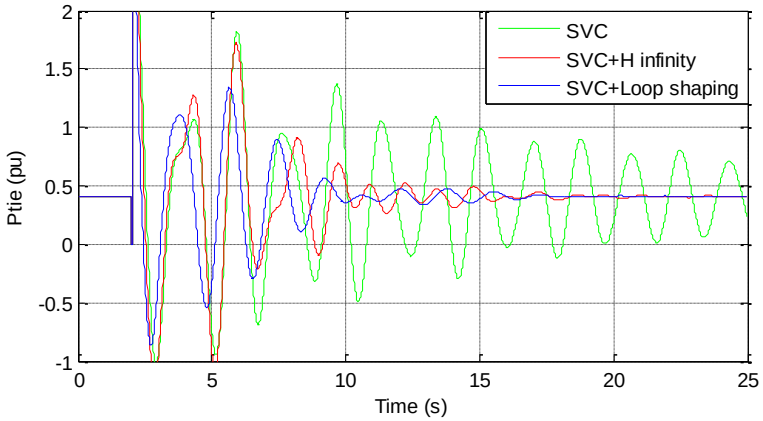

(g) 0.5MW tie-line, OP 3, fault at bus 52

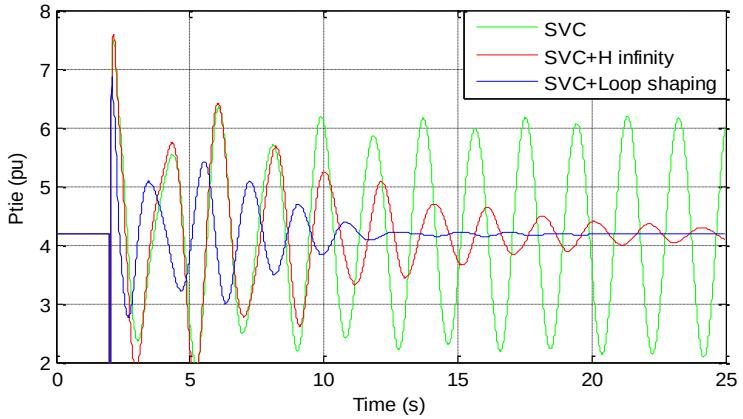

(h) 4.2MW tie-line, OP 4, fault at bus 52

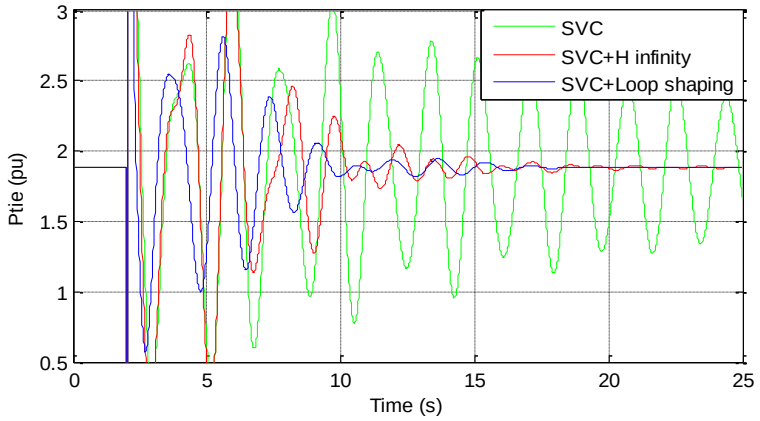

(i) 1.9MW tie-line, OP 5, fault at bus 52

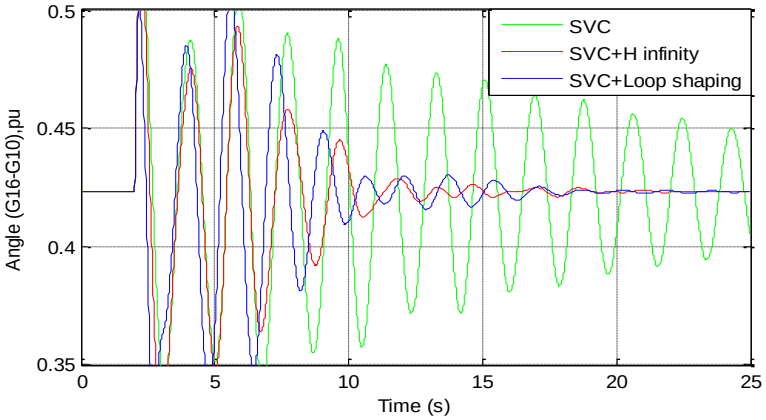

(j) Angle difference, OP 3, fault at bus 52

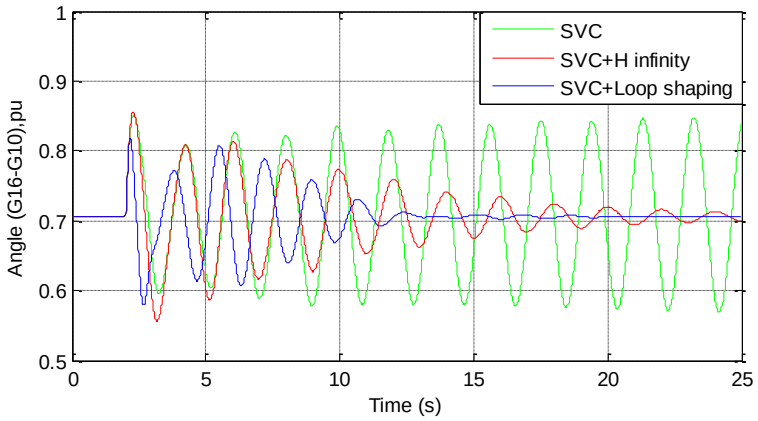

(k) Angle difference, OP 4, fault at bus 52

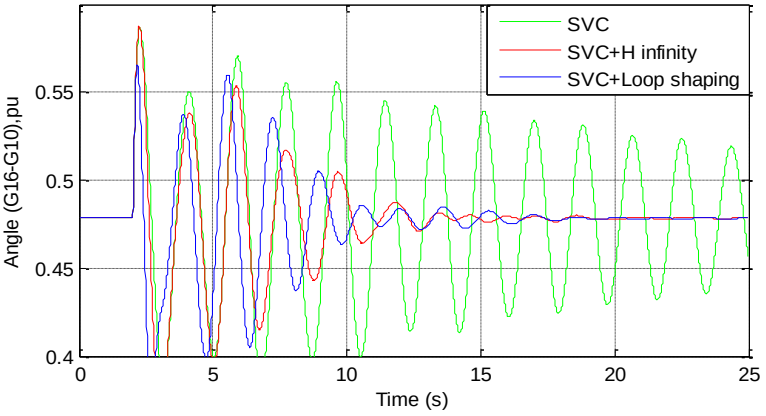

(l) Angle difference, OP 5, fault at bus 52

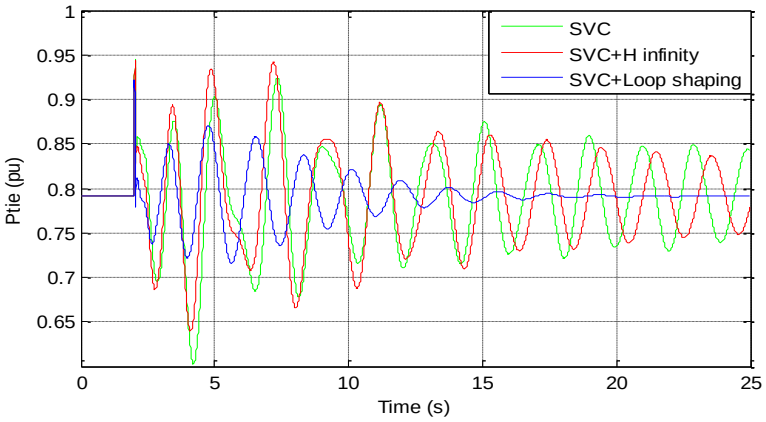

(m) 0.8MW tie-line, OP 3, fault at bus 38, trip line 46-49

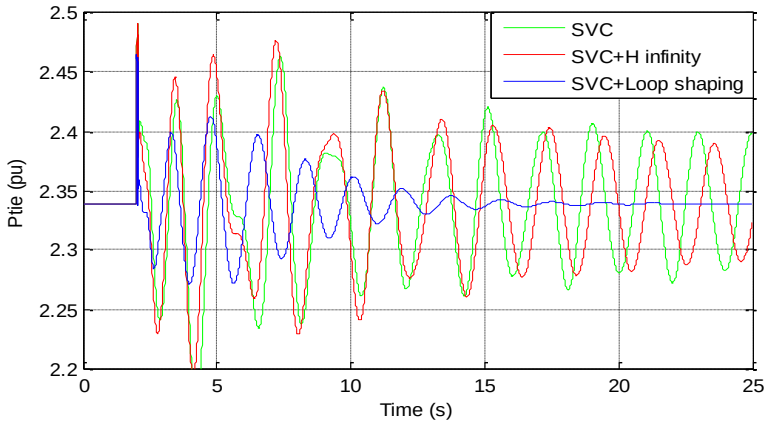

(n) 2.34MW tie-line, OP 5, fault at bus 38, trip line 46-49

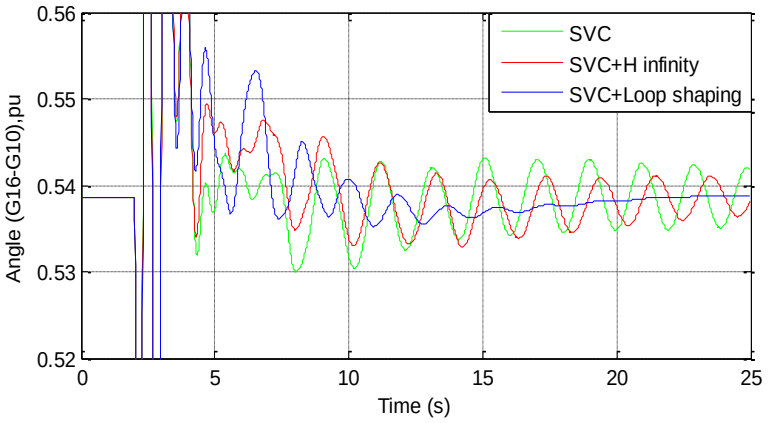

(o) Angle difference, OP3, fault at bus 38, trip line 46-49

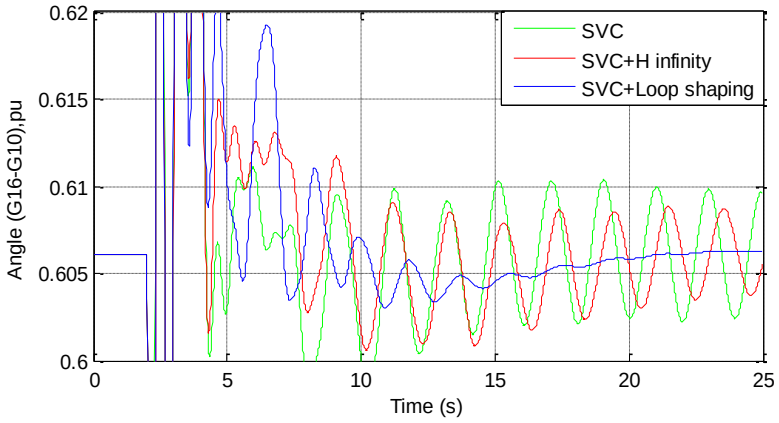

(p) Angle difference, OP5, fault at bus 38, trip line 46-49

Figure 4.6 Tie-line power and angle difference at varying load conditions, fault locations and changes in system topology

4.7.2.3 Eigenvalue Analysis

Table 4.7 summarized the damping ratios of the inter-area modes under different operating points with only SVC, SVC with the normal H_∞ and SVC with the proposed approach. The result shows that in all the scenarios the proposed approach is able to improve the damping ratio significantly and better than normal H_∞ .

Table 4.7 Damping and Frequencies of the Inter-Area Modes under Different Load Conditions

Operating point no.	*Mode no.*	*SVC*		*SVC with controller (H_∞)*		*SVC with controller (proposed approach)*	
		ξ	*f(Hz)*	ξ	*f(Hz)*	ξ	*f(Hz)*
1	Mode 1	0.01068	0.5363	0.10250	0.4819	0.1044	0.5057
	Mode 2	0.03420	0.7960	0.05454	0.8060	0.1863	0.8351
3	Mode 1	-0.00257	0.5268	0.05089	0.4991	0.1088	0.5147
	Mode 2	0.03111	0.7883	0.04761	0.7967	0.1367	0.7196
4	Mode 1	0.01188	0.5427	0.10280	0.4546	0.1122	0.4967
	Mode 2	0.03108	0.7875	0.05090	0.7934	0.1362	0.7201

4.8 Conclusion

A new method was introduced and implemented in this chapter to design a robust fixed-order loop-shaping controller. The controller is used to damp out the inter-area oscillations as an example. This approach is based on shaping the open-loop transfer function in the Nyquist diagram. The distance between the open-loop transfer function and the desired open-loop transfer function was minimized. The proposed controller was used to control an SVC on the two-area four- machines test system and 68 bus system. The advantages of using the proposed approach are as follows:

1- It considers the multi-model uncertainty.

2- It does not depend on selecting some weighting filters, thus making the controller design easier.

3- It deals with the entire plant model (large number of states) without reducing the plant and still leads to a low-order controller. For example, the controller for the 68 bus system with 190 states is also designed using the normal H_∞ approach and the order of the required controller was 9, whereas only the 4^{th}-order controller is needed in the proposed approach to achieve better performance.

Eigenvalue analysis is carried out for the two case studies. The proposed method showed promising results for damping the tie-line power oscillations under different operating points. In addition, the designed controller can maintain the stability of the system under topology changes. These changes make the system unstable without the controller.

CHAPTER FIVE

DATA DRIVEN CONTROL

5.1 Introduction

Controller design for a generic system can be broadly divided into two approaches based on the requirement of plant model:

1. The principles approach requires knowledge of the physics behind the system through which a mathematical model can be developed. Such a model of a power system can be described by a set of differential algebraic equations.
2. The data driven approach requires measured input/output data.

Most of the control approaches in literature that are used to damp inter-area oscillations are based on plant models (parametric models) [11, 30-35, 40] . However, it is difficult to find a parametric model for a large-scale power system based on a mathematical model. It becomes necessary to develop some control design techniques whereby the controller can be designed based only on input/output data.

If the physics behind a system is known and if a mathematical model to capture the phenomenon of interest exists, then the first approach is used. With respect to power systems, the modeling aspect can be divided into two separate subsystems: supply-side modeling and demand-side modeling. Supply-side modeling predominantly involves models for synchronous machines and their associated controls such as governor-turbine system and excitation system. Demand-side modeling, on the other hand, involves

modeling of consumer loads. Due to the sustained research efforts of researchers over the years, detailed supply-side models that capture phenomenon of different time scales of interest are available.

Demand-side modeling is an area that has captured the attention of researchers relatively recently. Nonetheless, significant advances have been made. For instance, the development of composite load models represents a step in that direction. The challenge, however, is the proper representation of these load models in a dynamic simulation model. This challenge is due to the fact that loads are represented as spot loads in a dynamic simulation model. Hence, the proportion of different load types that accurately captures the dynamic behavior of the system is at best a trial and error method. In addition, this proportion tends to change over time, as different types of loads are used at different times of day. As a result, matching the observed load behavior with the simulation model is a highly challenging task. On the other hand, the data-driven approach is a model-free approach that alleviates the requirement for such models.

The supplementary controller proposed in this work utilizes information from phasor measurement units (PMUs) to design a damping controller that sends supervisory signals to an installed SVC in the system [3, 19, 20]. This supplementary control signal improves the dynamic performance of the system through improved damping—the lack of which leads to sustained oscillation and eventually to blackouts.

The proposed approach requires remote signals, i.e. signals that are not at the same physical location as that of the SVC. Hence, any designed controller should address the issue of communication latency.

In this chapter a data-driven approach using input/output data is employed to design a fixed-order robust controller to damp inter-area oscillations and enhance power system stability. The proposed approach is based on frequency domain data. Frequency domain input/output data are common in several applications. Spectral models, which represent a function of frequency ω, can be simply identified from input/out data using Fourier Transform or spectral analysis. The proposed approach introduced in chapter four has been used in this chapter.

5.2 Problem Formulation

5.2.1 Class of models and controller

A model of a system can be represented as parametric or nonparametric; however, in this chapter a nonparametric model is considered. The plant model *G* in (5.1, see section 3.2.1.1) can be found from a set of input/output data by using spectral analysis [61, 66-68].

$$G = G_i(j\omega)[1 + W_{2i}(j\omega)\Delta]; \quad i = 1,2, \ldots\ldots, m \tag{5.1}$$

Assume a linear system as shown in Fig 5.1; such a system can be written in the discrete time as in (5.2).

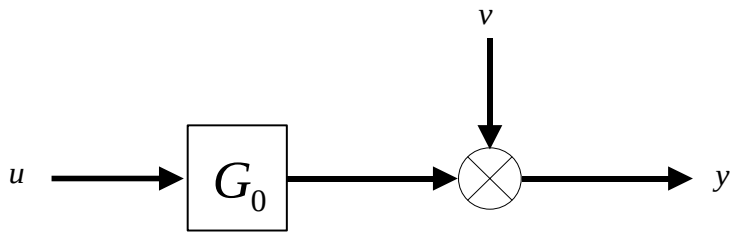

Figure 5.1 System representation

$$y(t) = G_0(t)u(t) + v(t) \tag{5.2}$$

where *v* is noise disturbance, *u* is the input signal, *y* is the output signal and G_0 is the discrete time transfer function.

The goal is to obtain frequency response of the test system based on a nonparametric model, i.e. time domain (input/output data). If the noise is ignored, the Fourier Transform of the system given in (5.1) can be written as:

$$Y(\omega) = G_0\left(e^{-j\omega T}\right)U(\omega) \tag{5.3}$$

thus

$$G_0\left(e^{-j\omega T}\right) = \frac{Y(\omega)}{U(\omega)} \tag{5.4}$$

The frequency response of the plane model $G_0\left(e^{-j\omega T}\right)$ can be estimated with Fourier Transform using *N* measurements input/output data as:

$$\acute{G_N}\left(e^{-j\omega T}\right) = \frac{Y_N(\omega)}{U_N(\omega)} \tag{5.5}$$

where

$$Y_N(\omega) = \frac{1}{\sqrt{N}}\sum_{t=1}^{N} y(t)e^{-j\omega t}$$

and

$$U_N(\omega) = \frac{1}{\sqrt{N}}\sum_{t=1}^{N} u(t)e^{-j\omega t}$$

However, in fact the measurement data has some noise, and it has to be considered. The estimator, including the disturbance noise, can be written as follows [61, 67]:

$$\acute{G_N}(e^{-j\omega T}) = G_0(e^{-j\omega T}) + \frac{V_N(\omega)}{U_N(\omega)} \tag{5.6}$$

The estimator $\acute{G_N}\left(e^{-j\omega T}\right)$ is unbiased, which means that the expectation of the effect of the noise *v(t) = 0*. The estimator is asymptotically uncorrelated, and the variance of this estimator is given by $\Phi_v(\omega)/\frac{1}{N}|U_N(\omega)|$. The noise *v(t)* in Fig. 5.1 can be estimated from (5.1) as $\acute{v}(t) = y(t) - G_0(z)u(t)$, and the spectrum of the noise $\Phi_v(\omega)$is given by

$$\grave{\Phi}_v(\omega) = \grave{\Phi}_y(\omega) - \frac{\left|\grave{\Phi}_{yu}(\omega)\right|^2}{\grave{\Phi}_u(\omega)}$$

This expression can be also written as follows:

$$\grave{\Phi}_v(\omega) = \grave{\Phi}_y(\omega) - \left[1 - \left(\grave{K}_{yu}(\omega)\right)^2\right] \tag{5.7}$$

in which

$$\grave{K}_{yu}(\omega) = \sqrt{\frac{\left|\grave{\Phi}_{yu}(\omega)\right|^2}{\grave{\Phi}_u(\omega)\grave{\Phi}_y(\omega)}}$$

Now, the model in (5.1) can be represented in the spectral model form by multiplicative uncertainty model as $G_0\left(e^{-j\omega T}\right)\left[1 + W_2\left((j\omega)\right)\Delta\right]$, where

$$W_2(j\omega) = \frac{1}{\acute{G_N}(e^{-j\omega T})}\sqrt{\frac{5.99\grave{\Phi}_v(\omega)}{2|U_N(\omega)|^2}}$$

The class of a controller can be low order such as the proportional-integral-derivative (PID) controller or high-order controller. The Laguerre function is a commonly used basis function as high-order controller and is shown in section (3.2).

5.3 Robust controller Constraints

The approach represented in chapter three (section 3.2) has been used to design the controller based on the identified model.

5.4 Controller design steps

The following steps can be followed to design a robust fixed-order controller:

1- Selecting inter-area modes that need to be damped, which are listed in Table 3.2 (see section 3.5).

2- Selecting input/output signals that ensure the damping of the inter-area modes. Such damping is achieved by using the controllability metric. It is very important to select appropriate input/output signals to ensure that the modes to be damped have a good controllability index.

3- Obtaining input/output data. To achieve the input/output data of the test system, the SVC has been excited by applying a Pseudo Random Binary Sequence (PRBS) signal with a given sampling time (*dt = 10ms)* on the input of the SVC. The output signal, which is the tie-line power, must be monitored. Fig. 5.1 shows the input/output identification data that is used to identify the plant model.

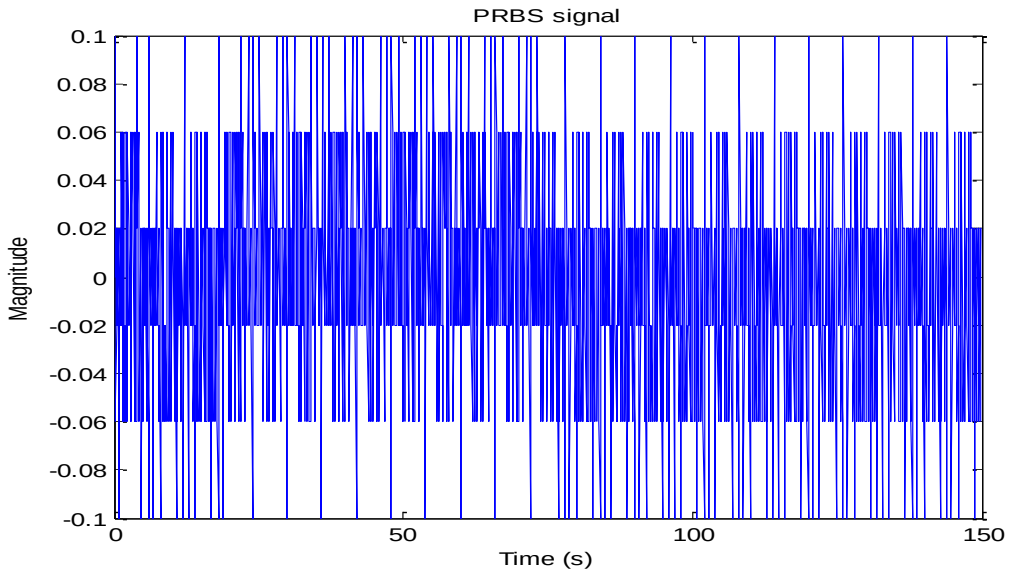

(a) PRBS signal (input signal).

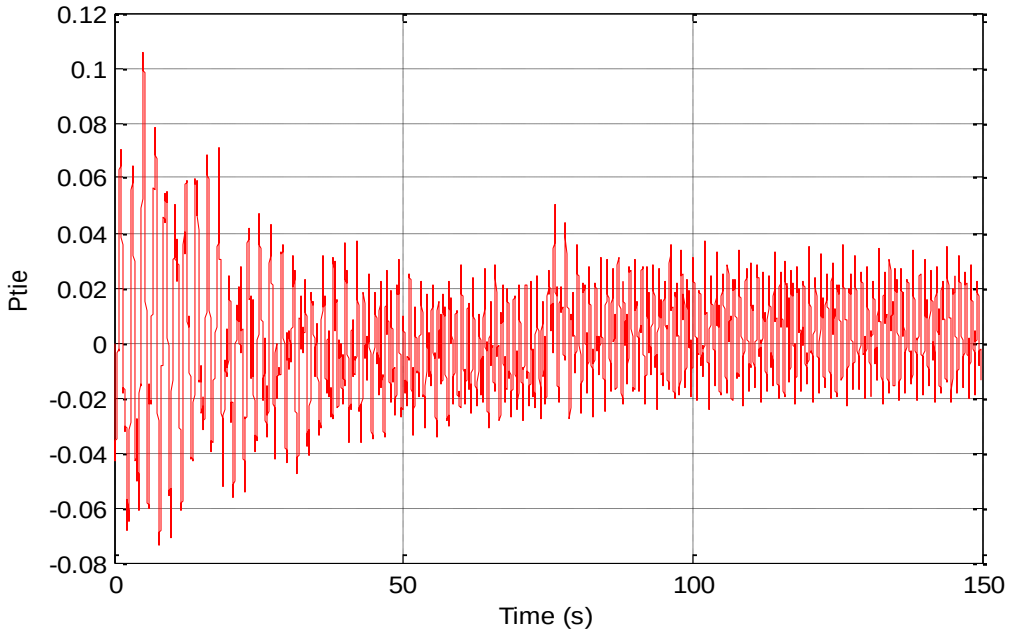

(b) Output signal

Figure 5.2 Input/output identification data

4- Identifying the plant model using MATLAB Identification Toolbox [69]. The identified model is compared with the original model to make sure that the identified model represents the original model. Fig. 5.2 (a) shows the frequency response of the original and the identified model, and it can be seen that they are identical in the range of frequency of interest, which means the identified model has the same response as the original one. The Eigenvalues of both models are obtained as shown in Fig 5.2 (b), and it is clear that they are matched. This identified model is used to design a fixed-order robust controller to damp the inter-area oscillations.

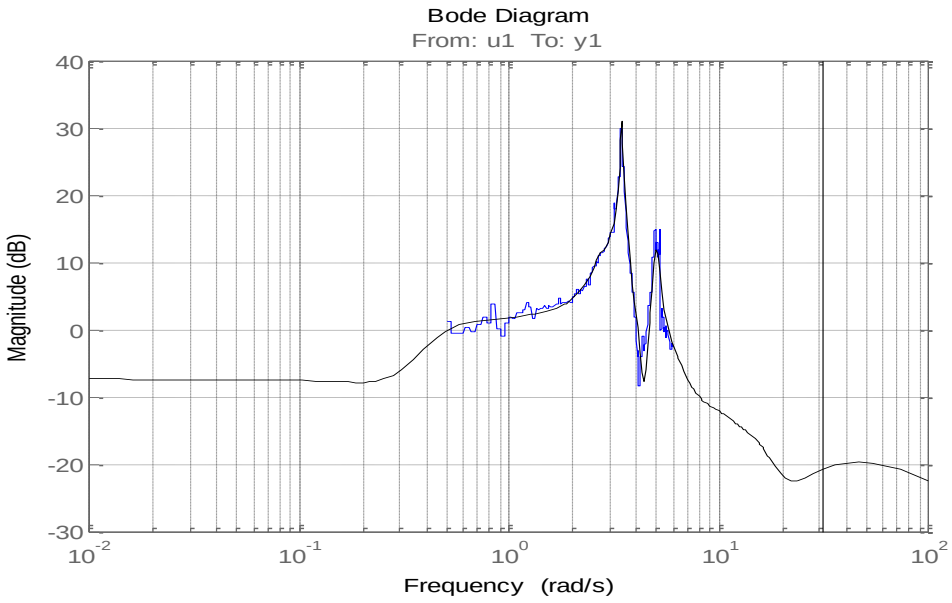

(a) Frequency response of the original and the identified model

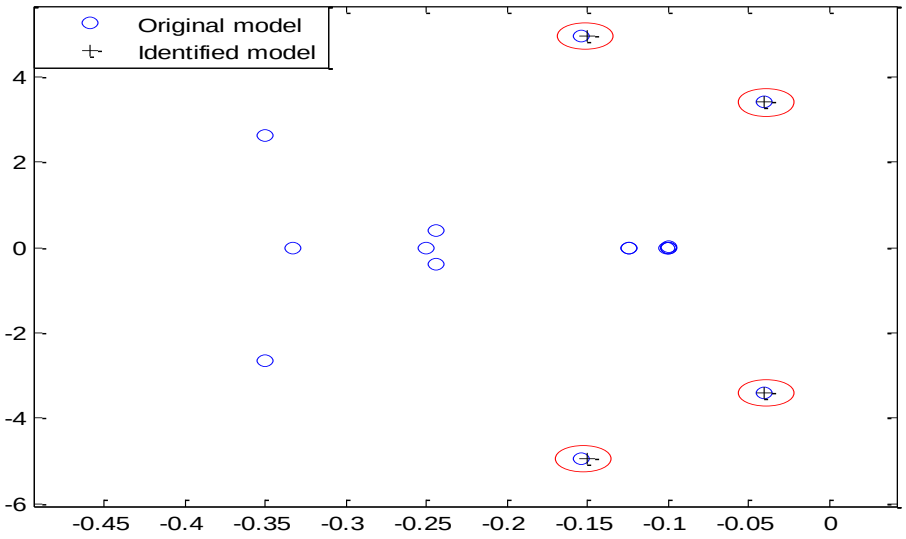

(b) Eigenvalue of the original and the identified model

Figure 5.3 Matching the original model with the identified model

The rest of the steps have already been explained in section (3.5).

5.5 Test system

The same test system that has been studied in chapter three is used here. Three phase fault is applied at different locations in the test system to test the response of the designed controller, as will be been shown in the results.

5.6 Simulation Results

To investigate the robustness of the proposed controller, three phase fault is placed at different areas with different operating points. Figures 5.4 (a) and (b) show the angle

difference between G16 and G10 under two different operating points (Op3 and 4) during three phase fault at bus 34. It can be see that the robust controller is able to damp the inter-area oscillations within a few seconds. The tie-line power at the same operating points is shown in Figure 5.4 (c) and (d); it is clear that the inter-area oscillations are damped out after adding the signal of the supplementary controller to the set point of the SVC.

Another scenario has been studied to investigate the robustness of the system including the controller. Three phase fault is applied at bus 49 and is cleared after 50ms. The results show that the controller is able to damp these oscillations under different load conditions as well as different locations as shown in Figures 5.5 (a)-(d).

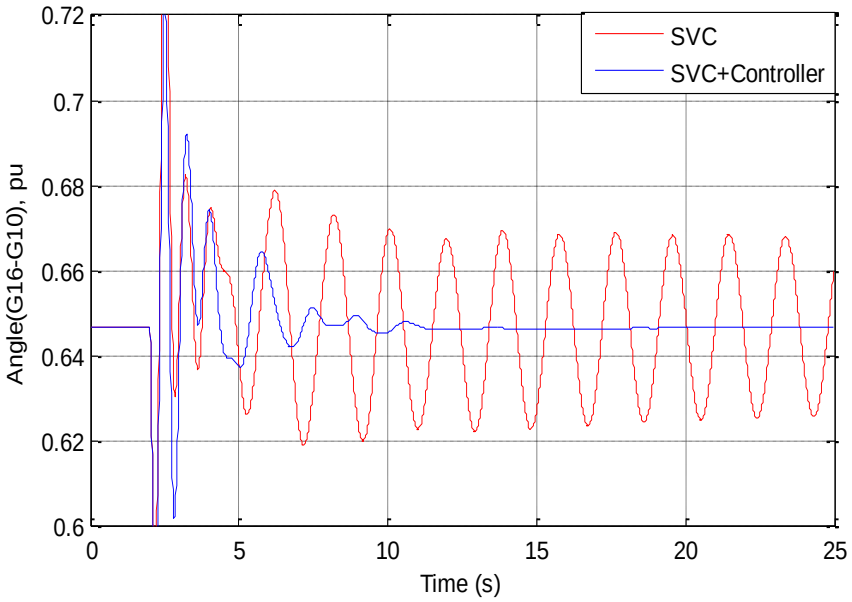

(a) Fault at 34-35, angle difference, G16 and G10, OP3

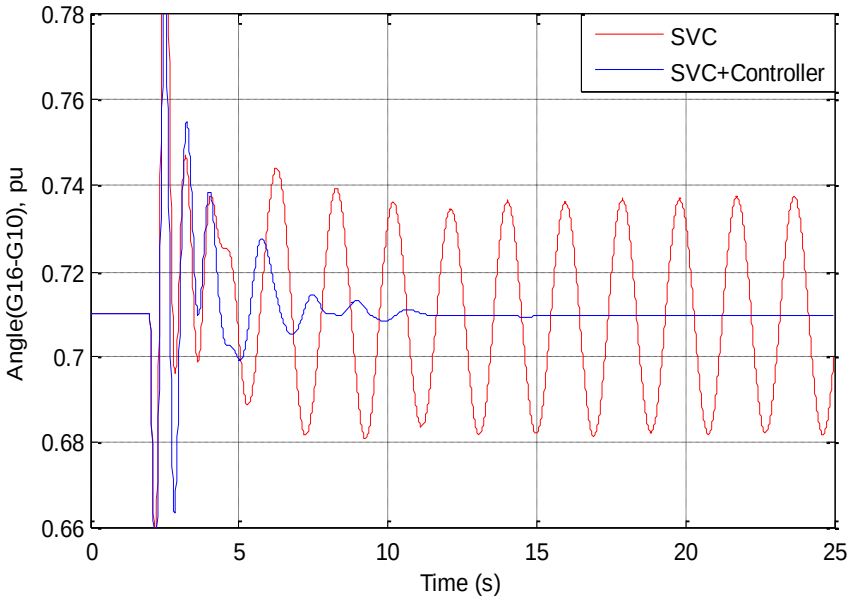

(b) Fault at 34-35, angle difference, G16 and G10, OP4

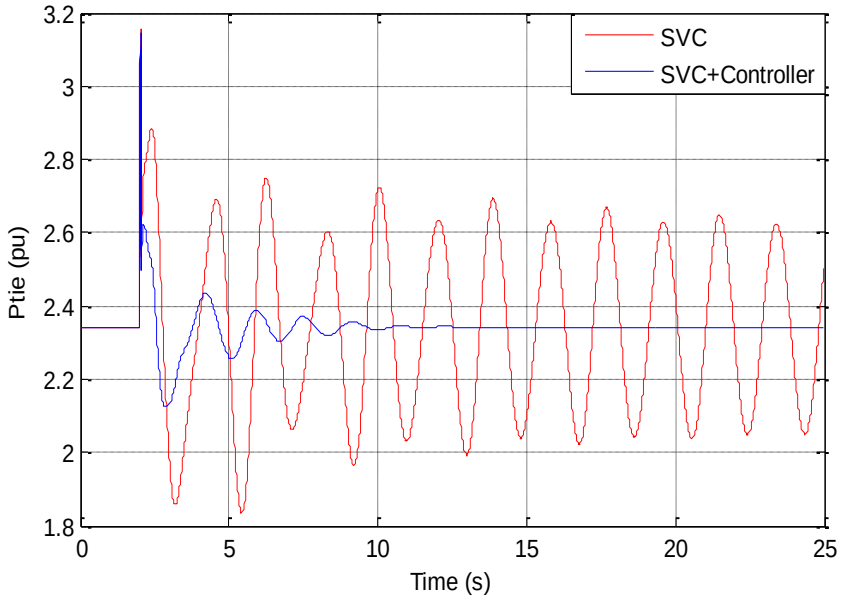

(c) Fault at 34-35, tie-line power, OP 3

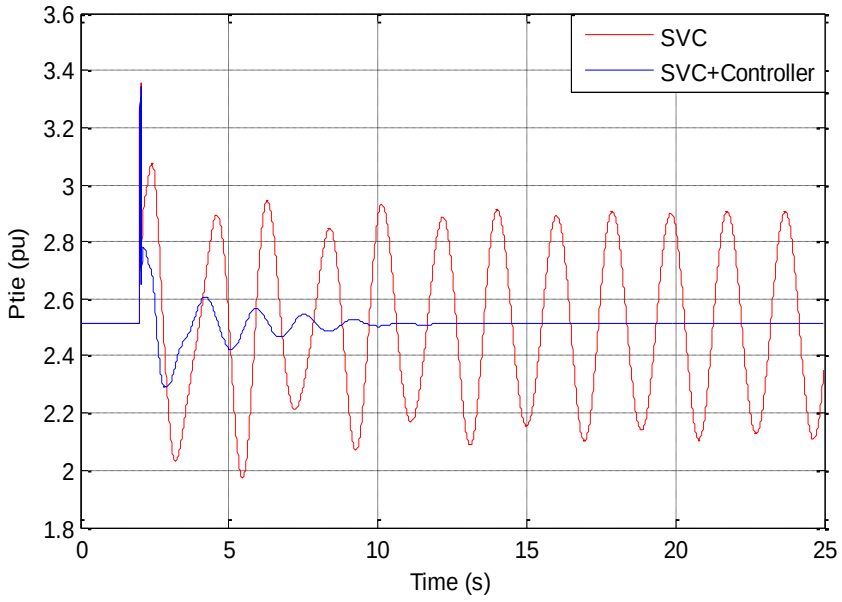

(d) Fault at 34, tie-line power, OP 4

Figure 5.4 Dynamic response of the system under three phase fault at bus 34 (Area 2)

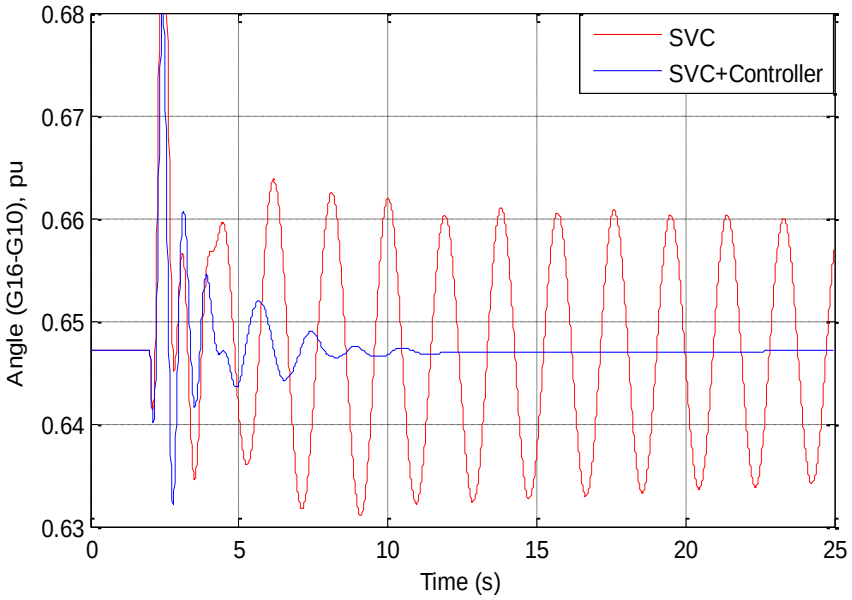

(a) Fault at 49-52 op3, Angle difference, G16 and G10, OP3

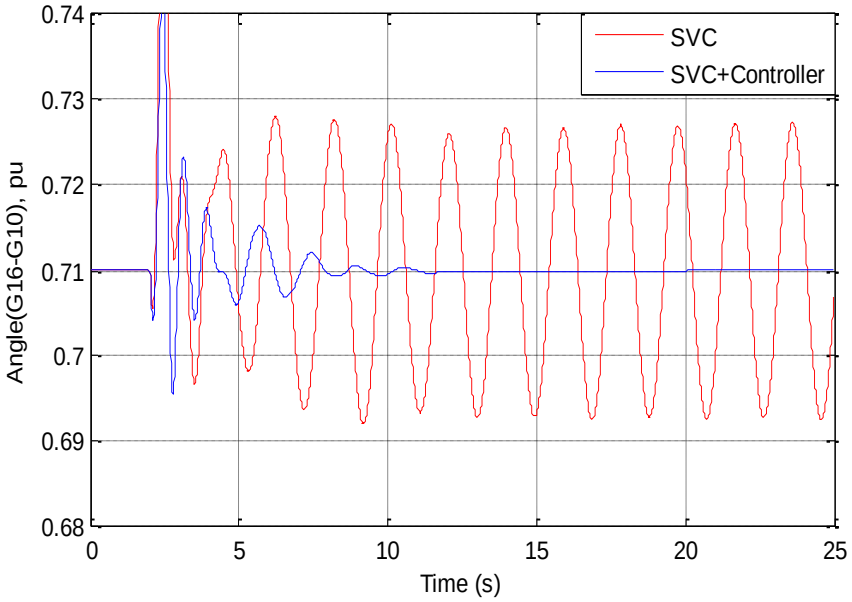

(b) Fault at 49-52 op4, Angle difference, G16 and G10, OP4

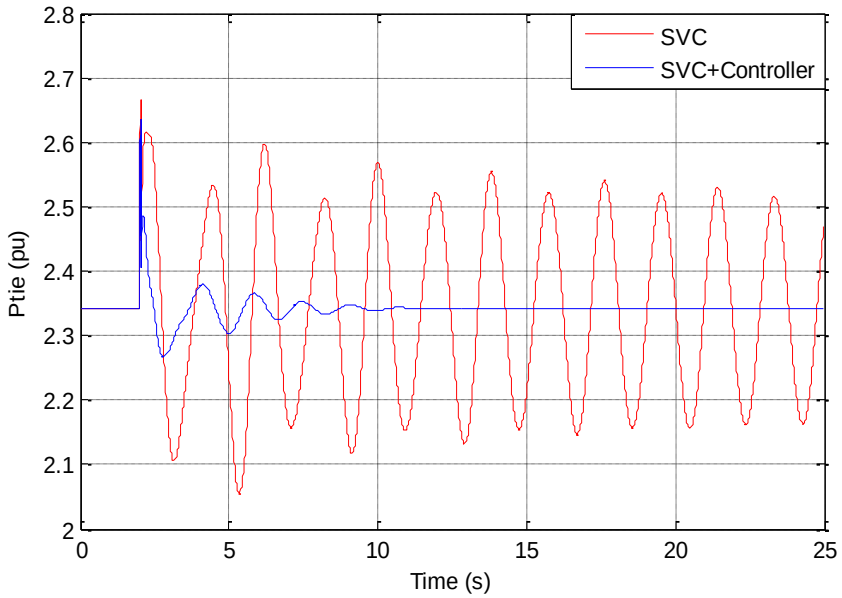

(c) Fault at 49-52 op3 Tie-line power, OP 3

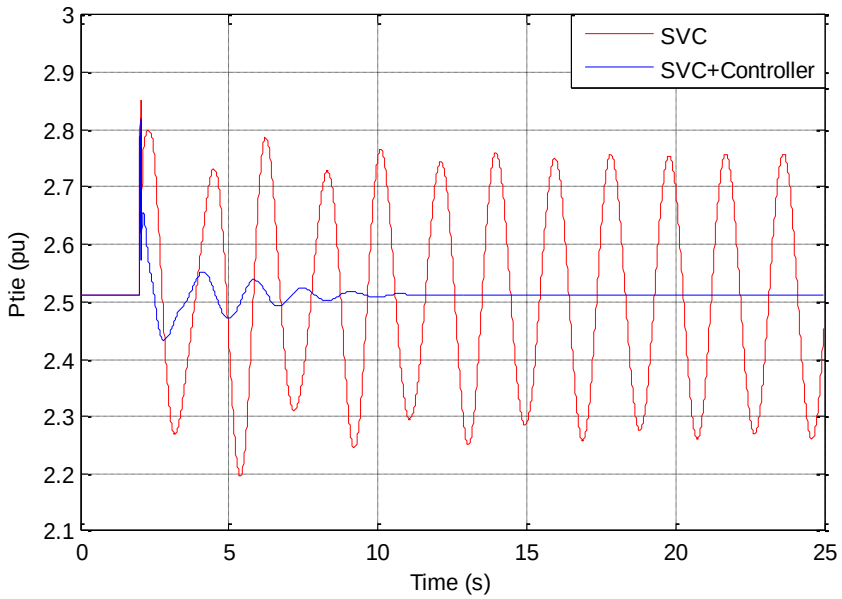

(d) Fault at 49-52 op4 Tie-line power, OP 4

Figure 5.5 Dynamic response of the system under three phase fault at bus 49 (Area 2)

5.7 Conclusion

In this chapter, the data driven controller approach is used to design a robust fixed-order controller to damp inter-area oscillations and maintain system stability. The data has been generated using PRBS function by exciting the set point of the SVC and monitoring the output signal. These data have been used to identify the spectral model using MATLAB Identification Toolbox. The dynamic response of the original model and the identified one has been investigated to make sure that they represent the same system (matching in the range of frequency of interest). The robust controller is designed based on the identified model, and different scenarios have been applied to test the robustness of the system with and without the controller. The IEEE 68 bus system is used as a test system. The results show that robustness can be achieved by adding a supplementary signal to the reference of the SVC.

CHAPTER SIX

CONCLUSION AND FUTURE WORK

6.1 Conclusion

In this dissertation, two approaches have been presented to design a fixed-order robust controller with the aim of damping inter-area oscillations and enhancing system stability. The designed fixed-order supplementary damping controller adjusts the voltage reference set point of SVC. These approaches are based on shaping the open-loop transfer function in the Nyquist diagram. The loop-shaping approach is based on shaping the open-loop transfer function by considering the phase and the gain margin on the Nyquist plot. The second approach is based on shaping the closed-loop sensitivity functions in the Nyquist plot under the $H\infty$ constraints. These constraints can be linearized by choosing a desired open-loop transfer function. The robust controller is designed to minimize the error between the open-loop transfer functions of the original and the desired plant model. This reduction can be achieved by using convex optimization methods. Convexity of the problem formulation ensures global optimality. The issue of delaying the feedback signal has been addressed using multi-model optimization.

The proposed approaches are compared with recent different existing techniques to design a robust controller; the result shows that the proposed approaches have some advantages over existing techniques.

The proposed controllers were used to control an SVC on the two-area four-machines test system and 68 bus system. The advantages of using the proposed approaches are listed below:

1- The multi-model uncertainty is considered, which means that the controller can be designed based on different operating scenarios, and by so doing, robustness is achieved for a wide range of operating points.
2- The loop-shaping approach is not dependent on selecting some weighting filters, which means controller design is easier.
3- The designed controller is fixed order, which means that the user can specify the order of the controller; it does not depend on the order of the system.
4- The entire plant model (large number of states) is dealt with without reducing the plant, yet still leads to a low-order controller. For example, the controller for the 68 bus system with 190 states is also designed using the normal H_∞ approach and the order of the required controller is 9, whereas only a 4th-order controller is needed when using the proposed approach to achieve better performance.
5- A fixed-order robust controller can be designed based only on frequency-domain data (obtained using spectral analysis of measured I/O data); no parametric model is required.

To investigate the robustness of the proposed controller, two-part validation of the proposed approaches is presented. Comparisons of the proposed method, both numerical and time-domain based, are made with the base case with only SVC and SVC with the controller. In the first part of validation, the Eigenvalue spectrum obtained using the

different methods is compared. Specifically, comparisons for damping ratios are drawn for different modes of interest. In the second part, time domain performance results are presented at different operating conditions and different fault locations. In addition, the effect of time delay on the remote signals has been considered, and the results show that the controller designed based on time delay improves the system dynamics and damping of inter-area oscillations; however, the controller which is designed without considering time delay is not able to handle large time delay (300ms).

The proposed methods showed promising results for damping the tie-line power oscillations under different operating points. In addition, the designed controller can maintain the stability of the system under topology changes. These changes make the system unstable without the controller in some cases.

6.2 Future Work

Future work focuses on the following:

1- In chapter five, a nonparametric model is used to design the robust controller based on frequency domain input/output data, and the effect of time delay has not been considered. A part of the future work will consider the issue of time delay signal and its effect on controller response.

2- Variable time-delay uncertainty as a stochastic variable in the stochastic optimization process. The use of variable time delay presents a more realistic case as communication channels have variable time delay wherein each data packet can have a different latency bounded by some observed lower and upper limit.

References

[1] P. Kundur, N. J. Balu, and M. G. Lauby, *Power system stability and control* vol. 7: McGraw-Hill New York, 1994.

[2] B. Pal and B. Chaudhuri, *Robust control in power systems*: Springer Science & Business Media, 2006.

[3] S. A. Al-Baiyat, "Design of a robust SVC damping controller using nonlinear H∞ technique," *Arabian Journal for Science and Engineering*, vol. 30, p. 66, 2005.

[4] F. Liu, Y. Li, M. Wu, Y. Zhou, and R. Yokoyama, "Robust wide-area damping controller design for inter-area oscillations with signals' delay," *IEEJ Transactions on Electrical and Electronic Engineering*, vol. 11, pp. 206-215, 2016.

[5] H. Shayeghi, H. Shayanfar, S. Jalilzadeh, and A. Safari, "TCSC robust damping controller design based on particle swarm optimization for a multi-machine power system," *Energy Conversion and Management*, vol. 51, pp. 1873-1882, 2010.

[6] A. Elices, L. Rouco, H. Bourles, and T. Margotin, "Design of robust controllers for damping interarea oscillations: Application to the European power system," *IEEE Transactions on Power Systems*, vol. 19, pp. 1058-1067, 2004.

[7] M. Abido, "Power system stability enhancement using FACTS controllers: A review," *The Arabian Journal for Science and Engineering*, vol. 34, pp. 153-172, 2009.

[8] E. Acha, C. R. Fuerte-Esquivel, H. Ambriz-Perez, and C. Angeles-Camacho, *FACTS: modelling and simulation in power networks*: John Wiley & Sons, 2004.

[9] B. Chaudhuri and B. C. Pal, "Robust damping of multiple swing modes employing global stabilizing signals with a TCSC," *IEEE Transactions on Power Systems,* vol. 19, pp. 499-506, 2004.

[10] J. Deng, C. Li, and X.-P. Zhang, "Coordinated design of multiple robust FACTS damping controllers: A BMI-based sequential approach with multi-model systems," *IEEE Transactions on Power Systems,* vol. 30, pp. 3150-3159, 2015.

[11] J. Deng and X.-P. Zhang, "Robust Damping Control of Power Systems With TCSC: A Multi-Model BMI Approach With H Performance," *IEEE Transactions on Power Systems,* vol. 29, pp. 1512-1521, 2014.

[12] N. G. Hingorani, "FACTS-flexible AC transmission system," *AC and DC Power Transmission, 1991, International Conference,* pp. 1-7, 1991.

[13] N. G. Hingorani, "Flexible AC transmission," *IEEE spectrum,* vol. 30, pp. 40-45, 1993.

[14] Y. Li, C. Rehtanz, S. Ruberg, L. Luo, and Y. Cao, "Wide-area robust coordination approach of HVDC and FACTS controllers for damping multiple interarea oscillations," *IEEE transactions on power delivery,* vol. 27, pp. 1096-1105, 2012.

[15] F. Liu, R. Yokoyama, Y. Zhou, and M. Wu, "TCSC wide-area damping controller to enhance the damping of inter-area oscillation for power systems with considering the time delay of wide-area signals," in *Power System Technology (POWERCON), 2010 International Conference,* pp. 1-6, 2010.

[16] R. Majumder, B. C. Pal, C. Dufour, and P. Korba, "Design and real-time implementation of robust FACTS controller for damping inter-area oscillation," *IEEE Transactions on Power Systems,* vol. 21, pp. 809-816, 2006.

[17] R. M. Mathur and R. K. Varma, *Thyristor-based FACTS controllers for electrical transmission systems*: John Wiley & Sons, 2002.

[18] P. Pourbeik and M. J. Gibbard, "Simultaneous coordination of power system stabilizers and FACTS device stabilizers in a multimachine power system for enhancing dynamic performance," *IEEE Transactions on Power Systems,* vol. 13, pp. 473-479, 1998.

[19] P. S. Rao and I. Sen, "A QFT-based robust SVC controller for improving the dynamic stability of power systems," *Electric Power Systems Research,* vol. 46, pp. 213-219, 1998.

[20] S. Robak, "Robust SVC controller design and analysis for uncertain power systems," *Control Engineering Practice,* vol. 17, pp. 1280-1290, 2009.

[21] K. M. Son and J. K. Park, "On the robust LQG control of TCSC for damping power system oscillations," *IEEE Transactions on Power Systems,* vol. 15, pp. 1306-1312, 2000.

[22] Y.-H. Song and A. Johns, *Flexible ac transmission systems (FACTS)*: IET, 1999.

[23] W. Yao, L. Jiang, J. Wen, Q. Wu, and S. Cheng, "Wide-area damping controller of FACTS devices for inter-area oscillations considering communication time delays," *IEEE Transactions on Power Systems,* vol. 29, pp. 318-329, 2014.

[24] M. Yue and R. Schlueter, "A μ-synthesis robust SVC control design," *Transmission and Distribution Conference and Exposition, 2003 IEEE PES*, pp. 705-710, 2003.

[25] Q. Zhao and J. Jiang, "Robust SVC controller design for improving power system damping," *IEEE Transactions on Power Systems*, vol. 10, pp. 1927-1932, 1995.

[26] Q. Zhao and J. Jiang, "A TCSC damping controller design using robust control theory," *International Journal of Electrical Power & Energy Systems*, vol. 20, pp. 25-33, 1998.

[27] C. Shankaralingappa and S. H. Jangamashetti, "FACTS controllers to improve voltage profile and enhancement of line loadability in EHV long transmission lines," *Power System Technology and IEEE Power India Conference, 2008. POWERCON 2008. Joint International Conference*, pp. 1-5, 2008.

[28] A. Abdlrahem, P. Saraf, K. Balasubramaniam, R. Hadidi, A. Karimi, and E. Makram, "Design of a Fixed-Order Robust Controller to Damp Inter-Area Oscillations in Power Systems," *Journal of Power and Energy Engineering*, vol. 4, p. 61, 2016.

[29] A. Abdlrahem, P. Saraf, R. Hadidi, A. Karimi, H. Sherwali, and E. Makram, "Design of a fixed-order robust controller using loop shaping method for damping inter-area oscillations in power systems," *2016 IEEE Power and Energy Conference at Illinois (PECI)*, pp. 1-6, 2016.

[30] B. Chaudhuri, B. C. Pal, A. C. Zolotas, I. M. Jaimoukha, and T. C. Green, "Mixed-sensitivity approach to H∞ control of power system oscillations

employing multiple FACTS devices," *IEEE Transactions on Power Systems*, vol. 18, pp. 1149-1156, 2003.

[31] M. Farsangi, Y. Song, and M. Tan, "Multi-objective design of damping controllers of FACTS devices via mixed H 2/H∞ with regional pole placement," *International journal of electrical power & energy systems*, vol. 25, pp. 339-346, 2003.

[32] S. Georges, M. Rita, and P.-D. Maria, "Mixed sensitivity H∞ control of doubly fed induction motor," *2007 IEEE International Symposium on Industrial Electronics*, pp. 1300-1304, 2007.

[33] M. J. Khosrowjerdi, R. Nikoukhah, and N. Safari-Shad, "A mixed H2/H∞ approach to simultaneous fault detection and control," *Automatica*, vol. 40, pp. 261-267, 2004.

[34] M. Klein, L. Le, G. Rogers, S. Farrokhpay, and N. Balu, "H {sub {infinity}} damping controller design in large power systems," *IEEE Transactions on Power Systems*, vol. 10, 1995.

[35] E. Prempain, I. Postlethwaite, and X. Sun, "Robust control of the gasifier using a mixed-sensitivity H∞ approach," *Proceedings of the Institution of Mechanical Engineers, Part I: Journal of Systems and Control Engineering*, vol. 214, pp. 415-427, 2000.

[36] A. Sil, T. Gangopadhyay, S. Paul, and A. Maitra, "Design of robust power system stabilizer using H∞ mixed sensitivity technique," *Power Systems, 2009. ICPS'09. International Conference*, pp. 1-4, 2009.

[37] P. Gahinet and P. Apkarian, "A linear matrix inequality approach to H∞ control," *International journal of robust and nonlinear control*, vol. 4, pp. 421-448, 1994.

[38] C. Zhu, M. Khammash, V. Vittal, and W. Qiu, "Robust power system stabilizer design using H∞ loop shaping approach," *IEEE Transactions on Power Systems*, vol. 18, pp. 810-818, 2003.

[39] B. C. Pal, A. H. Coonick, I. M. Jaimoukha, and H. El-Zobaidi, "A linear matrix inequality approach to robust damping control design in power systems with superconducting magnetic energy storage device," *IEEE Transactions on power systems*, vol. 15, pp. 356-362, 2000.

[40] B. Chaudhuri, R. Majumder, and B. C. Pal, "Wide-area measurement-based stabilizing control of power system considering signal transmission delay," *IEEE Transactions on Power Systems*, vol. 19, pp. 1971-1979, 2004.

[41] D. Dotta, A. S. e Silva, and I. C. Decker, "Wide-area measurements-based two-level control design considering signal transmission delay," *IEEE Transactions on Power Systems*, vol. 24, pp. 208-216, 2009.

[42] P. Saraf, R. Hadidi, and E. Makram, "Partial right eigenstructure assignment based mode selective damping in a power system," in *North American Power Symposium (NAPS), 2015*, pp. 1-5, 2015.

[43] Z. Duan, C. Zhang, Z. Hu, and Y. Zhang, "Robust control of interconnected power system based on wams considering signals transmission delay," *2009 Asia-Pacific Power and Energy Engineering Conference*, pp. 1-4, 2009.

[44] E. Ghahremani and I. Kamwa, "Joint improvement of system loadability and stability through a multi-stage planning of a UPFC with a PMU-based supplementary damping control," *2013 IEEE Power & Energy Society General Meeting*, pp. 1-5, 2013.

[45] R. Preece, J. V. Milanović, A. M. Almutairi, and O. Marjanovic, "Damping of inter-area oscillations in mixed AC/DC networks using WAMS based supplementary controller," *IEEE Transactions on Power Systems*, vol. 28, pp. 1160-1169, 2013.

[46] J. W. Stahlhut, T. J. Browne, G. T. Heydt, and V. Vittal, "Latency viewed as a stochastic process and its impact on wide area power system control signals," *IEEE Transactions on Power Systems*, vol. 23, pp. 84-91, 2008.

[47] H. Wu, Q. Wang, and X. Li, "PMU-based wide area damping control of power systems," *Power System Technology and IEEE Power India Conference, 2008. POWERCON 2008. Joint International Conference*, pp. 1-4, 2008.

[48] X. Xie, Y. Xin, J. Xiao, J. Wu, and Y. Han, "WAMS applications in Chinese power systems," *IEEE Power and Energy Magazine*, vol. 4, pp. 54-63, 2006.

[49] F. R. P. Safaei, S. G. Ghiocel, J. P. Hespanha, and J. H. Chow, "Stability of an adaptive switched controller for power system oscillation damping using remote synchrophasor signals," *53rd IEEE Conference on Decision and Control*, pp. 1695-1700, 2014.

[50] E. O. Schweitzer III, D. Whitehead, K. Fodero, and P. Robertson, "Merging SONET and Ethernet Communications for Power System Applications,"

Proceedings of the 38th Annual Western Protective Relay Conference, Spokane, WA, 2011.

[51] A. Karimi, "Frequency-domain robust control toolbox," *52nd IEEE Conference on Decision and Control*, pp. 3744-3749, 2013.

[52] Y. Zhang, "Design of wide-area damping control systems for power system low-frequency inter-area oscillations," Washington State University, 2007.

[53] J. Slootweg, H. Polinder, and W. Kling, "Dynamic modelling of a wind turbine with doubly fed induction generator," *Power Engineering Society Summer Meeting, 2001*, pp. 644-649, 2001.

[54] S. Heier, *Grid Integration of Wind Energy*, John Wiley & Sons, 520pp, 2014.

[55] A. Luna, F. d. A. Lima, D. Santos, P. Rodríguez, E. H. Watanabe, and S. Arnaltes, "Simplified modeling of a DFIG for transient studies in wind power applications," *IEEE Transactions on Industrial Electronics*, vol. 58, pp. 9-20, 2011.

[56] J. Slootweg, H. Polinder, and W. Kling, "Representing wind turbine electrical generating systems in fundamental frequency simulations," *IEEE Transactions on energy conversion*, vol. 18, pp. 516-524, 2003.

[57] G. Galdos, A. Karimi, and R. Longchamp, "H∞ controller design for spectral MIMO models by convex optimization," *Journal of Process Control*, vol. 20, pp. 1175-1182, 2010.

[58] G. Galdos Sanz de Galdeano, "Fixed-Order Robust Controller Design by Convex Optimization Using Spectral Models," 2010.

[59] A. Karimi and G. Galdos, "Fixed-order H∞ controller design for nonparametric models by convex optimization," *Automatica,* vol. 46, pp. 1388-1394, 2010.

[60] A. Karimi, G. Galdos, and R. Longchamp, "Robust fixed-order H∞ controller design for spectral models by convex optimization," *Decision and Control, 2008. CDC 2008. 47th IEEE Conference,* pp. 921-926, 2008.

[61] L. Ljung, "System Identification: Theory for the user," *Englewood Cliffs,* 1987.

[62] S. Skogestad and I. Postlethwaite, *Multivariable feedback control: analysis and design,* vol. 2: Wiley New York, 2007.

[63] J. Chow and G. Rogers, "Power system toolbox," *Cherry Tree Scientific Software,[Online] Available: http://www.ecse.rpi.edu/pst/PST. html,* vol. 48, p. 53, 2000.

[64] F. Milano, "An open source power system analysis toolbox," *IEEE Transactions on Power systems,* vol. 20, pp. 1199-1206, 2005.

[65] H. G. Far, H. Banakar, P. Li, C. Luo, and B.-T. Ooi, "Damping interarea oscillations by multiple modal selectivity method," *IEEE Transactions on Power Systems,* vol. 24, pp. 766-775, 2009.

[66] H. Wu, K. S. Tsakalis, and G. T. Heydt, "Evaluation of time delay effects to wide-area power system stabilizer design," *IEEE Transactions on Power Systems,* vol. 19, pp. 1935-1941, 2004.

[67] L. Ljung, "State of the art in linear system identification: Time and frequency domain methods," *American Control Conference, 2004. Proceedings of the 2004*, pp. 650-660, 2004.

[68] J. Taylor, "Robust Bode Methods for Feedback Controller Design of Uncertain Systems," 2014.

[69] L. Ljung, "System identification toolbox for use with {MATLAB}," 2007.

APPENDIX: IEEE 68 Bus System Data

Table A. 1 Bus data

Bus #	V (pu)	Angle (degree)	P_{gen}(pu)	Q_{gen}(pu)	P_{load}(pu)	Q_{load}(pu)	G_{shunt}(pu)
1	1.0634	7.1886	0	0	2.527	1.1856	0
2	1.0612	8.5706	0	0	0	0	0
3	1.0479	6.4222	0	0	3.22	0.02	0
4	1.034	7.5027	0	0	5	0.736	0
5	1.0338	8.3774	0	0	0	0	0
6	1.0342	8.9999	0	0	0	0	0
7	1.0291	6.9114	0	0	2.34	0.84	0
8	1.0311	6.4639	0	0	5.22	1.77	0
9	1.0441	3.7966	0	0	1.04	1.25	0
10	1.0375	11.182	0	0	0	0	0
11	1.0353	10.4313	0	0	0	0	0
12	0.9603	10.3784	0	0	0.09	0.88	0
13	1.0355	10.4512	0	0	0	0	0
14	1.0345	8.7404	0	0	0	0	0
15	1.0285	7.1708	0	0	3.2	1.53	0
16	1.0412	8.1345	0	0	3.29	0.32	0
17	1.0452	6.9648	0	0	0	0	0
18	1.0448	6.3019	0	0	1.58	0.3	0
19	1.054	12.7894	0	0	0	0	0
20	0.9937	11.5884	0	0	6.8	1.03	0
21	1.0375	10.5158	0	0	2.74	1.15	0
22	1.0532	15.0855	0	0	0	0	0
23	1.0477	14.744	0	0	2.48	0.85	0
24	1.0461	8.1757	0	0	3.09	-0.92	0
25	1.0639	9.6436	0	0	2.24	0.47	0
26	1.0602	7.6868	0	0	1.39	0.17	0
27	1.049	6.1244	0	0	2.81	0.76	0
28	1.0534	10.1063	0	0	2.06	0.28	0
29	1.052	12.6876	0	0	2.84	0.27	0
30	1.0577	6.8518	0	0	0	0	0
31	1.06	9.2447	0	0	0	0	0
32	1.052	11.494	0	0	0	0	0
33	1.057	7.9358	0	0	1.12	0	0

34	1.0657	2.9585	0	0	0	0	0
35	1.014	2.9166	0	0	0	0	0
36	1.0434	-0.3978	0	0	1.02	-0.1946	0
37	1.0294	-6.6793	0	0	60	3	0
38	1.0574	9.2134	0	0	0	0	0
39	1.0048	-8.3421	0	0	2.67	0.126	0
40	1.0657	14.9468	0	0	0.6563	0.2353	0
41	0.9993	44.8398	0	0	10	2.5	0
42	0.9991	39.6162	0	0	11.5	2.5	0
43	1.0142	-7.5187	0	0	0	0	0
44	1.0136	-7.5503	0	0	2.6755	0.0484	0
45	1.0168	2.7999	0	0	2.08	0.21	0
46	1.0322	10.077	0	0	1.507	0.285	0
47	1.0752	7.2969	0	0	2.0312	0.3259	0
48	1.0763	8.9727	0	0	2.412	0.022	0
49	1.0105	13.3573	0	0	1.64	0.29	0
50	1.0097	19.9016	0	0	1	-1.47	0
51	1.0207	6.8256	0	0	3.37	-1.22	0
52	0.9931	39.5554	0	0	24.7	1.23	0
53	1.045	10.852	2.5	0.6383	0	0	0
54	0.98	16.2167	5.45	0.9506	0	0	0
55	0.983	18.0233	6.5	1.1464	0	0	0
56	0.997	17.3346	6.32	0.9037	0	0	0
57	1.011	16.6598	5.052	1.4688	0	0	0
58	1.05	20.1518	7	2.0445	0	0	0
59	1.063	22.5822	5.6	0.8783	0	0	0
60	1.03	16.0538	5.4	-0.2074	0	0	0
61	1.025	19.1731	8	-0.0461	0	0	0
62	1.01	15.9493	5	-0.0941	0	0	0
63	1	18.3175	10	-0.3645	0	0	0
64	1.0156	4.8734	15.5	2.4363	0	0	0
65	1.011	0	38.1482	9.2781	0	0	0
66	1	46.3751	20.85	0.6926	0	0	0
67	1	40.4764	5	0.6617	0	0	0
68	1	46.4959	40	4.739	0	0	0
70	1	0	0	0	-5	-0.05	0

Bus #	B shunt (pu)	Bus Type	Q_{gen_max}(pu)	Q_{gen_min}(pu)	V_{rated} (kV)	V_{max} pu	V_{min} pu
1	0	3	0	0	345	1.1	0.9
2	0	3	0	0	345	1.1	0.9
3	0	3	0	0	345	1.1	0.9
4	0	3	0	0	345	1.1	0.9
5	0	3	0	0	345	1.1	0.9
6	0	3	0	0	345	1.1	0.9
7	0	3	0	0	345	1.1	0.9
8	0	3	0	0	345	1.1	0.9
9	0	3	0	0	345	1.1	0.9
10	0	3	0	0	345	1.1	0.9
11	0	3	0	0	345	1.1	0.9
12	0	3	0	0	345	1.1	0.9
13	0	3	0	0	345	1.1	0.9
14	0	3	0	0	345	1.1	0.9
15	0	3	0	0	345	1.1	0.9
16	0	3	0	0	345	1.1	0.9
17	0	3	0	0	345	1.1	0.9
18	0	3	0	0	345	1.1	0.9
19	0	3	0	0	345	1.1	0.9
20	0	3	0	0	345	1.1	0.9
21	0	3	0	0	345	1.1	0.9
22	0	3	0	0	345	1.1	0.9
23	0	3	0	0	345	1.1	0.9
24	0	3	0	0	345	1.1	0.9
25	0	3	0	0	345	1.1	0.9
26	0	3	0	0	345	1.1	0.9
27	0	3	0	0	345	1.1	0.9
28	0	3	0	0	345	1.1	0.9
29	0	3	0	0	345	1.1	0.9
30	0	3	0	0	345	1.1	0.9
31	0	3	0	0	345	1.1	0.9
32	0	3	0	0	345	1.1	0.9
33	0	3	0	0	345	1.1	0.9
34	0	3	0	0	345	1.1	0.9
35	0	3	0	0	345	1.1	0.9
36	0	3	0	0	345	1.1	0.9
37	0	3	0	0	345	1.1	0.9

38	0	3	0	0	345	1.1	0.9
39	0	3	0	0	345	1.1	0.9
40	0	3	0	0	345	1.1	0.9
41	0	3	0	0	345	1.1	0.9
42	0	3	0	0	345	1.1	0.9
43	0	3	0	0	345	1.1	0.9
44	0	3	0	0	345	1.1	0.9
45	0	3	0	0	345	1.1	0.9
46	0	3	0	0	345	1.1	0.9
47	0	3	0	0	345	1.1	0.9
48	0	3	0	0	345	1.1	0.9
49	0	3	0	0	345	1.1	0.9
50	0	3	0	0	345	1.1	0.9
51	0	3	0	0	345	1.1	0.9
52	0	3	0	0	345	1.1	0.9
53	0	2	999	-999	22	1.1	0.9
54	0	2	999	-999	22	1.1	0.9
55	0	2	999	-999	22	1.1	0.9
56	0	2	999	-999	22	1.1	0.9
57	0	2	999	-999	22	1.1	0.9
58	0	2	999	-999	22	1.1	0.9
59	0	2	999	-999	22	1.1	0.9
60	0	2	999	-999	22	1.1	0.9
61	0	2	999	-999	22	1.1	0.9
62	0	2	999	-999	22	1.1	0.9
63	0	2	999	-999	22	1.1	0.9
64	0	2	999	-999	22	1.1	0.9
65	0	1	0	0	345	1.1	0.9
66	0	2	999	-999	345	1.1	0.9
67	0	2	999	-999	345	1.1	0.9
68	0	2	999	-999	345	1.1	0.9
70	0	3	0	0	69	1.2	0.8

Table A. 2 Line data

From bus	To bus	Resistance (pu)	Reactance (pu)	Line charging (pu)	Tap ratio	Tap phase	Tap max	Tap min	Tap size
36	37	0.0005	0.0045	0.32	1	0	0	0	0
49	52	0.0076	0.1141	1.16	1	0	0	0	0
16	19	0.0016	0.0195	0.304	1	0	0	0	0
16	21	0.0008	0.0135	0.2548	1	0	0	0	0
21	22	0.0008	0.014	0.2565	1	0	0	0	0
22	23	0.0006	0.0096	0.1846	1	0	0	0	0
23	24	0.0022	0.035	0.361	1	0	0	0	0
16	24	0.0003	0.0059	0.068	1	0	0	0	0
2	25	0.007	0.0086	0.146	1	0	0	0	0
25	26	0.0032	0.0323	0.531	1	0	0	0	0
17	27	0.0013	0.0173	0.3216	1	0	0	0	0
26	27	0.0014	0.0147	0.2396	1	0	0	0	0
26	28	0.0043	0.0474	0.7802	1	0	0	0	0
26	29	0.0057	0.0625	1.029	1	0	0	0	0
28	29	0.0014	0.0151	0.249	1	0	0	0	0
1	30	0.0008	0.0074	0.48	1	0	0	0	0
9	30	0.0019	0.0183	0.29	1	0	0	0	0
9	30	0.0019	0.0183	0.29	1	0	0	0	0
30	31	0.0013	0.0187	0.333	1	0	0	0	0
1	31	0.0016	0.0163	0.25	1	0	0	0	0
30	32	0.0024	0.0288	0.488	1	0	0	0	0
32	33	0.0008	0.0099	0.168	1	0	0	0	0
33	34	0.0011	0.0157	0.202	1	0	0	0	0
34	36	0.0033	0.0111	1.45	1	0	0	0	0
9	36	0.0022	0.0196	0.34	1	0	0	0	0
9	36	0.0022	0.0196	0.34	1	0	0	0	0
16	17	0.0007	0.0089	0.1342	1	0	0	0	0
31	38	0.0011	0.0147	0.247	1	0	0	0	0
33	38	0.0036	0.0444	0.693	1	0	0	0	0
41	40	0.006	0.084	3.15	1	0	0	0	0
48	40	0.002	0.022	1.28	1	0	0	0	0
42	41	0.004	0.06	2.25	1	0	0	0	0
52	42	0.004	0.06	2.25	1	0	0	0	0
37	43	0.0005	0.0276	0	1	0	0	0	0
39	44	0	0.0411	0	1	0	0	0	0

43	44	0.0001	0.0011	0	1	0	0	0	0
35	45	0.0007	0.0175	1.39	1	0	0	0	0
39	45	0	0.0839	0	1	0	0	0	0
44	45	0.0025	0.073	0	1	0	0	0	0
38	46	0.0022	0.0284	0.43	1	0	0	0	0
1	47	0.0013	0.0188	1.31	1	0	0	0	0
47	48	0.0025	0.0268	0.4	1	0	0	0	0
47	48	0.0025	0.0268	0.4	1	0	0	0	0
46	49	0.0018	0.0274	0.27	1	0	0	0	0
45	51	0.0004	0.0105	0.72	1	0	0	0	0
50	51	0.0009	0.0221	1.62	1	0	0	0	0
17	18	0.0007	0.0082	0.1319	1	0	0	0	0
3	18	0.0011	0.0133	0.2138	1	0	0	0	0
1	2	0.0035	0.0411	0.6987	1	0	0	0	0
2	3	0.0013	0.0151	0.2572	1	0	0	0	0
3	4	0.0013	0.0213	0.2214	1	0	0	0	0
4	5	0.0008	0.0128	0.1342	1	0	0	0	0
5	6	0.0002	0.0026	0.0434	1	0	0	0	0
6	7	0.0006	0.0092	0.113	1	0	0	0	0
5	8	0.0008	0.0112	0.1476	1	0	0	0	0
7	8	0.0004	0.0046	0.078	1	0	0	0	0
8	9	0.0023	0.0363	0.3804	1	0	0	0	0
6	11	0.0007	0.0082	0.1389	1	0	0	0	0
10	11	0.0004	0.0043	0.0729	1	0	0	0	0
10	13	0.0004	0.0043	0.0729	1	0	0	0	0
4	14	0.0008	0.0129	0.1382	1	0	0	0	0
13	14	0.0009	0.0101	0.1723	1	0	0	0	0
14	15	0.0018	0.0217	0.366	1	0	0	0	0
15	16	0.0009	0.0094	0.171	1	0	0	0	0
1	27	0.032	0.32	0.41	1	0	0	0	0
50	52	0.0012	0.0288	2.06	1	0	0	0	0
39	70	0	0.005	0	1	0	1.2	0.8	0.02
2	53	0	0.0181	0	1.025	0	1.05	0.95	0.0063
6	54	0	0.025	0	1.07	0	1.08	0.92	0.0063
10	55	0	0.02	0	1.07	0	1.08	0.92	0.0063
19	56	0.0007	0.0142	0	1.07	0	1.08	0.92	0.0063
20	57	0.0009	0.018	0	1.009	0	1.05	0.95	0.0063
22	58	0	0.0143	0	1.025	0	1.05	0.95	0.0063
23	59	0.0005	0.0272	0	1	0	1.05	0.95	0.0063

25	60	0.0006	0.0232	0	1.025	0	1.05	0.95	0.0063
29	61	0.0008	0.0156	0	1.025	0	1.05	0.95	0.0063
31	62	0	0.026	0	1.04	0	1.05	0.95	0.0063
32	63	0	0.013	0	1.04	0	1.05	0.95	0.0063
36	64	0	0.0075	0	1.04	0	1.05	0.95	0.0063
37	65	0	0.0033	0	1.04	0	1.05	0.95	0.0063
41	66	0	0.0015	0	1	0	1.05	0.95	0.0063
42	67	0	0.0015	0	1	0	1.05	0.95	0.0063
52	68	0	0.003	0	1	0	1.05	0.95	0.0063
19	20	0.0007	0.0138	0	1.06	0	1.08	0.92	0.0063
35	34	0.0001	0.0074	0	0.946	0	1.06	0.92	0.0063
12	11	0.0016	0.0435	0	1.06	0	1.06	0.92	0.0063
12	13	0.0016	0.0435	0	1.06	0	1.08	0.92	0.0063

Table A. 3 Machine data

Mac #	Bus#	Base MVA	x_l(pu)	r_a(pu)	x_d(pu)	x'_d(pu)	x''_d(pu)	T'_{do} (sec)
1	53	800	0.1	0.002	0.8	0.248	0.2	10.2
2	54	850	0.298	0.002	2.508	0.592	0.425	6.56
3	55	1000	0.304	0.002	2.495	0.531	0.45	5.7
4	56	800	0.236	0.002	2.096	0.349	0.28	5.69
5	57	750	0.203	0.002	2.475	0.495	0.375	5.4
6	58	1000	0.224	0.002	2.54	0.5	0.4	7.3
7	59	750	0.242	0.002	2.213	0.368	0.3	5.66
8	60	700	0.196	0.002	2.03	0.399	0.315	6.7
9	61	1000	0.298	0.002	2.106	0.57	0.45	4.79
10	62	875	0.174	0.002	1.479	0.4	0.35	9.37
11	63	1300	0.134	0.002	1.664	0.234	0.156	4.1
12	64	2000	0.44	0.002	2.02	0.62	0.5	7.4
13	65	10000	0.15	0.002	1.48	0.275	0.2	5.9
14	66	10000	0.17	0.002	1.8	0.285	0.23	4.1
15	67	10000	0.17	0.002	1.8	0.285	0.23	4.1
16	68	10000	0.205	0.002	1.78	0.355	0.275	7.8

Mac#	***T''_{do} (sec)***	***x_q (pu)***	***x'_q (pu)***	***x''_q (pu)***	***T'_{qo} (sec)***	***T''_{qo} (sec)***	***H (sec)***	***d_o (pu)***	***d_1 (pu)***
1	0.05	0.552	0.224	0.2	1.5	0.035	5.25	0	0
2	0.05	2.397	0.51	0.425	1.5	0.035	3.553	0	0
3	0.05	2.37	0.5	0.45	1.5	0.035	3.58	0	0
4	0.05	2.064	0.32	0.28	1.5	0.035	3.575	0	0
5	0.05	2.325	0.45	0.375	0.44	0.035	3.467	0	0
6	0.05	2.41	0.45	0.4	0.4	0.035	3.48	0	0
7	0.05	2.19	0.338	0.3	1.5	0.035	3.52	0	0
8	0.05	1.96	0.35	0.315	0.41	0.035	3.471	0	0
9	0.05	2.05	0.5	0.45	1.96	0.035	3.45	0	0
10	0.05	1.006	0.394	0.35	1.5	0.035	3.543	0	0
11	0.05	1.599	0.195	0.156	1.5	0.035	2.169	0	0
12	0.05	1.9	0.56	0.5	1.5	0.035	4.615	0	0
13	0.05	1.43	0.25	0.2	1.5	0.035	4.96	0	0
14	0.05	1.73	0.25	0.23	1.5	0.035	3	0	0
15	0.05	1.73	0.25	0.23	1.5	0.035	3	0	0
16	0.05	1.67	0.3	0.275	1.5	0.035	4.5	0	0

Table A. 4 Governor data

Mac#	w_f*(pu)*	*1/R(pu)*	T_{max}*(pu)*	T_s*(sec)*	T_c*(sec)*	T_3*(sec)*	T_4*(sec)*	T_5*(sec)*
2	1	20	1.1	0.2	0.1	0	2.5	8
3	1	20	1.1	0.2	0.1	0	2.5	8
4	1	20	1.1	0.2	0.1	0	2.5	8
5	1	20	1.1	0.2	0.1	0	2.5	8
6	1	20	1.1	0.2	0.1	0	2.5	8
7	1	20	1.1	0.2	0.1	0	2.5	8
8	1	20	1.1	0.2	0.1	0	2.5	8
9	1	20	1.1	0.2	0.1	0	2.5	8
10	1	20	1.1	0.2	0.1	0	2.5	8
11	1	20	1.1	0.2	0.1	0	2.5	8
12	1	20	1.1	0.2	0.1	0	2.5	8

Table A. 5 PSS data

Mac#	*Gain*	T_w *(sec)*	T_{n1} *(sec)*	T_{d1} *(sec)*	T_{n2} *(sec)*	T_{d2} *(sec)*	Y_{max}	Y_{min}
1	80	10	0.1	0.02	0.08	0.02	0.2	-0.05
2	80	10	0.08	0.02	0.08	0.02	0.2	-0.05
3	80	10	0.08	0.02	0.08	0.02	0.2	-0.05
4	80	10	0.08	0.02	0.08	0.02	0.2	-0.05
5	80	10	0.08	0.02	0.08	0.02	0.2	-0.05
6	50	10	0.1	0.02	0.1	0.02	0.2	-0.05
7	80	10	0.08	0.02	0.08	0.02	0.2	-0.05
8	80	10	0.08	0.02	0.08	0.02	0.2	-0.05
9	100	10	0.08	0.03	0.05	0.01	0.2	-0.05
10	80	10	0.1	0.02	0.1	0.02	0.2	-0.05
11	50	10	0.08	0.03	0.05	0.01	0.2	-0.05
12	80	10	0.1	0.02	0.1	0.02	0.2	-0.05